T.C.

ALTINBAŞ UNIVERSITY

Institute of Graduate Studies

Mechanical Engineering

HEAT ASSISTED MACHINING OF SUPERALLOYS

Talha MUNIR

Master of Science

Supervisor

Asst. Prof. Dr. Armin TURKSOY

Istanbul, 2021

HEAT ASSISTED MACHINING OF SUPERALLOYS

by

Talha MUNIR

Mechanical Engineering

Submitted to the Institute of Graduate Studies

in partial fulfillment of the requirements for the degree of

Master of Science

ALTINBAŞ UNIVERSITY

2021

The thesis titled " HEAT ASSISTED MACHINING OF SUPERALLOYS " prepared and presented by Talha MUNIR was accepted as a master of science thesis in mechanical engineering.

____

Asst. Prof. Dr. Armin TURKSOY

Supervisor

Thesis Defense Jury Members:

Asst. Prof. Dr. Armin TURKSOY	Faculty of Engineering and Natural Sciences, Altınbaş University	________________
Asst.Prof. Dr. Hakan KAYGUSUZ	Faculty of Engineering and Natural Sciences, Altınbaş University	________________
Asst. Prof. Dr. Seyed Ehsan LAYEGH	Faculty of Engineering, MEF University	________________

I certify that this thesis satisfies all the requirements as a thesis for the degree of Master of Science.

Approval Date of Institute of Graduate Studies: ____/____/____

I hereby declare that all information in this document has been obtained and presented in accordance with academic rules and ethical conduct. I also declare that, as required by these rules and conduct, I have fully cited and referenced all material and results that are not original to this work.

Talha Munir

Signature

ACKNOWLEDGMENT

First of all, I would like to thank Almighty ALLAH, who made me complete this task. I would like to thank my family, my father, Abdul Razzaq, and my mother Naseem Akhter who have always been supportive and encouraging, they raised me to become a good person and a positive member of society and were patient with me through good and better days and everything I have accomplished is because of their effort and I hope I can make them happy in return for all they have done for me and also my brother Muhammad Sohaib and sister Fatima Noor for all the support and encouragement.

I would like to express my gratitude to my thesis advisor Asst. Prof. Dr. Armin Turksoy of Mechanical Engineering department at Altinbas University. The door to Dr. Armin Turksoy’s office was always open whenever I ran into a trouble spot or had a question. He consistently allowed this paper to be my work but steered me in the right direction whenever he thought I needed it.

I would like to thank all my teachers for having a great influence on me, I would like also to thank the Department of Mechanical Engineering and also Altinbas University and its library for providing me with access to all the books and articles that I needed to finish this work.

ABSTRACT

HEAT ASSISTED MACHINING OF SUPERALLOYS

Munir Talha,

M.Sc, Mechanical Engineering, Altınbaş University

Supervisor: Asst. Prof. Dr. Armin Turksoy

Co-Supervisor:

Date: 06/2021

Pages: 114

Superalloys are vastly used in the aerospace industry due to their alluring properties such as maintaining their strength at high-temperature applications. Nevertheless, manufacturing these raw materials to the desired geometrical shapes is one of the main challenges of the subtractive manufacturing industry and they are categorized as hard-to-machine materials. Several approaches such as High-Speed Machining (HSM), Cryogenic cooling, Minimum Quantity Lubrication (MQL), and Heat Assisted Machining (HAM) are introduced to tackle this matter.

HAM is a technique that introduces external heat sources to the workpiece (pre-heating or real-time heating methods) to increase the ductility of the superalloy and therefore reduce the yield and shear strength of the workpiece. By this means the machining parameters demonstrate an improvement compared to conventional machining.

This study focuses on the research approaches conducted to evaluate the effect of the various heat source applications (Gas flame, Induction, Laser, and Plasma) on the material properties and the machinability of the superalloys. Additionally, the heating methodology and heat assistance impact on cutting parameters (forces, tool life, surface integrity, and chip morphology) are outlined. Finally, a comparison of the heat source efficiency and the economics of the various heat applications are performed. The analysis of the Finite element method on the orthogonal cutting of Inconel 718 was evaluated. The material behavior can observe by the constitutive model, the effect of high strain, strain rate, and temperatures on the equivalent flow stresses observed by the modeling of conventional and modified Jhonson-cook. The induction heat source considered and the analytical solution of induction power is evaluated. the heat-induced in the Inconel 718 workpiece concerning time is studied in detail. The induction heating of Inconel 718 is simulated by using the COMSOL multiphysics model. The effect of frequency and current on the temperature inside the material has been discussed. A comparison of the stress-strain curve of the Inconel 718 modeled, the temperature effect on the strain rate

Keywords: Superalloys, Heat Assisted Machining, Laser, Induction, Flow stresses, Finite element analysis

TABLE OF CONTENTS

LISTS OF TABLES

Pages

LISTS OF FIGURES

Pages

ABBREVIATIONS

BUE	:	Build-up Edge
CBN	:	Cubic Boron Nitride
CM	:	Conventional Machining
CN	:	Carbon Nitride
CVD	:	Chemical Vapour Deposition
DOF	:	Degree of Freedom
FCC	:	Face Centered Cubic
HAM	:	Heat Assisted Machining
HAZ	:	Heat Affected Zone
HSM	:	High-Speed Machining
IAM	:	Induction Assisted Machining
IR	:	Infrared
JC	:	Jhonson-Cook
LAM	:	Laser-assisted Machining
LBM	:	Laser Beam Machining
LPG	:	Liquified Petroleum Gas
MC	:	Metal Carbide
MQL	:	Minimum Quantity Lubrication
MRR	:	Material Removal Rate
Nd: YAG	:	Neodymium Doped Yttrium Aluminum Garnet

ODS	:	Oxide Dispersion Strengthening
PAM	:	Plasma Assisted Machining
PEM	:	Plasma Enhanced Machining
PVD	:	Physical Vapor Deposition
RT	:	Room Temperature

LIST OF SYMBOL

	:	Beam divergence
Δ	:	Pulse duration
	:	Electrical permittivity
	:	Skin effect
	:	Thermal efficiency
	:	Magnetic permeability
	:	Electrical resistivity
	:	Density
	:	Electrical conductivity
	:	Width of cut
	:	Specific heat
	:	Laser spot diameter
	:	Diameter
$\bar{}$	:	Electric flux density
	:	Feed per revolution
	:	Feed force
	:	The focal length of the lens
	:	Radial force
	:	Tangential force
h	:	Depth of cut
$\bar{}$	:	Magnetic field intensity

: Inclination angle

: Current

: Angular frequency

: Current density

: Thermal conductivity

: Feed cutting constant

: Feed edge constant

: Radial cutting constant

: Radial edge constant

: Tangential cutting constant

: Tangential edge constant

: Laser power

: Power density

: Heat generation rate

: Input power

: Radius

: Time

: Temperature

0 : Initial thermal

1. INTRODUCTION

Since WWII, superalloys continue to be of use in the manufacturing of high-end products in various applications such as turbine blades, gas turbines, submarines, and oil industries [1]. The superior mechanical, physical, and thermal properties of these materials at elevated temperatures are the main motivation for pushing the performance limits in the aerospace industry [2]. In addition, the high-strength-to-weight ratio and corrosion resistance of superalloys is one of the main reasons that make them appealing raw materials in jet engines [3]. However, these inherent properties are the key to what makes them classified as “difficult-to-cut materials” [4]. Moreover, most materials under the aforementioned category require considerable energy while undergoing machining operations [5].

Superalloys are mainly categorized as Nickel-base, Cobalt-base, and Iron-based. Additionally, some of the main minor alloying elements are Tungsten, Titanium, Aluminum, and Vanadium. In the Iron-based types depending on the microstructure and the Iron-Carbon phases of austenitic and martensitic, the working temperature of the superalloy varies. In general, the Iron-based superalloy with the austenitic microstructure works at higher temperatures compared to the martensitic type. On the other hand, Nickel-based superalloys are commonly used in turbojet engines where the working temperature is approximately 1000°C. High thermal shock resistance, creep strength, and yield strength in the harsh exhaust environment are the main characteristics that make the Nickel-based superalloys a major material for exhaust turbines in jet engines. Moreover, for applications that higher temperatures are needed the main choice is Cobalt-based superalloys. The main reason is the minor addition of the refractory metals in the superalloy microstructure. Additionally, an adequate amount of chromium enhances corrosion resistance [6].

Mainly, superalloys have low thermal conductivity, high hardness, high shear strength, and work hardenability. Therefore, during the machining process, the high temperature at the primary and secondary contact zones, cannot dissipate. Additionally, due to the diffusion and adhesion mechanisms in between the cutting tool and the workpiece, high tool wear rates occur. Consequently, tool life becomes short and the final product cost increases drastically [7]. As an example, in turning operation, the machined workpiece is exposed to stress, strain, pressure as well as thermal and sometimes chemical loading which can eventually lead to strain aging, recrystallization, and plastic deformation. These effects are the main agents that cause microstructure alteration, generation of residual stresses, phase transformation, and work hardening [8]. It has been reported that the depth and degree of microstructure alteration depend on cutting parameters as well as tool geometry. Hence, it is of great importance to select appropriate conditions [9].

Several methods have been introduced by researchers to overcome superalloy machining problems. In some superalloy materials, high-speed machining is recommended due to higher material removal rate with a small amount of change in cutting forces. Ma et al. [4] conducted a series of experiments with different cutting conditions and reported that changing the spindle speed from 4000 to 4500 rpm reduced the cutting forces in high-speed machining of Inconel 718 (Nickel-based superalloy) significantly. On the other hand, Cai et al. [10] investigated the effect of cutting speed on the surface quality of the Inconel 718 and claimed that the high-speed machining resulted in higher cutting forces and residual stresses. However, beyond the 80 m/min cutting speed, the forces became stabilized. Moreover, Jin et al. [11] investigated the high-speed machining of powder metallurgy manufactured FGH95 superalloy (Nickel-based). The experiments showed that below 2400 m/min cutting speed, the surface roughness did not change significantly. However, higher than this cutting speed resulted in higher surface roughness. Considering these problems with the HSM of superalloys, another approach introduced was the combination of HSM with minimum quantity lubrication (MQL) or cryogenic cooling. By this means, high material removal rate, relatively lower cutting forces due to lubrication, higher machining accuracy as well as a good surface finish were achieved. Additionally, at higher cutting speeds, the flooded lubrication was not effective due to the formation of a high-temperature blanket. Therefore, the usage of the MQL method provided efficient droplet penetration in the cutting zone corresponding to better cooling [12]–[14]. Kaynak [15] compared the dry, Cryogenic, and MQL machining of the Inconel 718. At lower cutting speeds, the MQL method reduced the cutting forces significantly compared to cryogenic and dry machining. However, as the cutting speed rises, the cryogenic cooling becomes more effective in reducing the cutting forces which was mainly related to the tool-chip contact length. Besides, the cooling pressure affects the tool life considerably which needs further consideration. Nandy et al. [16] investigated the effect of sprayed coolant pressure on the cutting zone of the Ti-6Al-4V workpiece. Results demonstrate that spray pressures as high as 100 bar can increase the tool life by 250%. On the other hand, coolant and lubricant consumption increase production costs due to environmental concerns, thus, dry machining techniques with reasonable tool life introduce a more cost-effective approach along with environmental benefits. However, achieving high-quality finished products while dry machining is a well-known challenge [17].

Furthermore, some researchers explored the effect of cutting tool coating on enhancing the tool life and surface integrity while machining superalloys [18]. Zhou et al. [19] compared the role of Cubic Boron Nitride (CBN) coated tool on the surface roughness of Inconel 718. At cutting speeds below 300 m/min, the coated tool had approximately 20% higher tool life compared to the uncoated one. However, due to a larger nose radius in the CBN-coated tool, the machined part had higher surface roughness. Hao et al. [20] examined a Physical Vapor Deposition (PVD)-TiAlN-coated carbide tool at different cutting speeds in Inconel 718 turning operation. Although, the cutting forces and the tool wear reduces, at higher temperatures, the tool substance oxidation causes a reduction in the tool life and surface quality.

In addition to the effect of cutting parameters and tool material, the mechanical properties of the workpiece need to be taken into consideration. In metals, the ductile to brittle transition temperature plays an important role in the tensile, compression, and shear strength of the material. Using this phenomenon, several researchers, adopt a pre-heating approach to soften the superalloy and reduce the cutting forces. Figure 1.1 demonstrates the effect of temperature on the tensile strength of some hard-to-machine materials. As shown, in Figure 1.1, for most of the materials, after a threshold temperature, the tensile strength drops drastically.

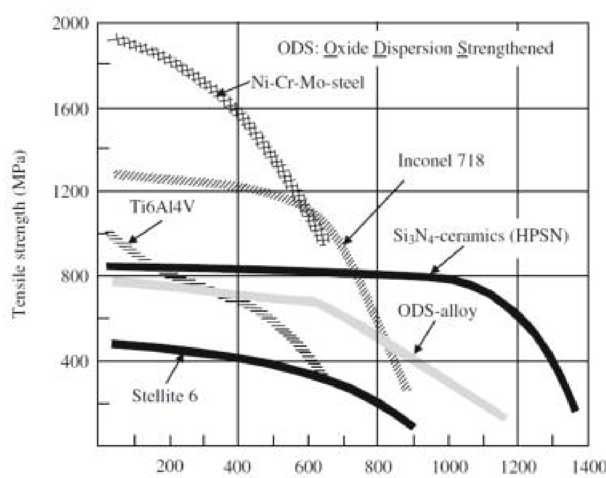

Figure 1.1: Effect of temperature on the ultimate tensile strength for various hard-to-machine materials [21].

HAM is a preheating method that reduces the chances of work hardening and minimizes the cutting forces [22]. Therefore, it mainly enhances the tool life in superalloy machining [23]. Several heat sources have been used to implement HAM in different industries for various materials. Although heat sources are readily available technologies, the challenge for engineers is how to integrate them within the machining centers under different conditions without harming machine and tooling devices [24]. Furthermore, machining complex geometries while implementing the heat source is limiting the use of this approach. This review study focuses on the HAM of superalloys using different heating techniques as well as how these heating systems are assimilated into different machining centers ranging from a basic lathe machine to the complex 5-axis CNC. The heating techniques discussed in this paper are Laser, plasma, gas Flame, Induction as well as some hybrid methods. The effect of these approaches on the machining characteristics such as cutting force, surface topology, chip morphology, tool wear, and material removal rate is evaluated in detail. A comparison is made between these methods to explore the most suitable techniques for specific superalloy. The finite element method plays a significant role in the development of different explicit and steady-state thermal simulations. The Ansys 2021 R1 is used for the simulation of Inconel 718. The explicit dynamics model was developed for the material. An orthogonal cutting operation is done and analyzes the result for the stresses and strain. Researchers developed many empirical formulas for the different kinds of material to observe the stress-strain curve. In this study, a conventional and modified constitutive model has been under consideration to study the flow stresses and strain rate concerning temperature for the Inconel 718. Additionally, the stress-strain curve has been modeled by using MATLAB. The effect of thermal softening on the flow stresses, strain rate hardening, and temperature was observed in detail. The conventional JC model has limitations and because of this the results are not appropriate while the modified JC model gives the effective results. This is because of the consideration of thermal softening in modified JC model. The power required to heat up the material by induction heating is analytical evaluated. Temperature is directly proportional to the induced induction power. The effect of frequency on the temperature is significant, temperature increases as the frequency increase if the current keeps constant. In chapter 5, COMSOL Multiphysics modeling results shows the effect of frequency and current on the temperature with respect to time.

2. LITERATURE REVIEW

2.1 HEATING METHODOLOGY

Compared to conventional superalloy machining, HAM demonstrates more promising results. However, most of the superalloys have a low thermal conductivity which pursues researchers to investigate various energy sources and heating strategies of superalloy pre-heating. In this chapter, the principles of the selected energy sources are discussed in detail and the integration methods in various machines are explained.

2.1.1 Gas Flame

The Liquified Petroleum Gas (LPG) and oxygen are used to provide the necessary heat to increase the workpiece temperature. This heating source is among the cheapest and commercially available considering the low initial investment costs. Kumar et al. [25] designed an experimental setup to investigate the hot turning of Monel 400 and Inconel 718. The regulator pressure was kept constant during the turning operation to provide a homogeneous heat distribution. As the workpiece reached the desired temperature, the flame torch automatically moved away from the workpiece, and whenever there was a reduction in the workpiece temperature, the flame handle moved towards the workpiece to maintain a constant temperature. Additionally, the pre-heating temperatures and the corresponding cutting forces were evaluated numerically and validated experimentally. As materials heated up, the cutting forces reduced, with the optimum temperature of 600°C. Additionally, the shear strength of the Inconel 718 was reduced by using the gas torch as an external pre-heating tool. Therefore, the specific cutting energy of the material was reduced which enhanced higher material removal rates and better productivity. Although the approach has notable advantages and is pretty much simple compared to the other methods, the low penetration depth, energy waste, and low controllability issues are the main disadvantages. Moreover, this method is not a proper technique for some superalloys, since the carbon particles diffuse to the superalloy microstructure and form oxides[25]–[27]. Figure 2.1 shows the schematic and experimental setup for Inconel 718 hot turning using the gas flame torch.

(a)

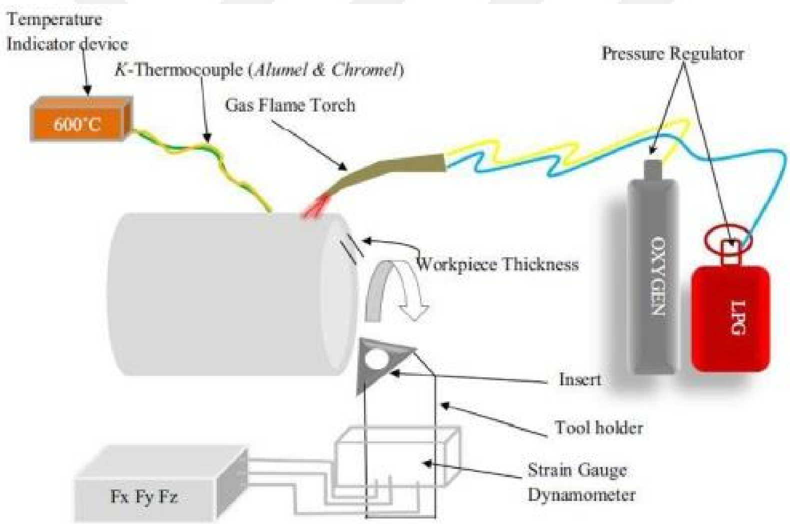

(b)

Figure 2.1: a) Experimental setup and measured force directions b) Schematic diagram of gas flame assisted machining [26].

2.1.2 Induction-assisted

Induction heating is a non-contact heating process that uses the induced electromagnetic current (eddy currents) to bond, soften or harden electrically conductive metals. The combination of speed, controllability, and uniform heat distribution within the material makes it one of the most efficient methods among the heating processes. A change in the magnetic field induces a current which is explained using the Maxwell Eq. (2.1 to 2.4).

$$\Delta^{-} = \quad + \underline{\;^{-}} \tag{2.1}$$

$$\Delta^{-} = -\underline{\;^{-}} = - \quad \underline{\;^{-}} \tag{2.2}$$

$$^{-} = \quad ^{-} = \quad o \quad ^{-} \tag{2.3}$$

$$^{-} = \quad ^{-} = \quad o \quad ^{-} \tag{2.4}$$

where‾ is the electric field strength,‾ is the electric flux density,‾ is the magnetic field intensity, ‾ is the magnetic flux density, is the current density, is the electrical permittivity (or dielectric constant), and is the magnetic permeability. The induced current causes heating in the conductive material due to the presence of an electric field in the medium and this can be related to Ohms' law.

$$= \quad ^{-} = \underline{\;^{-}} \tag{2.5}$$

where denotes the electrical conductivity of the material and is the electrical resistivity [28]. Additionally, the three-dimensional heat transfer generated by the induced magnetic field and current can be described as:

$$\underline{\quad} = \underline{\quad}\left(\underline{\;2\;2\;} + \underline{\;2\;2\;} + \underline{\;2\;2\;}\right) + \tag{2.6}$$

where is the thermal conductivity, is the density, is the specific heat, is the temperature, is the time, and is the heat generation rate [29].

Considering the induction heating potential in the electrically conductive materials, several researchers investigated the compatibility of this heating method with the machining of superalloys. Baili et al. [30] integrated a semi-circular induction coil which partially enveloped the workpiece for pre-heating the superalloy during the turning operation. The partial coil geometry gave the advantage of simultaneous heating and cutting during the process which resulted in a more homogenous heat distribution during the operation. Additionally, in this process, considering the relatively low thermal conductivity of the alloy, the workpiece was heated up to 1000°Cin a short period (2 minutes) which demonstrated the high heating rate of the induction heating process.

Furthermore, some researchers integrated induction heating in the milling process. Kim. et al [31] mounted a mobile induction coil with a constant height and distance from the end mill tool to the milling machine. The induced eddy currents on the surface of the Inconel 718 increased the surface temperature for an optimized depth of cut. Figure 2.2 demonstrates the schematic and positioning procedure for the milling operation.

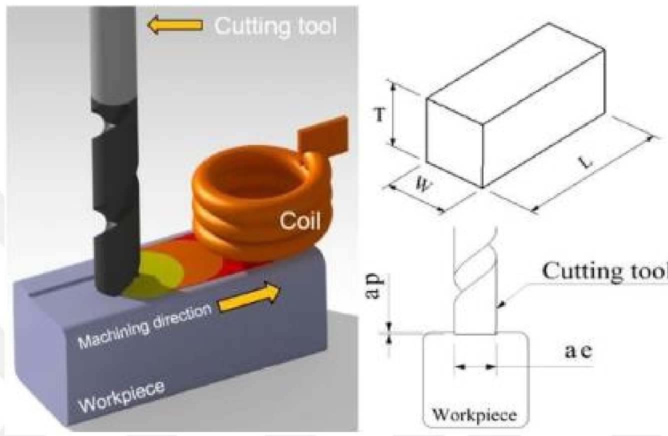

(a)

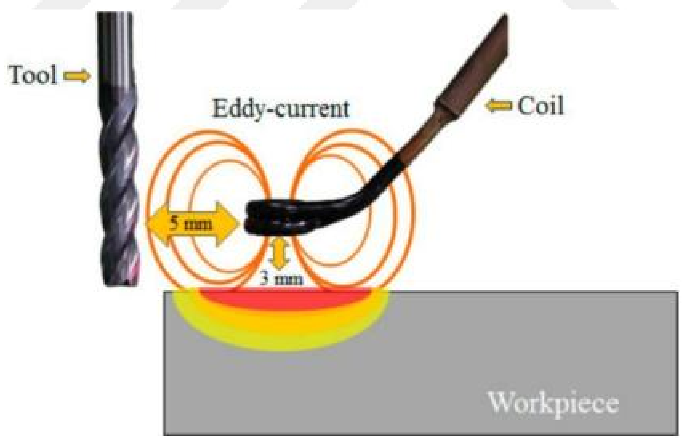

(b)

Figure 2.2: a) Schematic of the induction coil setup in milling b) Positioning dimensions of the induction coil concerning the tool and workpiece [31].

2.1.3 Laser-assisted

In a Laser setup, an optical amplifier condenses the electromagnetic radiation and emits the energy as the photons to the desired workpiece surface [35]. As the laser interacts with the workpiece surface, the energy of the light photons, is transferred to the workpiece surface causing a localized temperature rise.

The laser beam can be classified as the continuous and pulse mode, depending on the required amount of energy. Although the continuous laser beam generates huge amounts of energy in a short period, the pulse laser is preferred for heat-assisted machining operations due to the better control [32]. Furthermore, the Laser spot size dimension controls the amount of power delivered to the workpiece. The power density of the laser beam per unit time can be found as follows:

$$= \frac{4}{(\quad {}^{2}\quad {}^{2}\Delta\ )} \tag{2.7}$$

$$= \underline{\quad} \tag{2.8}$$

where is the Laser power, is the focal length of the lens, Δ is the pulse duration, is the beam divergence, and is the laser spot diameter. Additionally, the linear laser heat generation rate can be described as:

$$(\ ) = \frac{2}{\ {}^{2}}\exp\left(-\frac{2\ {}^{2}}{\ {}^{2}}\right) \tag{2.9}$$

where is the total input power of the laser, is the radius of the laser spot, and is the length in the cutting direction [33].

Moreover, the laser medium is selected depending on the application and the workpiece material. It can be solid (neodymium-doped YAG), liquid (dye), or gas (CO_2, He, Ne)[34], [35]. In Laser Beam Machining (LBM) and Laser-assisted Machining (LAM) operations, Nd: YAG and CO_2 are the main laser mediums. The main difference is related to the size of the wavelength, surface reflection, and peak power. The CO_2 laser has a higher wavelength compared to the Nd: YAG type. The higher wavelength of the CO_2 type causes a limitation in the energy absorption of metals. Therefore, YAG lasers are more preferred for HAM of superalloys [36], [37]. A series of experiments have been carried out to integrate the laser heat sources into various machining setups. Tadavani et al. [36] performed a laser-assisted turning of Inconel 718 using a pulsed laser method. The workpiece was preheated with the laser which was mounted on the lathe support at a 60° angle with the infrared (IR) thermal camera. Figure 2.3 represents the experimental setup of laser-assisted turning.

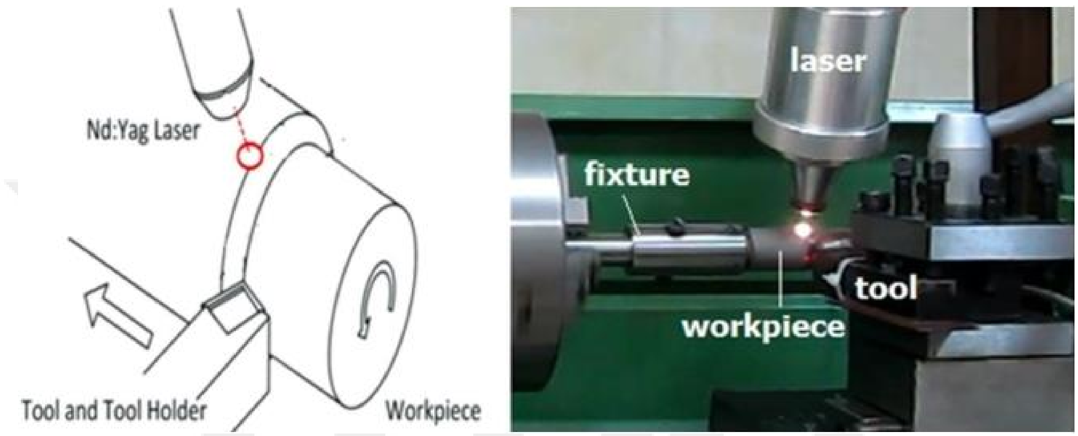

Figure 2.3: Experimental setup of laser integration in the Inconel 718 turning operation [36].

As an example of the laser integration in the milling operation, Kim et al. [38] mounted a laser head to the 5-axis milling machine to investigate Inconel 718 and AISI 1045 Steel. To achieve efficient heating in the desired workpiece surface, the inclination angle of the laser head was controlled in a way that the irradiation angle was perpendicular to the cutting surface. Therefore, the laser power density and the spot size were kept as optimal as possible. Figure 2.4 demonstrates the laser integrated experimental setup.

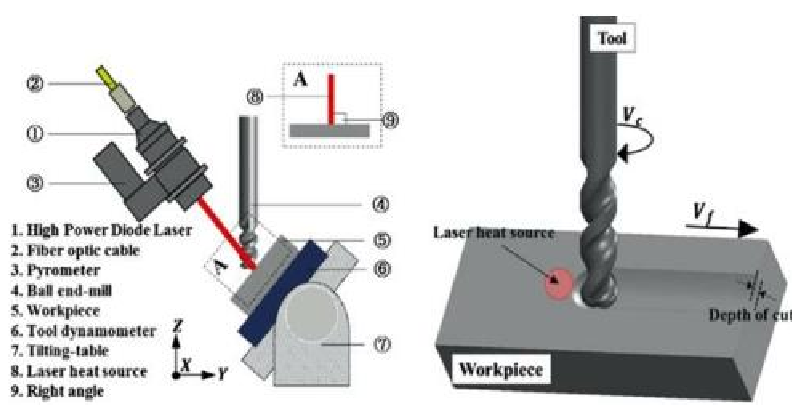

(a)

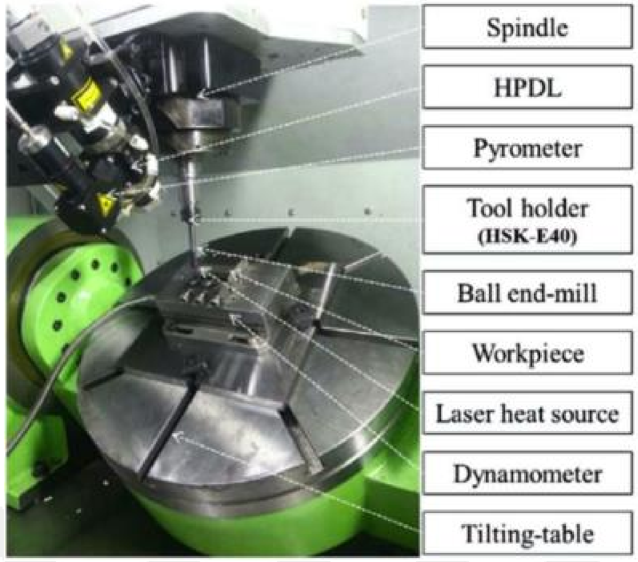

(b)

Figure: 2.4 a) Schematic of the laser integration b) The experimental setup with the components [38].

2.1.4 Plasma-assisted

In plasma heating, an electrical arc from a high current DC power supply energizes the gas atoms causing a superheated state of matter. Additionally, a nozzle is used to control the high-energy gas stream to the desired workpiece surface. The arc is made using a Tungsten electrode as a negative terminal and the workpiece as a positive terminal. The heating mechanism and plasma generation are mainly divided into two categories as transfer and non-transfer types. The transfer type generates the plasma state in between the workpiece and the torch while the non-transfer type generates the plasma state inside the torch. In the transfer type machine, the distance between the workpiece and the torch is kept constant. Additionally, this type only works on conductive materials which makes it more difficult to use compared to the non-transfer type [39], [40]. Moreover, the arc controlling parameters play an important role in magnifying the amount of energy by concentrating on the current density. Consequently, in a very short period, the selected surface of the superalloy faces a dense energy stream of 105-106 W/cm$_2$. Additionally, shielding gas protects the environment from oxygen burning [41].

The heat generated from the plasma torch can rise to 16000°Cwith a maximum speed of 6000 m/s air exit speed, which is more than enough to melt and blow metal away from the cutting zone [42]. If the heat distribution is assumed to be uniform, the thermal power can be calculated as:

$$= 0.24 * \quad * \quad * \qquad (2.10)$$

where is the plasma voltage, is the current, and is the thermal efficiency [41]. Additionally, the surface temperature of the plasma beam while hitting the workpiece surface can be modeled empirically as:

$$= 80.3275 \frac{\quad^{0.584} \quad^{0.06}}{\quad^{2.206} \quad^{0.405} \quad^{0.2026}} \qquad (2.11)$$

where, is the surface temperature, $_0$ is initial workpiece bulk temperature, is the cutting speed, is the workpiece diameter, is the feed per revolution [43]. Considering the plasma heating theory, several researchers performed experiments to investigate the possibility of system integration in superalloy machining. Lacalle et al. [44] integrated a plasma torch with the 3-axis milling machine and examined the machining performance of Inconel 718, Ti-6Al-4V, and Haynes 25 during the slot milling process. To perform the pre-heating operation, the plasma torch was mounted in a way that the workpiece heats up before the machining operation. Figure 2.5 shows the schematic of the PAM setup. On the other hand, Chen et al. [41] investigated the integration of the PAM in the turning of Inconel 718. Figure 2.6 represents the plasma torch mounting setup for the turning operation.

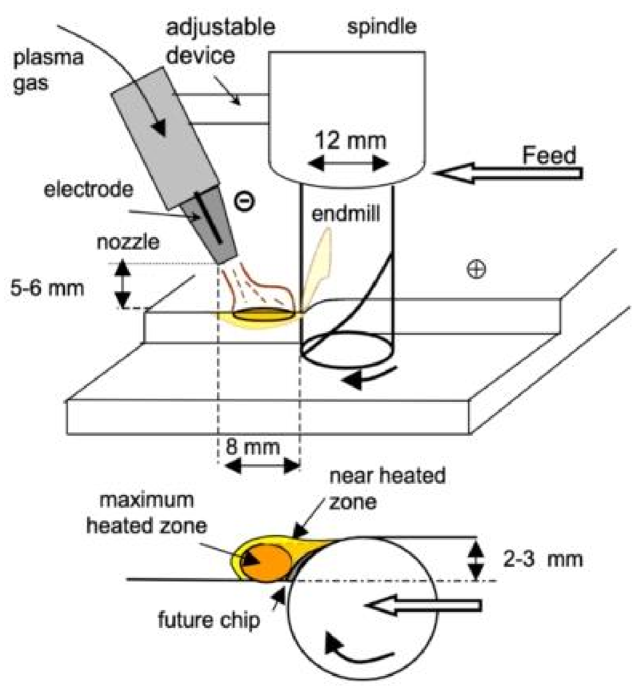

Figure 2.5: Schematic of Plasma torch integration during milling [44].

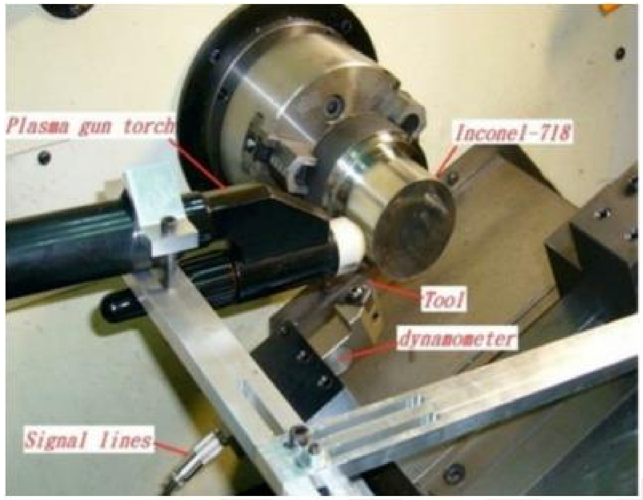

Figure 2.6: Experimental Layout for Plasma Assisted Machining [41].

Moon et al. [40] explored the effect of the plasma torch inclination angle on the milling of Inconel 718 and AISI 1045 Steel. Three inclination angles of 35°, 55°, and 70° were examined to explore the minimum and maximum preheating temperatures. The least temperature was generated at an angle of 35° and the highest temperature was generated at 70°. Additionally, the maximum effect of the preheating happened when the torch was near the workpiece surface. Therefore, the distance between the torch and workpiece was kept constant at 1.5mm to achieve the optimized preheating effect. Figure 2.7 demonstrates the schematic of different inclination angles in the experimental setup.

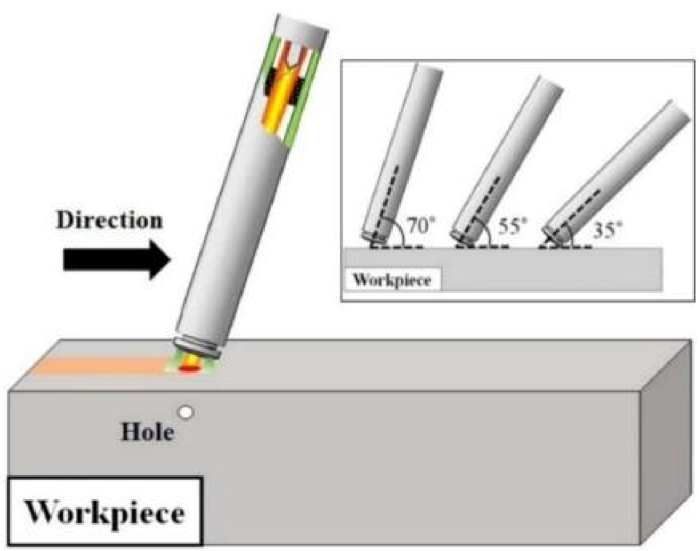

Figure 2.7: The position of Plasma torch based on angle [40].

Comparing all the heat sources, Laser and plasma tend to produce more intense localized heat. While laser and plasma work on the same principle, plasma produces larger heating spots. However, the power density produced by plasma is much less than laser. This can be a disadvantage in turning operation, as low density and large heating spots mean low heat penetration on the workpiece. In contrast, Lopez de Lacelle et al. [44] reported that during the milling operation, the large heating spot could be an advantage, which can pre-heat the end mill cutting zone including the entire radial depth of cut.

Table 2.1: A comparison of various heating techniques.

Heat source	Advantage	Disadvantage
Gas Flame	Easy to use. Low Initial setup cost	Risky and not environmentally friendly. Poor heating controllability. Distributed heat zone/less heat concentration
Induction	High heating capability Uniform heating Environmentally friendly Non-contact process	Limited tool mobility Distributed heat zone/less heat concentration
Laser	Easy control of heat source The high degree of heat concentration	Expensive initial setup High operational costs Non-Uniform heating/condensed heating
Plasma	The high degree of heat concentration Cheaper than Laser heat systems	High operational costs Non-Uniform heating/condensed heating

2.2 SUPERALLOYS PROPERTIES

Demands for high-performance products at elevated temperatures in various industries especially aerospace, lead to the development of superalloys. These materials sustain their static and dynamic strength at higher temperatures particularly higher than 650 ℃ Therefore, they are utilized as the raw material in the turbomachinery industry [45]. These properties are achieved mainly using the alloying method to engineer the microstructure of the material by generating phases. Additionally, specific heat treatment methods are applied to strengthen the material properties at elevated temperatures. Most of the superalloys, have a face-centered cubic (FCC) structure and can be divided into different groups such as Iron-based (Fe-based), Nickel-based (Ni-based), Cobalt-based (Co-based). These groups are differentiated based on the chemical composition with the highest percentage of the corresponding ingredient. Nickel, Cobalt, and Iron have a high melting temperature than other metals in their pure form. In addition, some other elements such as Aluminum (Al), Silicon (Si), Molybdenum (Mo), and Chromium (Cr) are added to excel the corrosion resistance, fatigue life cycle, and creep resistance of the alloy. Therefore, properties can be modified by altering the alloying element composition ratio in the metals. Table 2.2 represents the approximate ranges of the element composition in different superalloys [46].

Table 2.2: Minor element composition in various superalloys [46].

	Ranges %	
Element	Fe-Ni and Ni-base	Co-base
Chromium	5-25	19-30
Molybdenum, tungsten	0-12	0-11
Aluminum	0-6	0-4.5
Titanium	0-6	0-4
Niobium	0-5	0-4
Tantalum	0-12	0-9
Rhenium	0-6	0-2

These minor elements produce a secondary precipitated phase or a solid solution hardening within the superalloys. Additionally, the intermetallic compounds combined with the carbide phases and grain boundary refiners add required barriers to the dislocation motion which results in the strengthening of the material. Table 2.3 represents the common alloying elements and their application in the superalloy production procedure [46].

Table 2.3: Effect of elements in superalloy microstructure [46].

Effect(a)	Iron-base	Cobalt-base	Nickel-base
Solid-solution strengtheners	Cr, Mo	Nb, Cr, Mo, Ni, W, Ta	Co, Cr, Fe, Mo, W, Ta, Re
fcc matrix stabilizers	C, W, Ni	Ni	…
MC (metal carbide)	Ti	Ti	W, Ta, Ti, Mo, Nb, Hf
M_7C_3 (metal carbide)	…	Cr	Cr
$M_{23}C_6$ (metal carbide)	Cr	Cr	Cr, Mo, W
M_6C (metal carbide)	Mo	Mo, W	Mo, W, Nb
Carbonitrides: M(CN)	C, N	C, N	C, N
Promotes general precipitation of carbides	P	...	...
Retards formation of hexagonal η (Ni3Ti)	Al, Zr	...	...
Raises solvus temperature of γ'	...	...	Co
Hardening precipitates and/or intermetallics	Al, Ti, Nb	Al, Mo, Ti(b), W, Ta	Al, Ti, Nb
Oxidation resistance	Cr	Al, Cr	Al, Cr, Y, La, Ce
Improve hot corrosion resistance	La, Y	La, Y, Th	La, Th
Sulfidation resistance	Cr	Cr	Cr, Co, Si
Improves creep properties	B	...	B, Ta

Increases rupture strength	B	B, Zr	B(c)
Grain-boundary refiners	...	...	B, C, Zr, Hf
Facilitates working	...	Ni3Ti	...
Retard γ ′ coarsening	...	...	Re
(a) Not all these effects necessarily occur in a given alloy. (b) Hardening by precipitation of Ni_3Ti also occurs if sufficient Ni is present. (c) If present in large amounts, borides are formed.			

As discussed earlier, in addition to the effect of the superalloy composition, the metallurgical microstructure of the superalloy (engineered by the heat treatment methods), the working temperature, and the time that the superalloy is exposed to the heat are the main factors changing the mechanical properties of the material. Figure 2.8 represents the creep rupture strength of different superalloy groups at various working conditions. Physical properties of superalloys such as thermal conductivity and thermal expansion coefficients are lower compared to the other metal alloys which cause some problems in HAM applications. The reason is the addition of the transition elements and the occurrence of the refractory metals in the superalloys [47]. In this section, mechanical properties, chemical composition, and the microstructure of different superalloy groups are discussed in detail.

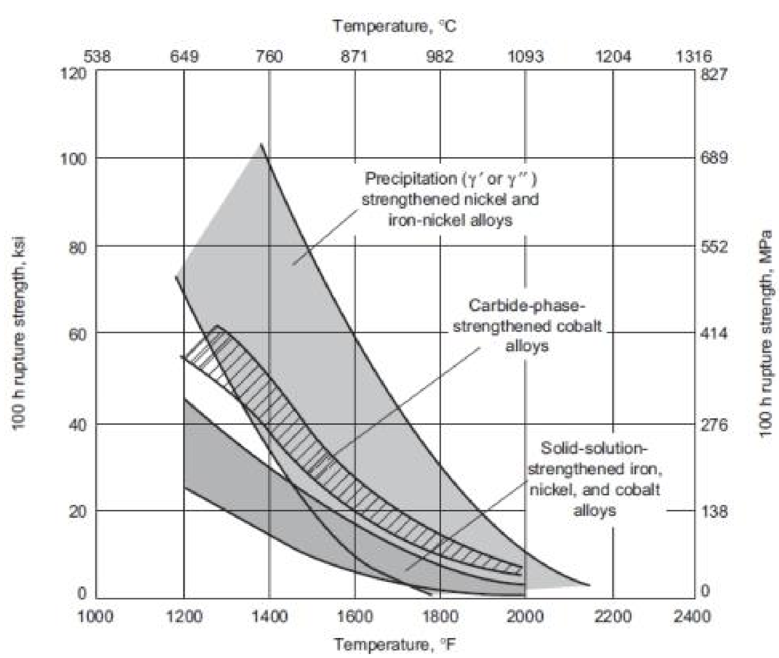

Figure 2.8: Creep rupture strength of superalloys after 100 hr [46].

2.2.1 Iron-base(Fe-based) Superalloys

The Iron-base superalloys were established with the advancement in the chemical and phase composition of the austenitic steels. The FCC crystal matrix combined with the secondary intermetallic precipitated phase particles and the solid solution hardening elements are the substructures of the material. The precipitation as a secondary phase is named as the ′ phase (Ni_3Al, Ni_3Ti) and ″phase (Ni_3Nb) which holds the material strength up to 750 ℃ It is produced upon the addition of the high Nickel percentage with a low amount of Aluminum, Titanium, and Niobium. These precipitated phases result in the higher creep strength of the Iron-base superalloys at a temperature range of 540-700 ℃, compared to the Nickel and the Cobalt base ones. Additionally, approximately 20% of Chromium is added to the microstructure. This high percentage of the Chromium is related to the solid solution hardening mechanism within the austenitic matrix [48].

The iron-base superalloys are sometimes referred to as Nickel-Iron-based superalloys. The reason is related to the high percentage of Nickel (more than 25%) within the austenitic FCC matrix. As the temperature of the material increases above the 750 ℃, the ′ phase converts to the -Ni_3Ti phase. The new phase has a lamellar and hexagonal crystal morphology. This conversion of the crystal shape causes a reduction in the creep strength of the material at the working conditions of 900-1000 ℃ Therefore, metal carbide (MC) and carbon nitride (CN) particles are added to the Iron-base superalloys as strengthening agents at elevated temperatures [48], [49].

Among the superalloy types, the Iron base ones generate the least cutting forces while machining. The reason is related to the lower strength of these alloys at elevated temperatures compared to the other types. However, at lower temperatures (540-700 $_{o}$C), they demonstrate promising strength, creep, and wear resistance. Additionally, the low thermal expansion coefficient of these alloys makes them a suitable material for shafts, rings, and casing parts [50].

2.2.2 Nickel-base(Ni-based) Superalloys

Nickel-based superalloys are among the most used and metallurgically developed superalloys due to their superior yield, fatigue, and creep strength at elevated temperatures [51]. These alloys can be classified into three main groups regarding their strengthening mechanism within the microstructure. The first class is strengthened with the secondary precipitated phase particles of the intermetallic compounds within the austenitic FCC matrix (phase). Two precipitated phases of ′ and ″ are generated with respect to the added metallic elements. The Nickel-Titanium/Aluminum alloys make the ′ and the Nickel-Niobium alloys initiate the ″ phases.

The second class is developed using the solid solution strengthening mechanism. This is done by taking atoms from alloying elements and adding them to the crystalline lattice of the base metal to increase the strength of the metal. The elements used for alloying in solid solution hardening have high melting temperatures which promote reduced diffusion rate as well as good lattice cohesion at relatively high temperatures. In addition to this main mechanism, some of them can utilize minor carbide/intermetallic precipitation for further durability at elevated temperatures. The optimized percentage of the carbide phases enhances the rupture strength of the alloy. However, higher amounts of them initiate the crack propagation considering the brittle characteristics of the particles. Consequently, it will result in reduced ductility and rupture strength.

Finally, the other class of Nickel-based superalloys is engineered by Oxide Dispersion Strengthening (ODS) method in which the inert particles such as yttria oxide (Y_2O_3) are dispersed into the microstructure to bound with the precipitated phases [46], [52]. The mechanism is mainly conducted by mechanical alloying and a secondary recrystallization heat treatment method that generates coarse elongated grains in the precipitated phase. This modification causes a transfer in the steady-state zone to the creep-rupture response which prolongs the creep performance of the material at elevated temperatures [53]. The microstructure and strength of the Nickel-based superalloys change with the temperature and strain rate drastically [54]. In addition, these alloys do not demonstrate promising fatigue, creep, and yield strength at high-temperature applications due to the low corrosion resistance. This defect resulted in the development of a new category of superalloys as Nickel-Chromium based ones used in the combustion chambers of spacecraft rockets [55]. Additionally, the relatively high yield and ultimate tensile strengths of these alloys open a vast application opportunity in the nuclear and aerospace industries [56].

Generally, Nickel-based superalloys maintain their strength at high temperatures (metal cutting temperatures). Therefore, compared to the other types, a sophisticated machining lathe, and the cutting tool is necessary. Additionally, for optimal cutting performance, an unconventional approach is demanding to reduce the high amounts of shear and friction forces, tool wear, and chatter vibrations. Considering all this, pre-heating the workpiece and reducing the tensile and shear strength of the material is a promising approach for the optimal cutting process [57].

2.2.3 Cobalt-base(CO-based) Superalloys

Like other superalloys, the core structure of the Cobalt superalloy is the austenitic FCC matrix (phase) strengthened with the solid solution hardening and carbide phases [46]. Compared to the Nickel and Iron-based superalloys, in the Cobalt-based superalloys, the precipitated secondary phases of the intermetallic compounds (′and ′′ phases) are inactive. However, the solid solution mechanism is similar to the Nickel-based superalloys [58]. In fact, both Nickel and Cobalt are austenitizing agents meaning that depending on the strength and corrosion resistance at elevated temperatures, they can be substituted with each other. Generally, the Cobalt-based superalloys have lower strength compared to the Nickel-based ones at temperatures below 800℃ However, as the temperature rises, they sustain their strength, fatigue, and corrosion resistance, which makes them a more appealing material for higher temperature applications [48]. Additionally, the higher wear resistance of the Cobalt-based superalloys (Stellite 6B) makes them a coating material for high-temperature applications. Figure 2.9 demonstrates the yield strength of some of the common Iron-base, Nickel-base, and Cobalt-base superalloys at various working temperatures based on their microstructure difference.

Similar to the other superalloy types, the Cobalt-based superalloys provide high tensile and corrosion resistance in harsh circumstances. However, during the machining process, the low thermal conductivity of the workpiece and the high necessary shear force for cutting result in reduced tool life and surface quality. Additionally, the use of the cutting fluids and the coolants as an aid for the cutting force reduction causes several issues such as microstructure changes due to diffusion, environmental pollution, and health risks. These problems pursue the researchers to investigate other alternatives to improve the machineabilities of the superalloys [59].

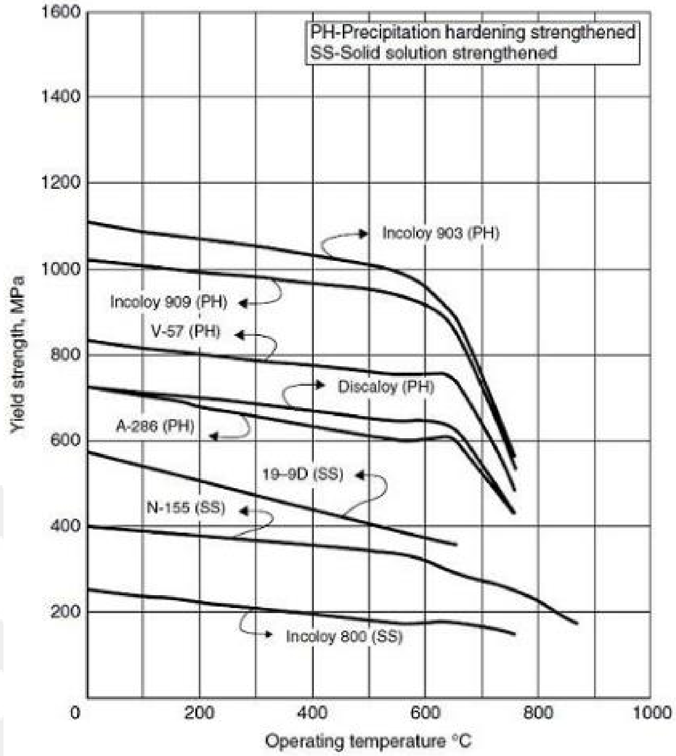
PH-Precipitation hardening strengthened
SS-Solid solution strengthened
Incoloy 903 (PH)
Incoloy 909 (PH)
V-57 (PH)
Discaloy (PH)
A-286 (PH)
19–9D (SS)
N-155 (SS)
Incoloy 800 (SS)
Yield strength, MPa
Operating temperature °C

(a)

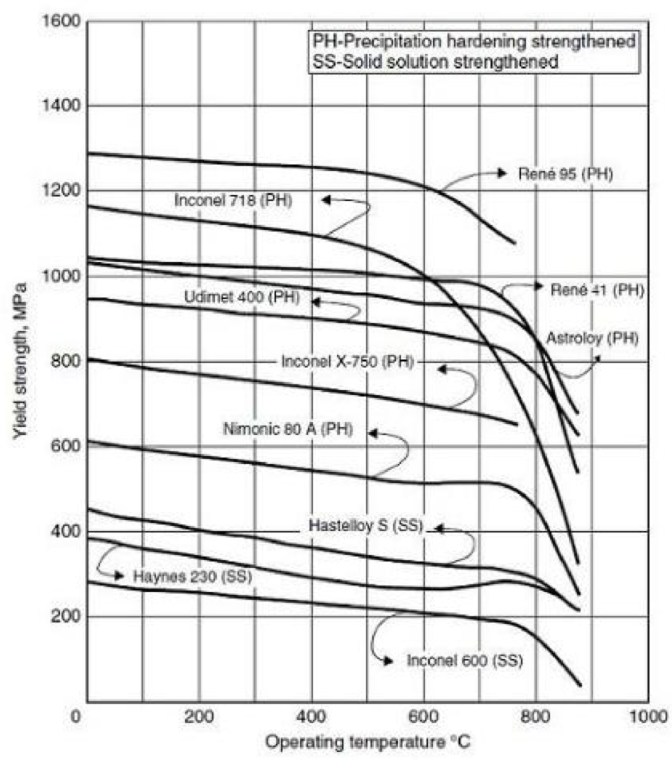
PH-Precipitation hardening strengthened
SS-Solid solution strengthened
René 95 (PH)
Inconel 718 (PH)
René 41 (PH)
Udimet 400 (PH)
Astroloy (PH)
Inconel X-750 (PH)
Nimonic 80 A (PH)
Hastelloy S (SS)
Haynes 230 (SS)
Inconel 600 (SS)
Yield strength, MPa
Operating temperature °C

(b)

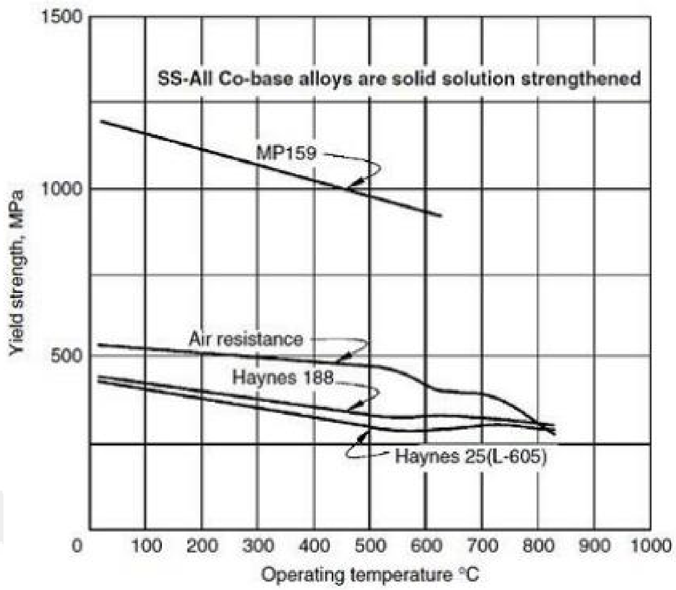

(c)

Figure 2.9: Yield strength of superalloys at various working temperatures a) Iron-based b) Nickel-based c) Cobalt-based [48].

2.3 EFFECT OF HEAT ASSISTANCE ON MACHINING PARAMETERS

The material properties of the superalloys are engineered in a way that they can sustain high strength, corrosion resistance, fatigue life cycle, and creep resistance at elevated temperatures. However, the microstructure developments, hot hardness, and strength result in poor machinability in these materials. This is the main reason that superalloys are categorized as difficult to cut materials. Additionally, the superior properties lead to an increase in the resultant cutting forces and power consumption. Therefore, the high temperature generated during the machining in the cutting zone causes diffusion and build-up edge (BUE) in the cutting tool. Moreover, the low thermal conductivity of the workpiece does not let the appropriate heat dissipation in between the cutting tool and the workpiece. The mentioned issues conclude in accelerated tool wear, low surface quality, and high machining cost. These problems become prominent during the rough machining with a high depth of cut. Pre-heating of the superalloy in specific temperatures can soften the material resulting in an optimal machining process. Hence, it is of great importance to examine the impact of external heat sources on the machining characteristics of superalloys. In this section, the effect of pre-heating in different cutting parameters such as cutting forces, material removal rate (MRR), tool wear, surface quality, and chip morphology are discussed in detail.

2.3.1 Cutting Forces

Although cutting forces have an important impact on the machining performance, it affects the machining center directly. The amount of power, bearing load, tool type, and the machine structure is in correlation with the generated cutting forces during the operation. Additionally, they are indicators of machinability, tool wear, chatter, and operation failure for various workpiece materials. Moreover, cutting forces tend to rise with the material hardness and cutting speed which affects machinability [60] and the tool wear rate [61]. The real-time cutting force measurement is conducted with the strain gauge or more accurately by the means of piezoelectric base dynamometers [62]. However, several researchers have modeled cutting forces analytically before conducting experiments.

Altintas [63] gathered the cutting force models and presented the mechanics of material removal using the 2-D orthogonal cutting model in which the cutting edge is perpendicular to the direction of cutting velocity ( ). Using the model, the 2-D cutting force is decomposed in the velocity and the uncut chip thickness directions as tangential ( ) and feed forces ( ) respectively. Then, the model is used to interpret the more realistic 3-D oblique cutting condition in which the cutting velocity is inclined to the cutting edge with an inclination angle ( ). The inclination angle results in another cutting force component known as radial force ( ).

In addition to the force decomposition, the cutting zone (area in which the tool and workpiece makes a contact and generates the chip) is of essential importance. The cutting zone can be distinguished into three plastically deformed zones as primary, secondary, and tertiary. The primary zone is the area that the tool and workpiece make a contact initially and due to the shearing, the chip formation happens. In the secondary zone, the sheared chip moves along the rake face of the tool. Finally, the tertiary zone is the contact area of the tool and the machined surface.

Furthermore, as an alternative to the orthogonal-oblique cutting mechanics, the mechanistic force estimation method is introduced. In this method, some experiments are carried out to identify tool-workpiece cutting constants [64]. As an example, in 3D oblique cutting, forces are related to the constants as:

$$= \quad h + \tag{2.12}$$

$$= \quad h + \qquad (2.13)$$

$$= \quad h + \qquad (2.14)$$

where, , , and are tangential, feed, and radial cutting constants, , , and are tangential, feed, and radial edge coefficients, is the width of cut, and h is the depth of cut. The mechanistic approach predicts the forces concerning the certain cutting tool and the workpiece material. Therefore, each time that these conditions change, a recalibration of the constants is necessary. In addition to the mechanistic approach, the cutting and edge coefficients can be estimated using the maximum shear stress [65] and minimum energy [66] principles. Finally, by implementing the classical orthogonal to oblique transformation model [67], the cutting and edge coefficients can be estimated analytically and compared with the mechanistic approach. The analytical models and the mechanistic approach try to estimate cutting forces before the operation. Consequently, the desired machine, cutting tool, vibration amplitude, material removal rate, and other characteristics can be predicted for optimal machining. The focus on the heat-assisted application is the possibility of cutting force reduction using material science and the mobility of the setup. Meanwhile, several researchers examined the effect of heat sources on superalloy machining experimentally and reported the impact of cutting conditions on the cutting forces.

Kumar et al. [25] investigated the gas flame heat-assisted turning of Monel-400. An uncoated carbide insert was used as the cutting tool and the workpiece was preheated to 700 °C Additionally, the cutting forces were recorded at each 100 °Ctemperature interval. Figure 2.10 represents the experimental forces at various working temperatures.

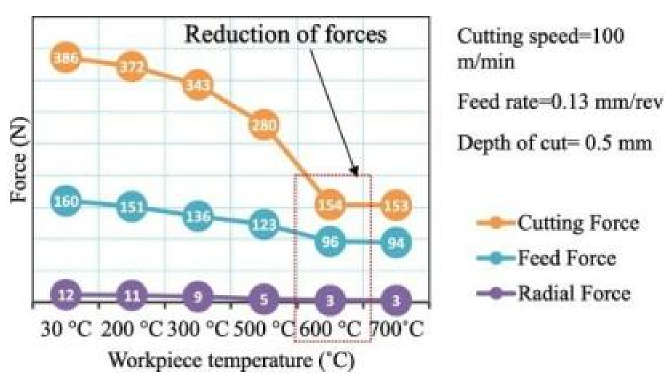

Figure 2.10: Forces generated at various working temperatures [25].

As shown in the figure, the cutting forces in all directions reduce with an increase in the temperature. The rate of the reduction in 600 °Cat tangential, feed, and radial directions are 60, 40, and 75 percentages, respectively. Beyond this point, the cutting tool diffusion, and drastic reduction of the material strength are visible which makes 600 °Cas an optimal cutting temperature of gas flame-assisted turning of Monel-400.

Additionally, the same authors compared the machinability of Nickel-based superalloys of Inconel 625, Inconel 718, and Monel 400 with gas flame-assisted turning. The experiments were performed at 30, 300, and 600 $_{o}$C with the same cutting parameters of the depth of cut, feed rate, and cutting velocity. All the forces in tangential, feed, and radial directions were reduced by an increase in the workpiece temperature, except the radial force in Inconel 625 at 300 $_{o}$C. It should be noted that the HAM of the superalloys with higher tensile strengths such as Inconel 718 and Inconel 625 is more beneficial due to higher force reduction amplitude. Figure 2.11 presents the experimental force measurements of three superalloys at various preheating temperatures [68]. Additionally, a more focused numerical and experimental evaluation of the Inconel 718 turning operation was performed by the same authors. The uncoated carbide inserts were selected as a cutting tool. The simulated results and the experimental data were validated, and a 5% value deviation was reported [26]. Table 2.4 summarizes the numerical and experimental cutting force validation at different preheating temperatures and machining parameters. Although the cutting forces reduce by heating the workpiece, a transient temperature analysis of the workpiece and cutting zone would have given more realistic numerical analysis results.

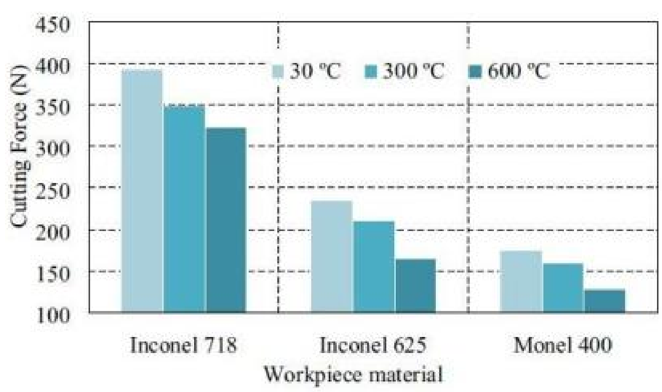

(a)

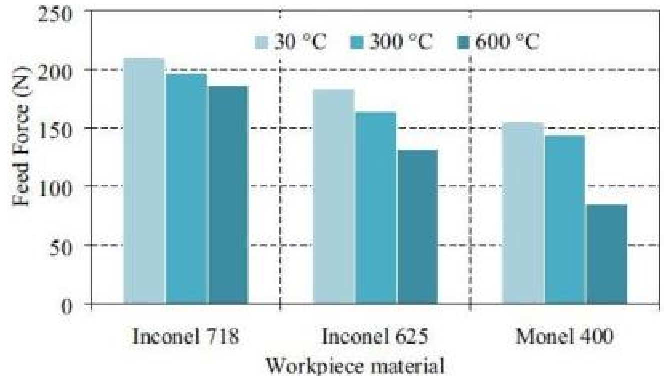

(b)

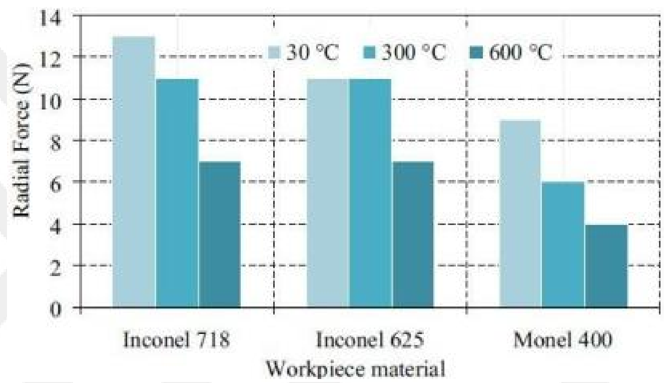

(c)

Figure 2.11: Force measurements of three superalloys at 100 m/min cutting velocity, 0.5 mm depth of cut, and 0.13 mm/rev feed rate a) Tangential cutting force b) Feed cutting force c) Radial cutting force [68].

Table 2.4: Experimental and numerical evaluation of gas flame assisted turning of Inconel 718 [68].

No	Cutting Speed (m/min)	Feed Rate (mm/rev)	Cutting Force (N) Numerical			Cutting Force (N) Experimental			Error %		
			30 oC	300 oC	600 oC	30 oC	300 oC	600 oC	30 oC	300 oC	600 oC
1	66	0.1	329	325	274	268	271	281	1.21	1.09	4.62
2	188	0.1	302	310	265	260	270	270	2.5	1.85	3.7
3	66	1.5	500	508	466	417	470	415	0.09	0.85	0.47
4	188	1.5	450	439	396	389	400	395	2.44	1	1.51

In addition to the gas flame-assisted machining, some researchers investigated the effect of induction-assisted machining on the cutting force behavior of superalloys. Choi et al. [69]

investigated the milling operation as ramping and contouring in the cone-shaped Inconel 718 workpiece. The experiment was carried out on a 5-axis CNC machine, using an 8mm diameter carbide endmill. Additionally, the induction coil was fixed to the spindle head with an arrangement that provided a 2mm constant distance from the workpiece surface. Moreover, in between the cutting tool and the induction coil, a 5mm distance was designed to avoid direct heat exposure. Figure 2.12 demonstrates the schematic of the heat assistance setup.

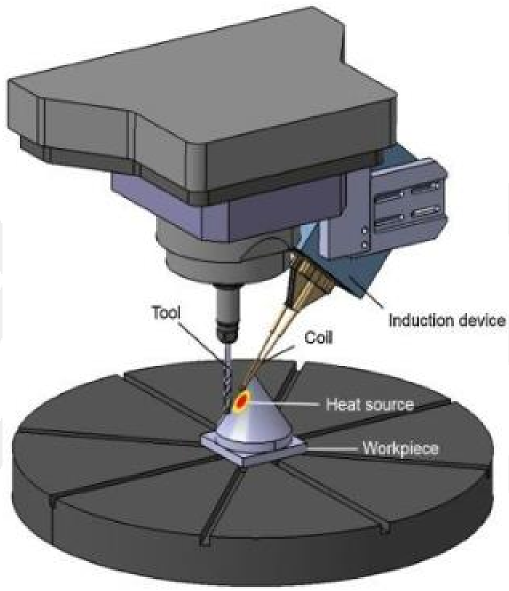

Figure 2.12: Schematic of induction assisted machining on circular cone shape workpiece [69].

The induction power and frequency were adjusted in a way that the workpiece surface became 900 °C at a maximum which is below the recrystallization temperature of Inconel 718. The cutting forces of induction-assisted machining (IAM) were measured and compared with the conventional machining (CM) for ramping and contouring operations. Figure 2.13 shows the cutting force comparison at various feed rates. The highest cutting force reduction percentage occurred at a low feed rate (50 mm/min) by 34.3% for ramping and 29.2% for contouring operations. The reason is related to the necessary preheating time of Inconel 718. As the feed rate increases, the low conductivity of the workpiece material does not provide sufficient time for the heating of the cutting zone. Additionally, Baek et al. [70] did the same procedure for slot milling of the Inconel 718 at higher feed rates. The authors utilized a hybrid method by combining the induction with laser assistance. Using the hybrid method of induction and laser assistance, the cutting forces were reduced even more by approximately 67% compared to conventional machining. Figure 2.14 represents the schematic of the hybrid heat-assisted machining approach.

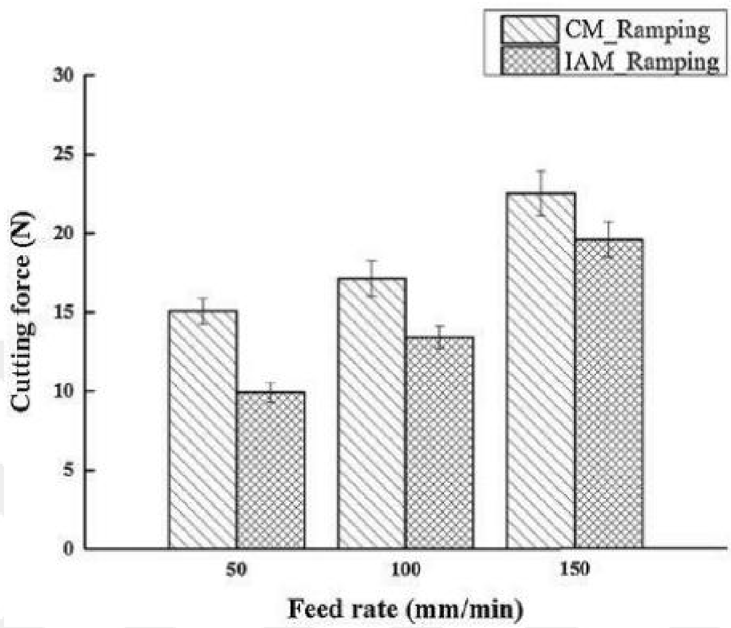

(a)

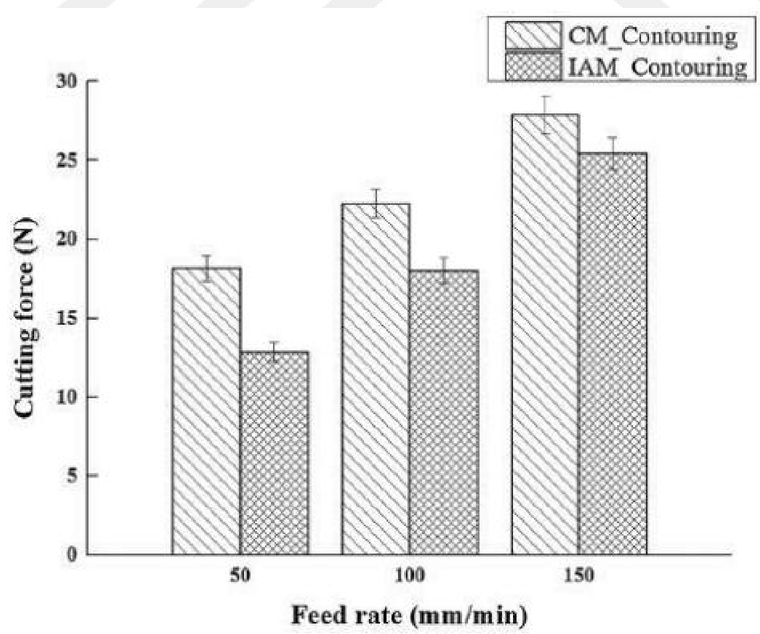

(b)

Figure 2.13: Cutting forces at 3000 rpm spindle speed at 0.5 mm depth of cut for Inconel 718 at various feed rates. a) ramping b) contouring [69].

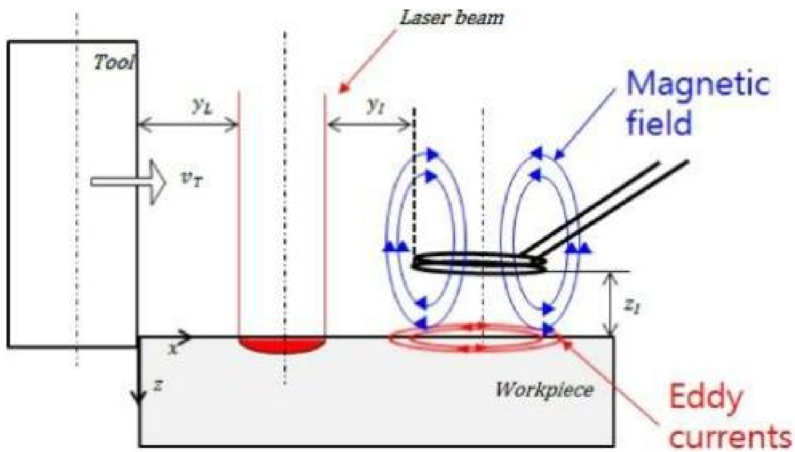

Figure 2.14: Schematic of the hybrid system [70].

Similarly, Ha et al. [29] utilized a hybrid method of induction and laser assistance. Experiments were classified into two main heating approaches. In the first method, the induction heat source was preceded by a laser (Method 1), and in the second the laser heat source was preceded by an induction (Method 2). Figure 2.15 represents the comparison of the cutting forces in method 1, method 2, Induction Assisted Machining (IAM), and Laser Assisted Machining (LAM) at three specific feed rates. As shown in the figure, using method 1, the cutting forces became least at each specific feed rate. Additionally, in all these feed rates, hybrid methods generated fewer cutting forces compared to the single preheating approaches.

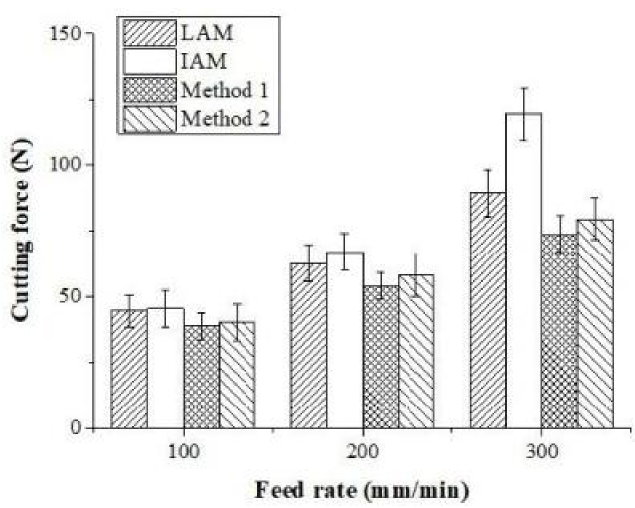

Figure 2.15: Cutting force measurement of Inconel 718 using four different pre-heating approaches [29].

Laser-assisted machining (LAM) is among the most known heat-assisted machining approaches due to its controlled localized heat source. It can decrease the magnitude of cutting forces and tool wear [71]. Furthermore, the preheating method and temperature affect the machining efficiency significantly [72]. Several researchers investigated the effect of a laser beam on the cutting force reduction in superalloy machining. Kong et al. [73] investigated the cutting performance of K24 (Nickel-based superalloy) in laser-assisted milling. A 500 W Nd-YAG laser with a 60° mount angle, ahead of the cutting tool, was placed. The spot diameter of the 6 Degree of Freedom (DOF) laser nozzle was kept constant as 3mm and at different cutting velocities and feed rates, cutting forces were measured using a piezoelectric dynamometer. Additionally, the workpiece material was coated with graphite initially to increase the laser heat absorption. The elevated temperature at the cutting zone caused a reduction in all components of the cutting forces. Figure 16 illustrates the effect of preheating temperatures on the various cutting force components. The laser heat source results in a temperature increase in the primary shear zone which reduces the flow stress (plastic deformation stress) of the workpiece. Whereas, in conventional machining, the compressive stress field in between the tool and workpiece promotes higher cutting forces. Using the laser assistance, the tangential, feed, and radial forces were reduced by 63 %, 32%, and 71%, respectively at 600°Cpreheating temperature.

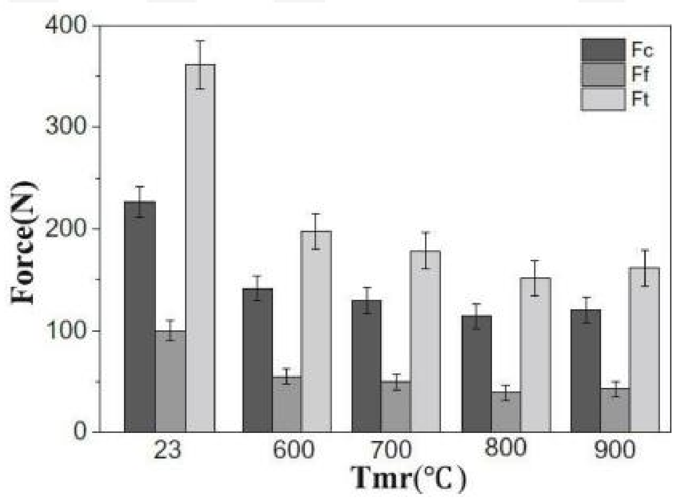

Figure 2.16: Experimental force component measurement for various preheating temperatures at 30 m/min cutting velocity, 0.1 mm/tooth feed rate, and 0.2 mm depth of cut [73].

Ding et al. [74] investigated the machinability of Nickel-based superalloy AMS 5704-Waspaloy with laser-assisted turning. A series of tests at various cutting speeds (1-3 m/s), feed rates (0.075 and 0.1 mm/rev), and preheating temperatures (20, 300, 400, and 500 $_{o}$C) were performed. The depth of cut was kept constant as 0.76 mm and a ceramic cutting insert was utilized. For this specific superalloy, it was claimed that the 400℃ preheating temperature showed the optimal cutting force reduction percentage as 20% compared to the conventional turning operation. Higher temperatures did not improve the cutting force reduction and the tool life of the turning operation.

Venkatesan et al. [75] studied the effect of various laser power and cutting parameters in turning Inconel 718. The authors claimed that the cutting force reduction with laser assistance occurs in cutting velocities below 60m/min. Additionally, as the feed rate increases, the cutting force reduction percentage with laser assistance reduces. As a solution to this problem higher power laser nozzles are suggested (1300 W). Similarly, Wu et al. [76] investigated the milling of Inconel 718 under the influence of laser heating using simulated and experimental results. The numerical heat-assisted cutting forces and experimental results were validated in the milling operation and a 15% force estimation error was observed. Additionally, a force reduction percentage of 23-45% was measured at preheating temperatures of 400-700 °C. Figure 2.17 demonstrates the numerical and experimental cutting forces at various preheating temperatures.

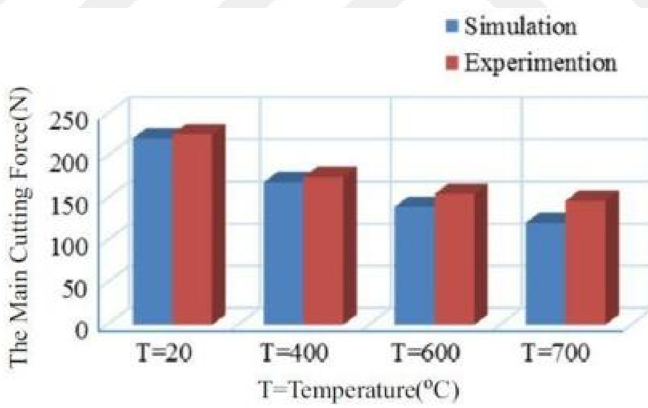

Figure 2.17: Simulated and Experimental cutting forces at various temperatures. = 60 / , = 0.05 / , depth of cut = 0.5mm [76].

Plasma-assisted machining (PAM) is an alternative to the LAM method. Several researchers investigated the effect of PAM on superalloys and claimed that for some specific cutting velocities, the process demonstrates lower cutting forces and for others, higher cutting forces compared to LAM. Additionally, in both methods, the cutting force reduction is observed. Moon et al. [40] investigated the cutting forces of Inconel 718 with PAM at various spindle speeds as 6000, 7000, and 8000 rpm with a constant feed rate (100mm/min) and depth of cut (0.3mm). At these incremental spindle speeds, the cutting forces were reduced by 42%, 43%, and 57% compared to conventional dry machining. Additionally, at the spindle speeds of 6000 and 8000 rpm, the cutting force reduction percentage was similar for both PAM and LAM. Whereas, at 7000 rpm spindle speed, LAM demonstrated a higher cutting force reduction percentage. Similarly, Chen et al. [41] discussed the effect of cutting speed, feed rate, and depth of cut on the tangential cutting forces of Inconel 718 turning operation using plasma assistance. As shown in Figure 2.18, at various cutting conditions, the tangential cutting forces reduce using the plasma preheating technique.

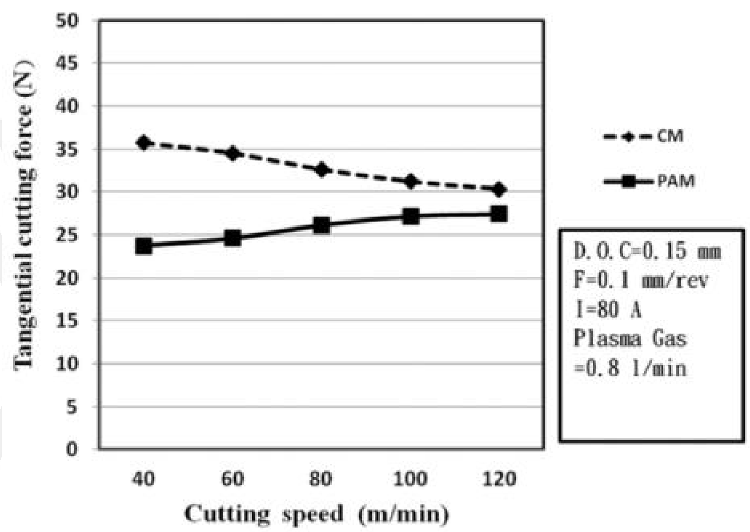

(a)

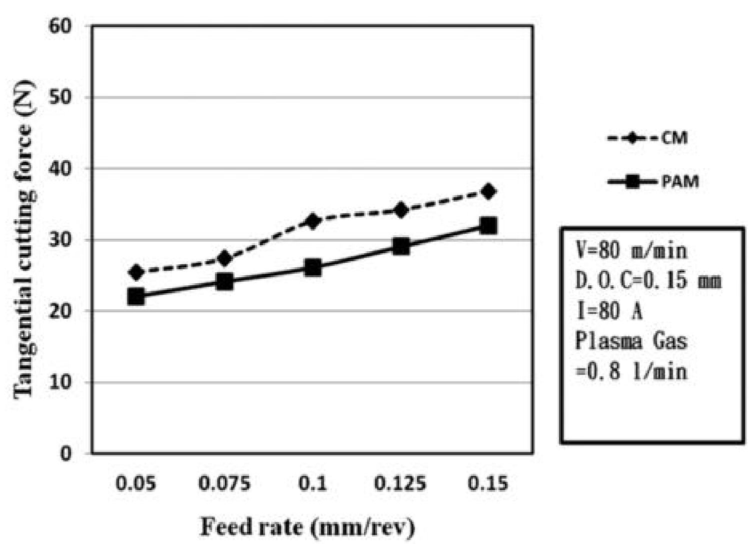

(b)

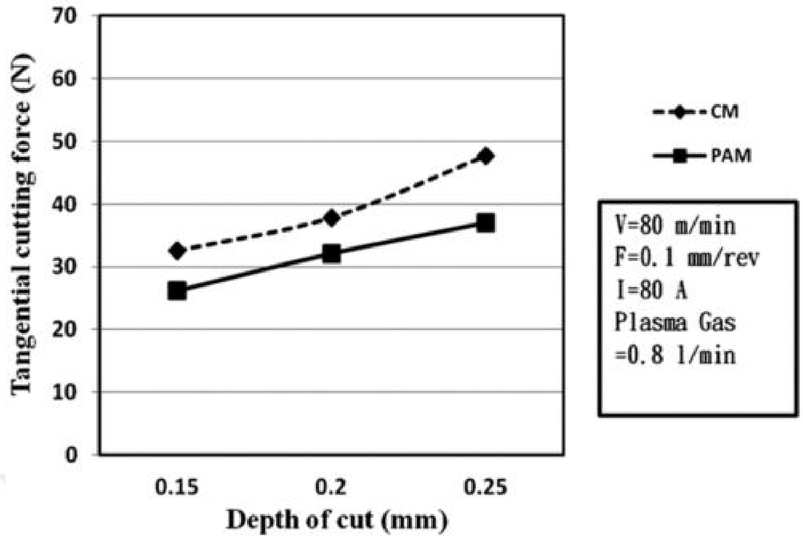

(c)

Figure 2.18: Tangential Cutting forces at constant plasma arc intensities. a) various cutting speeds b) various feed rates c) Various depth of cuts [41].

Lacalle et al. [44] studied the Plasma assisted milling of Cobalt-based superalloy (Haynes 25). Using the PAM, the tangential cutting force reduced as a function of plasma arc intensity. However, as the power supply current for the plasma generation increased (more than 60A), weld beads appear on the workpiece surface. Therefore, the power supply current was limited to 60A at maximum. Table 2.5 shows the tangential cutting force reduction percentages at various arc intensities.

Table 2.5 Tangential cutting force reduction as a function of the plasma intensity [44]

Arc Intensity (A)	Reduction of F_t (%)
30	21.56
40	21.60
50	21.52
60	28.70
70	Weld bead

2.3.2 Tool Wear

The cutting tool should possess specific characteristics such as hot hardness, toughness, chemical stability, and acceptable wear resistance to the workpiece material. Therefore, the selection of the proper cutting tool and excelling the tool life results in an economically acceptable machining operation with better surface quality. Additionally, the tool wear mechanisms help to better understand the dynamics of cutting operations. Generally, during the machining, tool wear does not form with a single mechanism. A combination of wear mechanisms pursues the tool life reduction. Typical tool wear mechanisms are categorized as abrasion, adhesion, diffusion, fatigue, and corrosion (oxidation).

Abrasive wear is caused by the friction between the chips and the cutting tool contact surface. The hard chip particles press into the friction interface under the cutting loads and while sliding over the cutting tool, the groove-shaped indentation occurs by the abrasive plowing. Additionally, excessive heat and cutting pressure promote the tool wear resulting in worn flank/rake surfaces in the cutting tool. Therefore, the hot hardness properties of the cutting tool play an important role in the tool life promotion. Moreover, in these harsh conditions, some of the chip particles adhere to the fresh flank/rake surfaces of the cutting tool. The relative motion of adhesive particles on these two friction surfaces causes a wear type which is called adhesive wear. The build-up edges in the cutting tools are mainly related to this wear mechanism.

The diffusion mechanism happens when the necessary activation energy for the atom motion is provided in the cutting zone. The atoms in the crystal lattice tend to migrate from the high concentration region to the low concentration zone. This results in an atom motion within the cutting tool to the chips or workpiece and worn tool surfaces.

The fatigue wear occurs due to the cyclic loads generated between the tool and workpiece. In the contact zone, the microscopic roughness of the tool and workpiece results in cyclic cutting stress. The fatigue wear mechanism mainly promotes the other wear mechanisms by generating microscopic surface cracks within the cutting tool surface. Likewise, the edge chipping mechanism usually appears due to high shear stresses in the vicinity of the cutting tip. At high cutting zone temperatures, the corresponding stresses lead to ductile behavior and cutting tool failure.

Finally, the excessive temperature and existence of the air and Oxygen generate a suitable environment for oxidation wear. Therefore, layer by layer corrosion of the cutting tool weakens the cutting edge. Hence, the chemical stability of the cutting tool concerning the environmental circumstances affects the tool's life expectancy. As discussed in section 2.2, superalloys are engineered to sustain their strength at high temperatures. Therefore, compared to conventional materials, excessive shear, and friction stresses during the machining result in higher rates of flank, crater, and notch wears. Mainly, abrasion wear combined with the adhesion of the superalloy particles and diffusion of the cutting tool atoms to the workpiece surface promotes the cutting tool wear. In this section, similar to the cutting force evaluation strategy, the effect of superalloy workpiece preheating techniques on the tool life is explored.

Kumar et al. [68] investigated the machinability and tool life variation of the common superalloys as Inconel 718, Inconel 625, and Monel 400 under the influence of gas flame-assisted preheating for turning operation. The operation was performed Using coated Kennametal SNMG square carbide cutting inserts. Authors concluded that higher tool life especially for Inconel 625 with 238% improvement is achieved compared to the conventional machining procedure. Figure 2.19 represents the experimental evaluation of the tool life at various pre-heating temperatures.

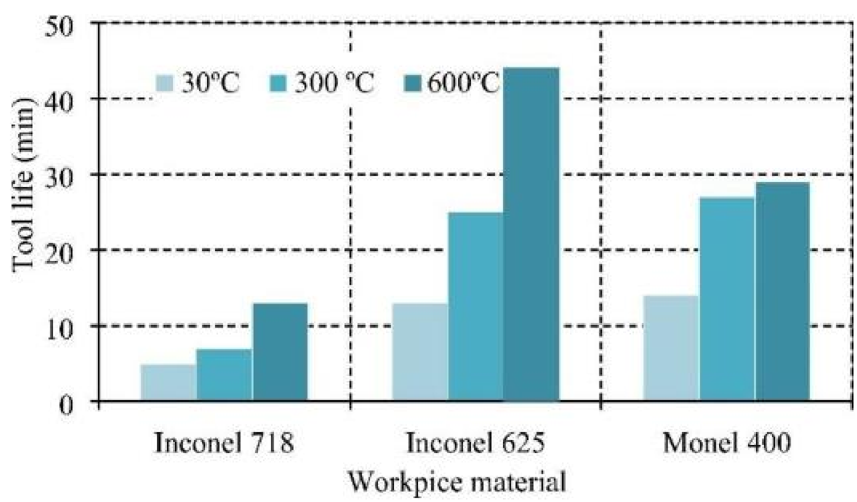

Figure 2.19: Effect of preheating temperature on the tool life of superalloys using the gas flame heating method at $V_c = 100$ m/min, f= 0.13 mm/rev, and 0.5 mm depth of cut [68].

Additionally, the authors investigated the major tool wear mechanisms in these superalloys. The permanent wear mechanisms are diffusion wear in Inconel 718, notch wear in Inconel 625, and a combination of abrasion/adhesion in Monel 400 [68].

Similarly, the same authors in another approach focused on the machinability of Monel 400 with uncoated carbide inserts at different depths of cut, cutting speeds, feed rates, and preheating temperatures using the gas flame technique [25]. The experiments showed that at a specific preheating temperature, as the cutting speed, depth of cut, and feed rate increases the tool life reduces. However, by an increase in the preheating temperature, the tool life improves in a way that compensates for the effect of these parameters. As an example, at 600 $_{o}$C preheating temperature with 100 m/min cutting velocity, the tool life is slightly higher than 30 $_{o}$C workpiece temperature with 40 m/min cutting velocity. Figure 2.20 represents the effect of cutting velocity, depth of cut, and feed rate on the tool life at various preheating temperatures of the Monel400 workpiece in turning operation.

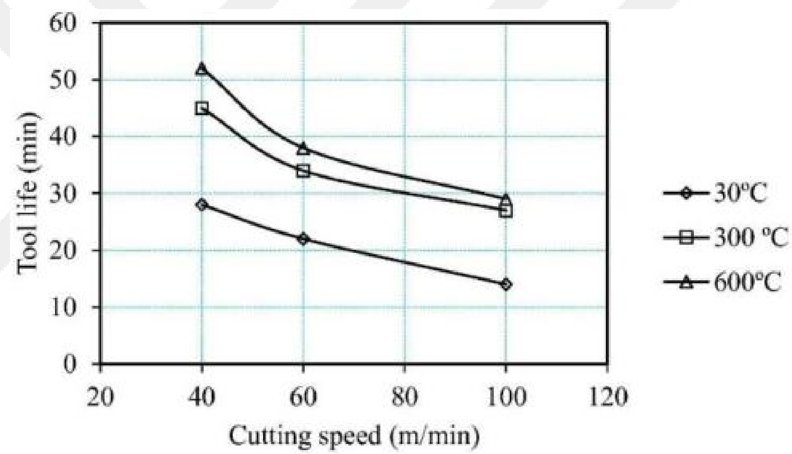

(a)

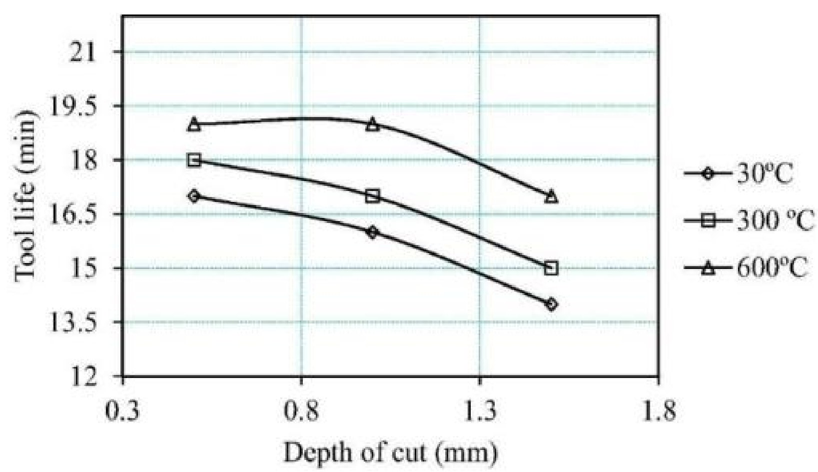

(b)

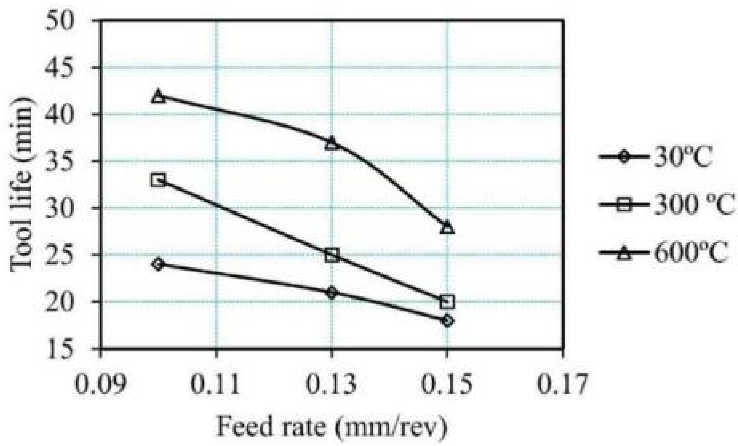

(c)

Figure 2.20: Tool life behavior at various preheating temperatures of Monel 400 a) effect of cutting speed b) effect of depth of cut c) effect of feed rate [25].

As discussed earlier, the gas flame technique is a cheap and simple method of preheating. However, due to the explosive nature of the fuel and chemical instability of the workpiece surface, other preheating techniques are utilized especially in CNC machines. For materials with magnetic properties, induction heating is preferred due to its fast and localized heat capabilities. Similarly, some researchers explored the cutting tool life improvements in superalloys using this technique. Amin et al. [77] performed the end milling of Inconel 718 using TiAlN coated carbide inserts. The cutting zone was preheated to a constant temperature of 420 $_{o}$C (PH) and a constant axial depth of cut of 0.57mm. Additionally, the tool life was evaluated with the same cutting parameters at room temperature (RT). Six trials were carried out in which at the first three, the feed rate was constant as 0.07 mm/tooth and cutting velocity varied from 16 to 50 m/min, in the second three, the cutting speed was constant as 28 m/min and the feed rates were varying from 0.03 to 0.16 mm/tooth. the tool life increased for all cases using the preheating method. Lowest feed rate (0.03 mm/tooth) and moderate cutting velocity (28 m/min) demonstrated the highest tool life improvement with an increase of 83% (trial 4).

Kim et al. [31] investigated the optimized machining parameters for induction-assisted milling of Inconel 718 using AlTiN+HH (High Heat special coating) coated and uncoated carbide cutting tools. From the tool wear perspective, the authors focused on the effect of coating durability with induction assistance. The diffusion wear was more significant in the uncoated endmill since only a small portion of the generated heat in the cutting zone was transferred to the chip/workpiece regions and most of the heat was encapsulated in the cutting tool. Additionally, the uncoated tool was more affected by the induction heat source. However, using the AlTiN+HH coated carbide tool, the heat generated in the cutting zone was transferred to the workpiece more than to the cutting tool due to the thermal properties of the coating material. Hence, the thermal-related wear of the coated tool was relatively insignificant. Figure 2.21 represents the worn surfaces of the coated and uncoated endmills in induction-assisted milling of Inconel 718 [31].

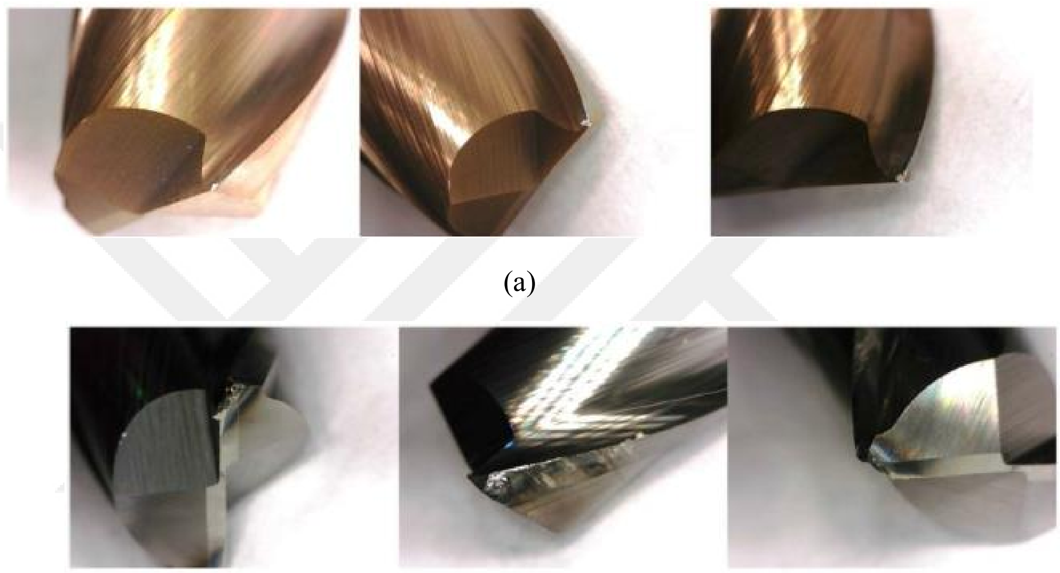

(a)

(b)

Figure 2.21: visual inspection of tool wear in induction assisted milling of Inconel 718 at 10000 rpm spindle speed, 100 mm/min feed rate, and 0.25 mm depth of cut a) AlTiN+HH coated end mill b) Uncoated end mill [31].

Although induction-assisted machining shows promising results by lowering cutting forces and increasing the tool life, in some cases, it is reported that due to the excessive workpiece temperature in bigger cutting zones, the process can have reverse effects. Therefore, some researchers developed a hybrid process of induction and laser assistance to explore the possible tool life improvements. Beak et al. [70] studied the milling characteristics of Inconel 718 under the influence of induction and laser-induction machining using a carbide cutting tool. While keeping the feed rate constant at 120 mm/min, three experiments were carried out at 3000, 5000, and 7000 rpm spindle speed and 0.1, 0.3, and 0.5mm depth of cut, respectively. Additionally, the workpiece preheating temperature for both operations was 900 $_{o}$C. The maximum tool wear of conventional, induction assisted, and induction-laser assisted were 0.288, 0.341, and 0.255 mm, respectively.

While induction-assisted machining demonstrated larger tool wear compared to conventional machining, the wear points were less. Overall, laser-induction assisted machining demonstrated the least tool wear among them all [70]. Figure 2.22 represents the tool wear and surface roughness behavior of these operations.

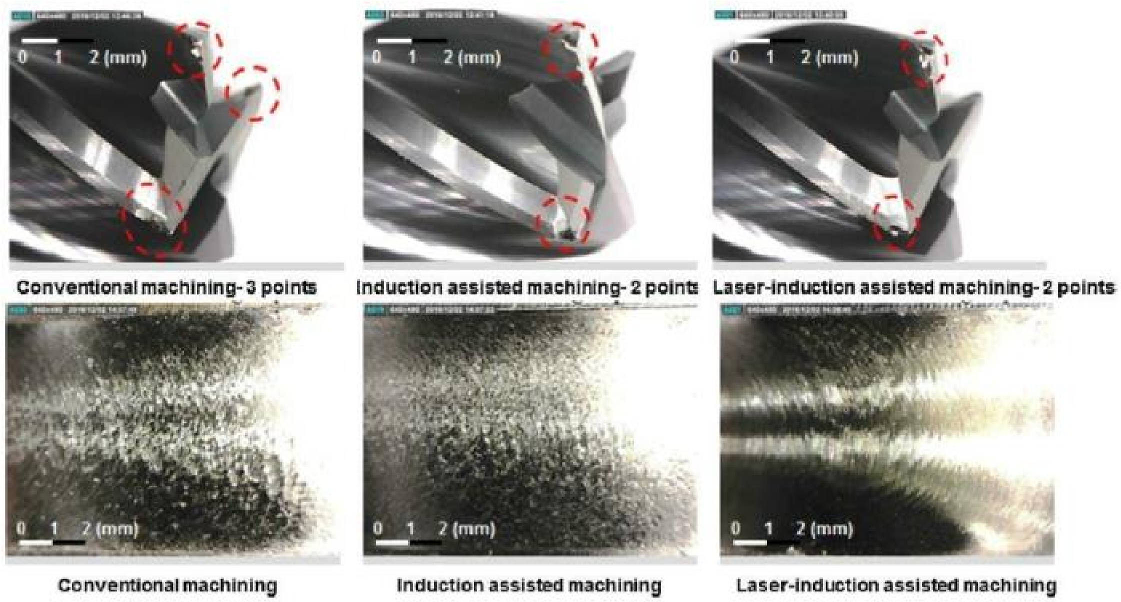

Figure 2.22: Tool wear and machined surface texture of Inconel 718 at 5000 rpm spindle speed, 1.2 mm depth of cut, and 120mm/min feed rate [78].

Kong et al. [73] focused on the wear mechanism of coated tungsten carbide (WC) tool in the laser-assisted milling of K24 (Nickel-based) superalloy. Three different types of coated WC tools denoted A, B, and C were utilized. Tool A was consisting of a single layer (TiAlN) Physical Vapor Deposition (PVD) coated, whereas tool B was a triple layer ($TiCN/Al_2O_3/TiN$) Chemical Vapor Deposition (CVD) coated WC tool. Finally, tool C consisted of a single-layered (TiCN) PVD-coated surface. Using laser-assisted machining, the tool life was increased by approximately 46% compared to conventional machining. Additionally, the laser heat source caused a difference in the wear behavior of these cutting tools compared to conventional machining. To better understand and interpret the differences, the wear behavior of the cutting tools was categorized in three distinguished stages as the initial stage with fast wear growth, a steady stage with linear wear growth, and a final stage of rapid wear growth. At each stage, the effect of coating and the major wear mechanisms were evaluated. Tool A (TiAlN) represented the highest wear resistance among others at the average cutting velocity (30 m/min) [73].

Although workpiece pre-heating by the means of laser reduces the shear strength of the material and the required cutting forces, the amount of laser power and cutting tool material from the thermal properties' perspective plays an important role in the tool life performance. Brecher et al. [79] investigated the milling of Inconel 718 using TiAlN-coated cemented carbide cutting tool. The flank wear of the inserts at various laser powers with 1000 mm^3 chip volume was recorded. Figure 2.23 represents the experimental results of the flank wear at various laser powers. The 1540 W laser power shows the most optimized results considering the tool wear and cutting force reduction percentage. As the laser power increases, the tool wear becomes more significant due to higher thermal edge wear.

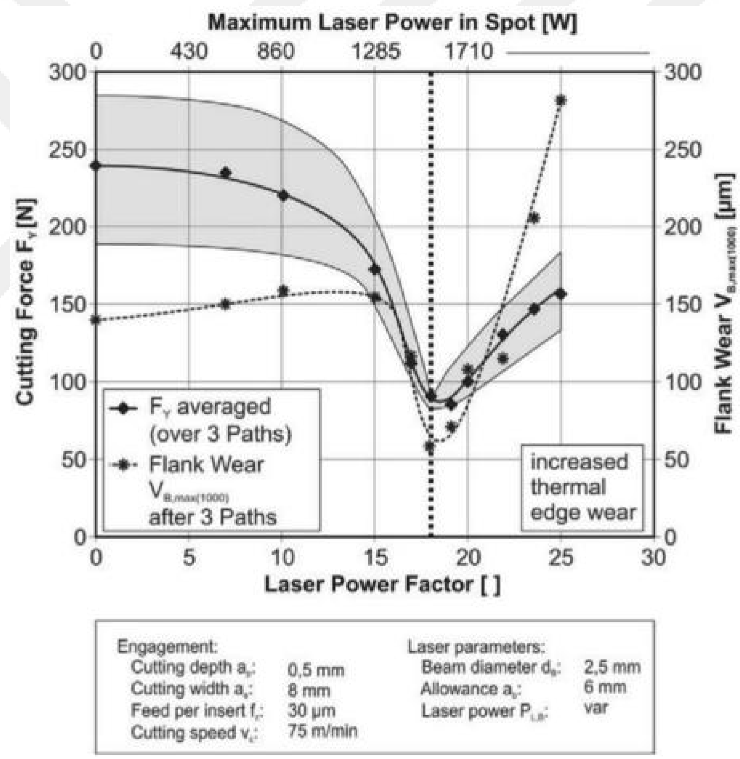

Figure 2.23: Flank wear and cutting forces at various laser power in Inconel 718 milling [79].

In addition to the laser assistance, some researchers investigated the tool wear performance of the plasma-assisted machining. Leshock et al. [80] experimentally validated the modeling of the plasma-enhanced turning of Inconel 718. Experiments were carried out at various cutting speeds (2-6.5 m/s) and workpiece preheating temperatures (20-700 ^oC) using WG-300 cutting inserts (Aluminum oxide reinforced with Silicon carbide whiskers). In conventional turning, the deep notching is the main reason for the tool failure. However, the introduction of plasma heating virtually eliminated this failure mechanism, thus elongating tool life [80], [81].

Lacalle et al. [44] investigated the milling of the Haynes 25 and Inconel 718 under plasma assistance. A TiAlN coated tungsten carbide end mill was used for Haynes 25 milling and a ceramic insert (Aluminum oxide ceramic with Silicon carbide whiskers) was used for Inconel 718. In both materials, plasma assistance leads to a reduction in tool wear compared to conventional milling. For the Haynes 25 milling, the flank wear was reduced from 0.5 mm to 0.1 mm at a cutting speed of 70 m/min, 110 A of plasma intensity, and 500 mm of cutting length. For the Inconel 718 milling, the flank wear of 0.4 mm happened in 17 seconds for conventional machining and the same wear happened twice the period (34 seconds) by plasma assistance [44]. Figure 2.24 represents the effect of plasma assistance at various machining lengths of Inconel 718. Although the plasma assistance reduces the amount of tool wear, the high machine cost and energy consumption make it less appealing compared to the other methods.

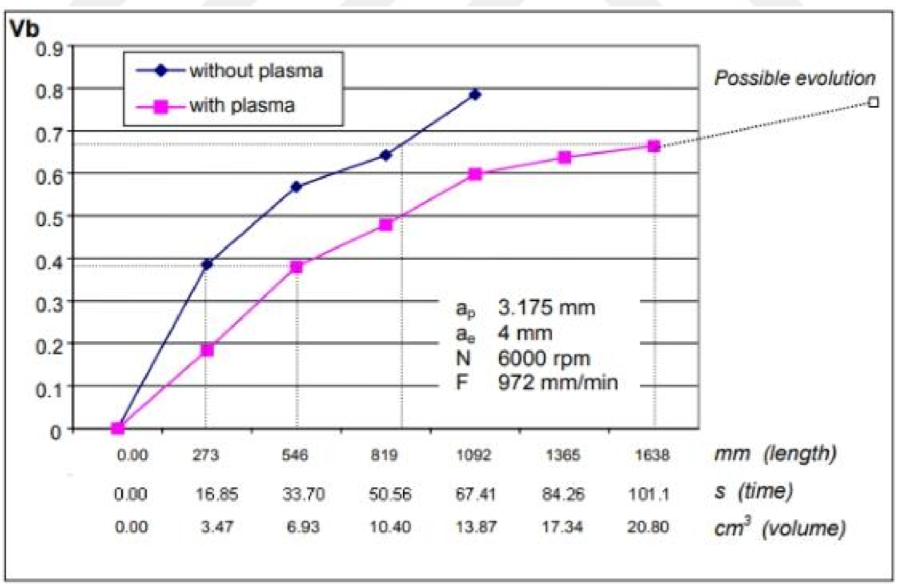

Figure 2.24: Effect of plasma assistance in increasing the machining length and reducing the tool flank wear [44].

2.3.3 Surface Quality and Chip Morphology

The surface integrity, texture, and roughness are in direct relation with the machining parameters such as cutting velocity, feed rate, depth of cut, and tool nose radius. Moreover, the surface topology of the workpiece affects its mechanical properties (residual stresses, fatigue performance, hardness, etc.) and frictional performance (static and dynamic friction coefficients, wear resistance, contact area, etc.). Therefore, the optimum surface finish of the workpiece can guarantee the durability and accuracy of the part with possibly fewer costs [82]. In the aerospace industry and especially in superalloy machining, the workpiece needs to be manufactured with high levels of dimensional accuracy and finished surface quality to satisfy its functionality criteria [83]. Residual stresses, cracks, and metallurgical alterations of the workpiece while machining affect the surface quality drastically [84]–[86]. Additionally, it was shown that during the dry machining of superalloys (Inconel 718), the cutting speed variation did not affect the surface roughness of the workpiece. However, the feed rate and tool nose radius are the more dominant factors influencing surface quality. An increase in the amount of the cutting load and the tool contact zone temperature results in severe plastic deformation and consequently higher surface roughness [87]. Moreover, it has been shown that in conventional dry turning of Inconel 718, a combination of large cutting speed and low feed rate results in the optimum surface quality of the machined workpiece [88]. On the other hand, when external heat is introduced to the workpiece, the shear strength and dynamics of the machining alters. In addition, a study on the shape, size, geometry, and microstructure of the produced chips during the machining process provides a series of useful information on the cutting zone dynamics and characteristics of the machining. The morphology of chips is characterized mainly by the operation method (such as milling, turning, boring, etc.), machining parameters (speed, feed rate, depth of cut), cutting tool and workpiece properties (strength, hardness, brittleness, etc.) [11], [89]. Meanwhile, continuous chips are not desired in the operation from the safety perspective [90]. Therefore, chip breakers are utilized to divide the chip's length into smaller dimensions. Additionally, the amount of heat generated in the cutting zone, chip cooling rate, thermal softening, and strain hardening of the workpiece are in direct correlation with the chip morphology [91]. As demonstrated by several researchers, an increase in the feed rate and cutting velocity results in a larger helical gap between the chip serrated ribbons. On the other hand, a cutting operation with a lower depth of cut consequence in a shorter gap amplitude between the ribbons. As a result, chip morphology can interpret the dynamics of the cutting process [92]. In this section, an overview of the superalloy's surface integrity and chip morphology will be investigated regarding the effect of various heat assistance techniques.

Kumar et al. [68] examined the effect of heat assistance using the gas flame while machining Inconel 625, Inconel 718, and Monel 400 at similar machining conditions (100 m/min cutting velocity, 0.13 mm/rev feed rate, and 0.5 mm depth of cut). Figure 2.25 represents the average surface roughness of the machined workpieces at various preheated temperatures. The surface roughness of all workpieces reduces as the preheating temperature rises with the highest reduction of 50% in Monel 400 at 600 $_{o}$C. Additionally, the authors reported that the chip morphology of these materials started to demonstrate distinctive characteristics as the preheating temperature rises.

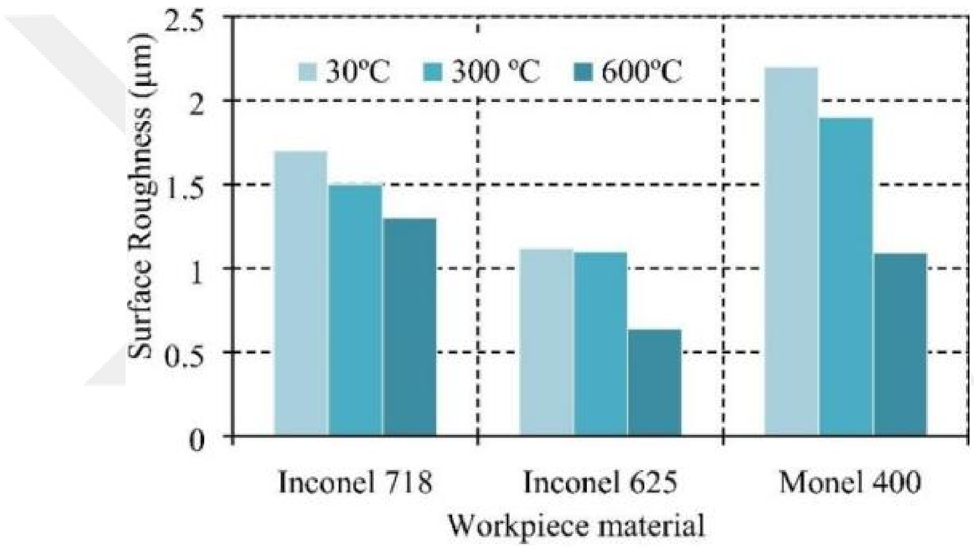

Figure 2.25: Surface roughness evaluation of superalloys at various pre-heating temperatures using the gas flame heating method [68].

Although all the superalloy workpieces had helical and discontinuous chips at room temperature, Monel 400 turning operation generated non-spiral continuous chips, Inconel 718 resulted in a continuous and spiral chip, and Inconel 625 machining demonstrated smaller discontinuous chips with spiral geometry at elevated temperatures.

Choi et al. [69] examined the effect of preheating temperature (900 $_{o}$C) on the surface roughness of Inconel 718 using induction-assisted heating. The surface roughness was improved for both operations as the high temperature was applied. Figure 2.26 demonstrates the surface roughness values for these operations at various feed rates. The highest improvement occurred at a feed rate of 50 mm/min with 45.2% for ramping operation and 39.7% for the contouring operation. In both operations, as the feed rate increased the amount of improvement in the surface roughness reduced.

The reason for the surface roughness improvement is laying behind the reduction of cutting resistance and vibration amplitude during the operation.

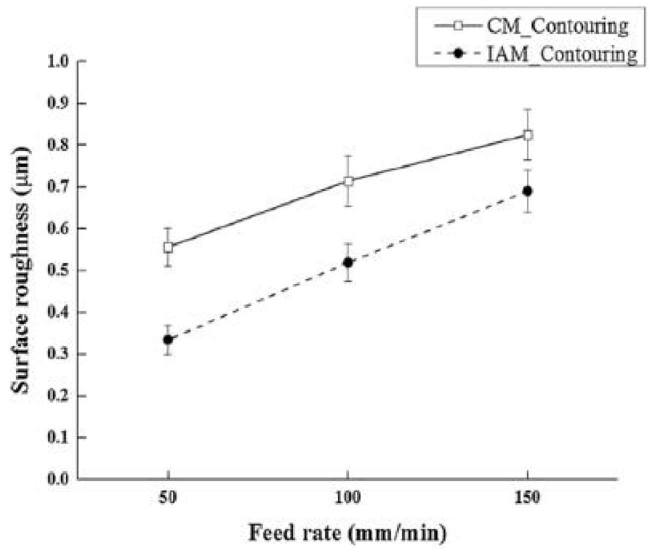

(a)

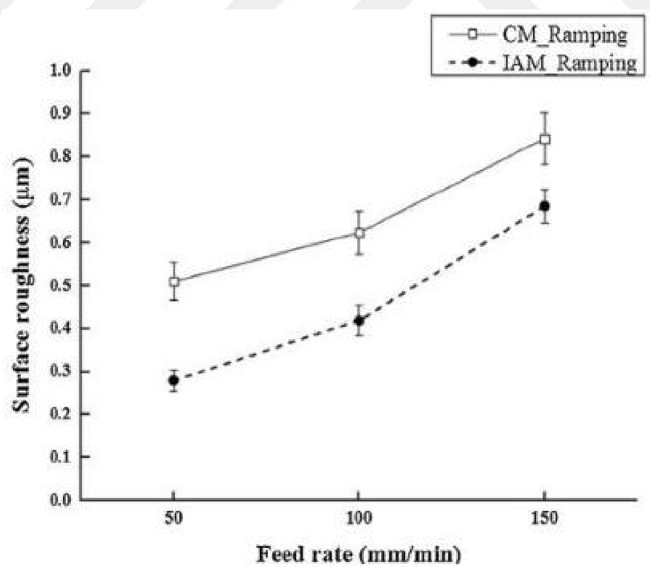

(b)

Figure 2.26: Experimental surface roughness values of Inconel 718 machining using induction assistance with 900°Cpreheating temperature at various feed rates. a) Contouring b) ramping [69].

In addition to induction assistance, some researchers investigated the effect of laser power on the surface quality of the machined superalloys. Germain et al. [93] examined the effect of laser power on the surface quality (roughness) of Inconel 718 using carbide and ceramic inserts. The arithmetic average surface roughness (R_a), peak surface roughness (R_{max}), and the average height peak/valley (R_z) were measured at various laser powers. Figure 2.27 represents the effect of laser power on the surface quality of the workpiece using carbide inserts and similarly, Figure 2.28 explores the effect of the laser assistance on average surface roughness using ceramic cutting inserts. As shown in the figures, the laser assistance does not have a significant effect on the surface roughness improvement while using the carbide tools. However, when ceramic cutting tools are utilized the surface quality becomes better as the cutting length increases.

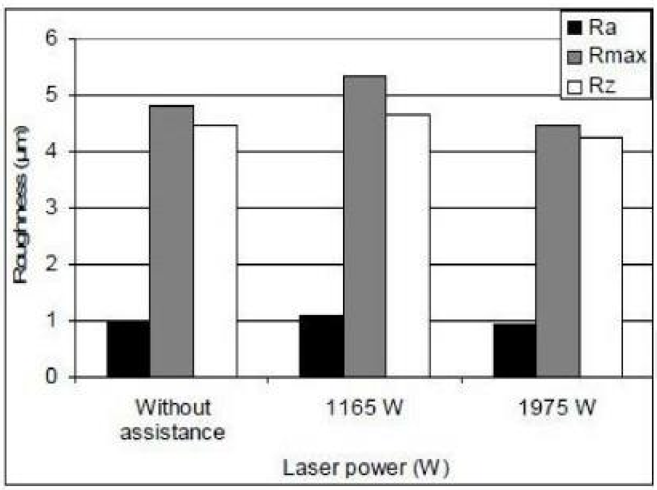

Figure 2.27: Surface roughness using carbide insert [93].

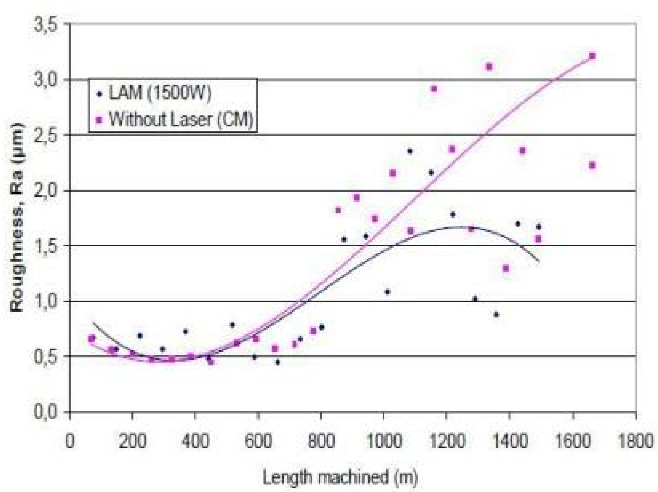

Fi Figure 2.28: Surface roughness using ceramic insert [93].

In addition to the surface quality, alteration of the chip morphology with laser assistance provides an insight into the impact of external heat sources on the characteristics of the machining. Tadavani et al. [36] compared the chip morphology in conventional and pulsed assisted laser turning of Inconel 718. Although, the cutting conditions were exact (15 m/min cutting velocity and 0.052 mm/rev feed rate) in both operations, the color and geometry of generated chips were inequivalent. In conventional turning, chips were silver in color, curly, and semi-continuous. Additionally, severe plastic deformation was observed on the chip edge, and in the middle of the chip, uniform plastic deformation was recorded. However, with laser assistance, chips were more curved, continuous, and brown. Additionally, uniform chip deformation occurred in most of the chips. The main reason for the color and shape difference was related to the presence of radiation and localized heating using Laser. Moreover, due to the relevant relation of the chip formation, temperature, and shear bands in laser assistance, chips demonstrate continuous geometry with uniform plastic deformation. Figure 2.29 represents the chip morphology of conventional and laser assistant turning of Inconel 718.

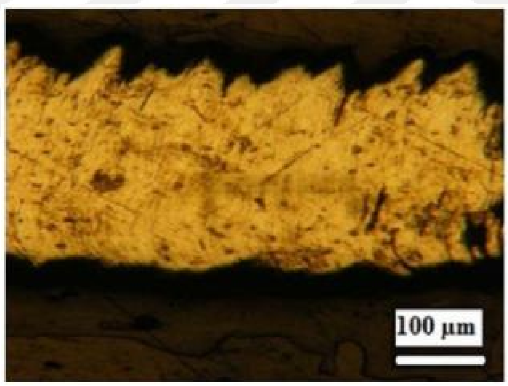

(a)

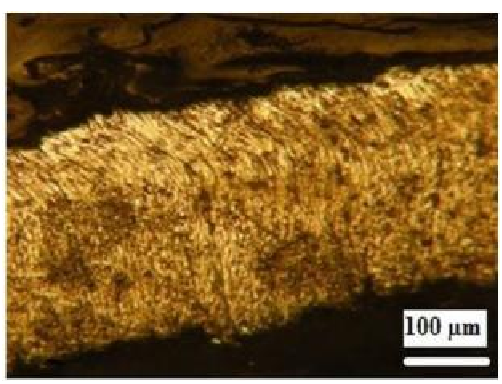

(b)

Figure 2.29: Chip morphology of Inconel 718 turning a) Conventional machining b)Laser assistant machining [36].

Similar to the laser assistance, the effect of the plasma-assisted machining on the surface roughness was investigated. Leshock et al. [94] modeled the temperature distribution of Inconel 718 plasma-assisted turning and validated the results with the experimental values. Experiments were carried out at various workpiece preheating temperatures (20-700 oC), cutting speeds (2- 6.5 m/s), and a constant depth of cut of 0.83mm with 0.124 mm/rev feed rate. It was reported that a significant improvement in surface roughness was achieved when the workpiece was heated to 500 oC. However, above 530 oC, surface oxidation occurred which caused higher surface roughness. Additionally, the authors claimed that it is possible to minimize surface oxidation by proper optimization of plasma parameters. Figure 2.30 shows the average surface roughness at various workpiece preheating temperatures.

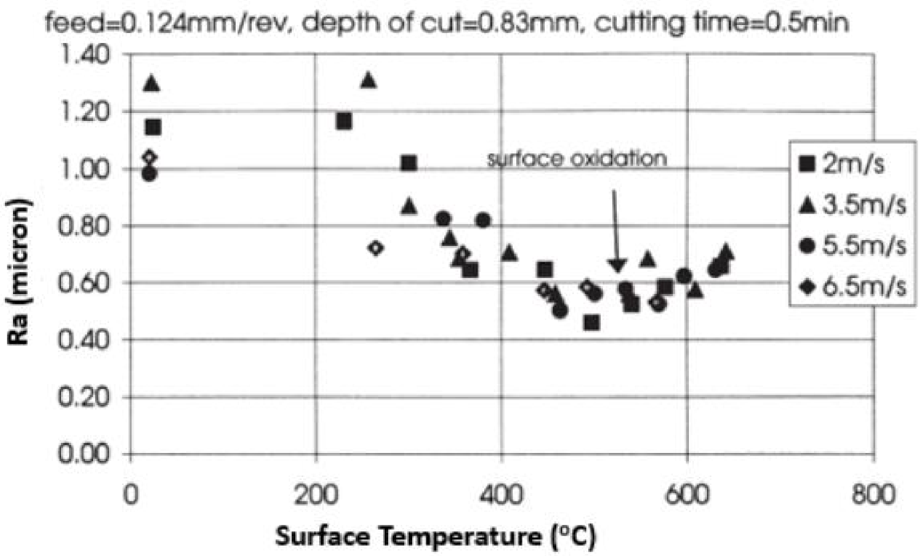

Figure 2.30: Surface roughness of plasma-assisted Inconel 718 Turing at various pre-heating temperatures. Chip [94].

Zhuang et al. [95] compared the surface integrity in conventional (dry machining), plasma-enhanced machining (PEM), and cryogenic assisted cooling (Cryo) in Inconel 718 turning. Although both cryogenic cooling and plasma-enhanced machining showed lower surface roughness at various cutting speeds compared to conventional dry machining, cryogenic cooling demonstrated more promising results at lower cutting speeds. However, as the cutting speed increased to 200 m/min, the plasma-enhanced machining and cryogenic cooling showed approximately the same surface roughness. Figure 2.31 represents the experimental values of surface roughness at various cutting speeds using these techniques.

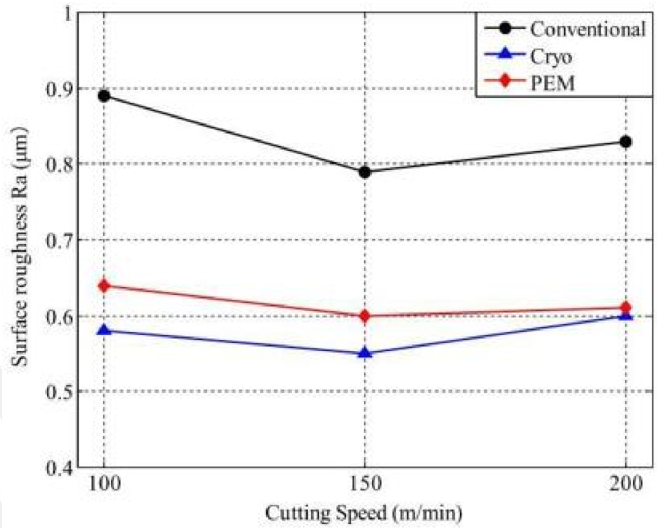

Figure 2.31: A comparison of Inconel 718 surface roughness at various cutting speeds [95].

2.4 COMPARISON OF HEATING TECHNIQUE

In previous sections, different heating techniques and their effect on the microstructure and machining parameters are discussed in detail. The main difference between the heating techniques is related to the efficiency of the heat source, thermal gradient, heating power, heat affected zone (HAZ), and the heat transfer method (conduction, convection, and radiation). While these methods lead to an improvement in the machining results, a detailed comparison can provide better knowledge on selecting the suitable method. In this section, the influence of mentioned heating techniques on Inconel 718 machining is compared with a focus on machinability, heat efficiency, and cost. The reason for choosing Inconel 718 is related to its high demand among other superalloys.

2.4.1 Machinability

The main aim of the heating methods is to improve the machinability of the superalloys by reducing the cutting forces, elongating the tool life, and achieving better surface quality. However, due to the nature of the workpiece material and the method of application, the percentage of the improvement and the efficiency of the process vary. In this section, the impact of the various heat assistance techniques on the machinability of the Inconel 718 is compared.

Several researchers reported cutting force reduction while using heat assistance in Inconel 718 machining. Figure 2.32 represents a comparison between these techniques and their force reduction percentages with a reference to dry machining. As shown in the figure, flame torch assistance demonstrates the least amount of reduction (17%) [68], and induction assistance resulted in the highest amount of reduction (70%) [70] when a single heat source was applied. Moreover, a combination of laser and induction assistance (LIAM hybrid method) provided even a higher force reduction percentage.

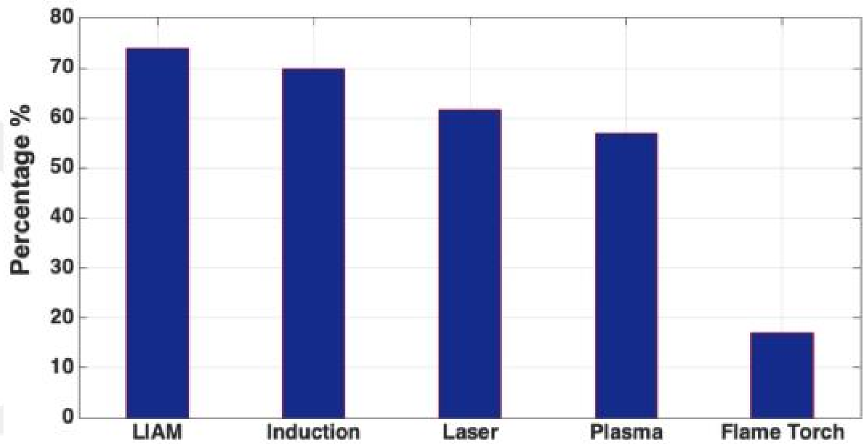

Figure 2.32: A comparison of force reduction with a reference to dry machining of Inconel 718.

In addition to the cutting forces, the tool wear mechanism and the tool life plays an important role in maintaining competitive machining. Kumar et al. [68] investigated the tool wear mechanism of Inconel 718 at 600 °Cusing the gas flame heating technique. The prominent wear mechanism was diffusion wear. However in the Induction Assisted Machining (IAM) of Inconel 718, due to the subsequent increase in temperature, an increase in the chemical reactivity of the chip and tool material occurred, resulting in the formation of the built-up edge [77]. Additionally, it has been observed that at elevated temperatures the tool wear increases compared to the machining conditions in the room temperature, but the number of wear points reduces relatively. Moreover, using hybrid assisted machining (Laser-induction) the amount of tool wear reduced as compared to conventional and induction assisted machining [70]. Furthermore, the tool material affects the tool life drastically. It has been shown that the coated carbide tool (AlTiN+HH) has relatively lower tool wear (390%) compared to the uncoated carbide tools in Inconel 718 machining. The main aim of the coating is to block the heat transfer from the preheated workpiece to the tool contact surface. Therefore, the coated tool will face less wear compared to the uncoated ones [31].

Germain et al. [93] demonstrated that the carbide cutting tool was not suitable for laser-assisted Inconel 718 machining. The process caused a poor tool life compared to conventional machining. However, changing the cutting tool to the ceramic material resulted in a 25% tool life improvement compared to conventional machining. Moreover, Lacalle et al. [44] reported that the ceramic cutting tools (Al_2O_3 with CiS whiskers) in plasma-assisted machining performs better when compared to the coated carbide tools (TiAlN coated). The main reason for this performance is that the hardness and fracture strength of the ceramic cutting tool does not drop immediately at elevated temperatures in contrast with coated carbide tools. Therefore, it was reported that the tool life of plasma-assisted Inconel 718 machining was 200% more than conventional machining. The surface roughness of the machined workpiece has great importance in the dimensional accuracy, fatigue life, and productivity of the process. Hence, a comparison of the various techniques will provide valuable knowledge on selecting the proper method. Figure 2.33 compares the surface quality of the machined Inconel 718 with dry machining using the mentioned techniques. As shown in the figure, the gas flame torch resulted in the least percentage of improvement (23%) [68] and laser-assisted machining caused the highest improvement (82%) [40]. Moreover, the amount of improvement with laser assistance was only slightly higher (4%) as compared to the plasma assistant machining.

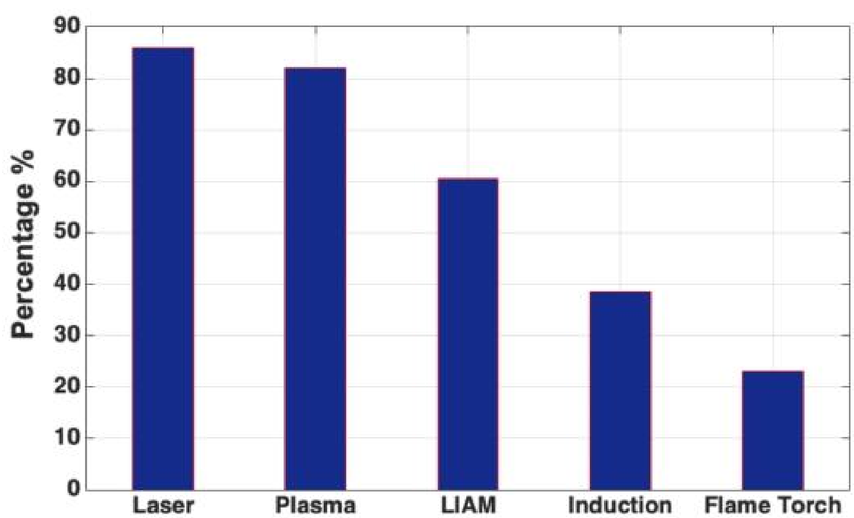

Figure 2.33: A comparison of surface roughness improvements with a reference to dry machining of Inconel 718.

2.4.2 Heating Efficiency

The efficiency of the heating technique has an important impact on the preheating energy consumption, product cost, and homogenous distribution of the heat throughout the workpiece cutting zone. Additionally, the physical properties (thermal conductivity, specific heat, thermal expansion coefficient) of the superalloy directly affect the production efficiency and suitable heating method selection procedure. In this section, an overview of the heating methods from the efficiency perspective is explored.

Among the heat sources, the gas flame torch is the cheapest and the most easily available option. However, the enormous percentages of heat loss due to convection and radiation, make it hard to reach the desired preheating temperatures for superalloy machining. Moreover, the efficiency of the process is so low that to obtain a homogeneous heat distribution in the workpiece, a huge amount of fuel energy and time (stabilizing the temperature) is necessary. The existence of the carbon particles and other elements on the surface layer of the workpiece can alter the microstructure and color (burned surface) of the part leading to poor machining enhancement. Therefore, other heat assistance techniques are more desirable if productivity is considered.

The US department of energy reported that [96] induction heating transfers 84% of the power to load as compared to resistance heating transferring 71% and gas flame 40%. Additionally, as the induction heating is controlled with the frequency and duty cycle of the pulse, in some percentages of the cycle the power is turned off which leads to higher savings of the electrical power. Table 2.6 demonstrates a comparison of power efficiency in induction, resistive, and gas flame heating while the input power is set as 1Kw. As shown in the table, the energy losses of the induction heating are the least as compared to the above-mentioned techniques.

Table 2.6: Required input power for 1kW delivered power and associated power saving [96].

Type	Input Power (kW)	Efficiency	Delivered Power (kW)	Power Savings
Induction	1.11	90%	1.0	-
Electric-Radiant	1.82	55%	1.0	29%
Gas	2.00	50%	1.0	44%

Induction heating is generally implemented in ferrous alloys due to its high magnetic properties. Moreover, nonferrous alloys (Aluminum, Copper, and Silver) with proper chemical compositions and high thermal conductivity utilize this method because of uniform heat distribution in heat treatment, casting furnace, and hot forming processes. In contrast, alloys with low thermal conductivity properties (Stainless Steel, Titanium, Carbon Steel) require an optimized frequency, power, duty cycle, and pulse mode selection to achieve the desired efficient preheating with induction. Additionally, the coil length and thickness, heating period, and material properties are the main parameters that influence the induction heating efficiency. Among them, frequency has crucial importance. Low-frequency results in an eddy current cancellation effect and high frequency causes the skin effect (concentration of the current on a thin surface layer). Moreover, the duty cycle controls the time on and time off periods of the pulse. A high duty cycle causes a concentrated eddy current with fast heating and a low duty cycle results in a low concentration of eddy current with more homogenous heat distribution. Therefore, the selection of the proper duty cycle controls the heating time and radiation/convection losses of the workpiece after preheating [97]. Another important factor is the inductor width. Although the width variation does not affect the current density distribution, it changes the inductor heating efficiency. As the width increases the efficiency reduces, respectively. Therefore, low inductor width with a high-frequency rate (taking skin effect into account) demonstrates efficient induction heating [98].

Several superalloys do not demonstrate proper magnetic properties for induction heating. Additionally, in some machining operations, there is a need for an intense localized heat source in the cutting zone which results in the usage of an alternative heat source such as the laser. Although the heating efficiency of the laser is low as compared to the induction, the environmental advantages of using the limited energy source and employing the optimized short pulse duration with limited heat affected zone (HAZ) improves the heating efficiency of the method drastically [99].

As discussed earlier, two main sources of laser are CO_2 and Nd: YAG. The wavelength of the CO_2 laser is approximately 10 μm and Nd: YAG is 1 μm. As the light wavelength length reduces, the intensity of the power and heat source will be higher. Therefore, it is more preferred to utilize Nd: YAG type lasers for preheating the superalloys with low thermal conductivity to achieve the desired temperature in a short period. Additionally, the CO_2-type lasers have low heat absorption nature which corresponds to lower heating efficiency [36]. Meanwhile, the beam impingement angle, polarization (electric field orientation in the light wave), intensity (a combination of the power and focal spot size) are the main parameters affecting the efficiency of the laser preheating process.

On the other hand, the elemental composition of the superalloy has a significant importance when the light interacts with the electrons to accelerate them and transfer the photon packs within the workpiece lattice. Additionally, the surface texture and roughness of the workpiece trap the laser energy pack resulting in higher radiation heat absorption. Therefore, the emissivity coefficient of the superalloy and surface textures are other important parameters affecting heating efficiency [100], [101]. Furthermore, considering all optimized laser heating parameters, approximately 35% of the beam energy is absorbed by the workpiece and the rest of the energy is wasted (at higher temperatures the heat efficiency even reduces more) [102]. Hence, a combination of laser and induction heat sources can improve machining productivity and heating efficiency. A narrow/deep HAZ of the low power output laser source and wide/shallow HAZ of the high power output induction heat source merge to excel the overall heating efficiency and reduce the required heating time [70]. Additionally, this hybrid heat source approach reduces the thermal effect on the tool by increasing the required distance between the heat source and the cutting tool [103].

Another approach for the efficient heating process is the plasma heat source. Especially, for the applications that require a high amount of intense heat at low time intervals, plasma is an appealing alternative considering its relatively low cost compared to the laser machinery [104]. The amount of the heat power generated with the plasma assistance is in direct relation with the transferred arc intensity and the translation motion speed of the torch to the workpiece [44]. The ionized gas is generated between two electrodes when a high potential difference is applied. To assist the power generation efficiency, a packing of dielectric material is introduced in the gap between two electrodes to initiate the polarization mechanism and electron energy. Microwave type plasmas operating at low pressures (approximately 0.1 bar) demonstrate thermal equilibrium with higher efficiencies at high temperatures [105]. Furthermore, depending on the machining operation (turning or milling) the required plasma intensity will vary. Generally, in a milling operation, the plasma torch is fixed to the cutting tool platform, and it applies uniform heat distribution to the workpiece cutting zone without pausing. Additionally, the heated zone in milling is larger than the amount of feed per tooth which evolves more cutting zones. However, in the turning operation, the heat of the plasma torch is applied to the workpiece surface with interruption caused by the rotational spindle speed. Therefore, a higher intensity of plasma arc is required in turning processes as compared to milling [44]. Moreover, in the turning operation, when the cutting tool and the plasma torch are near to the rotating chuck, the turbulent airflow affects the plasma gas stream intensity which reduces the heating efficiency and there is a need for a special chuck encloser design [94]. Additionally, at higher speeds, the efficiency of plasma heating can drop drastically [106]. As the required preheating volume of the workpiece increases, the amount of heating power to sustain a required temperature in the desired period increases which leads to the intense heat flow with lower efficiency [107].

Overall, comparing a single heat source, induction heating will have the highest efficiency. However, for the workpiece without magnetic properties, the laser will be a better option, since, the power intensity of the plasma is lower than the laser and it needs a more complex procedure [108]. Gas flame heat source has the least efficiency with the highest ease of application. On the other hand, as discussed earlier, a hybrid method (a combination of induction and laser) leads to even higher heating efficiency.

2.4.3 Economics

The cost of the subtractive manufacturing process is in direct relation to the desired quality of the final products. In addition to the proper machining setup, the labor, cutting tool, raw material, and cutting fluid costs are the prominent factors in an efficient manufacturing process. As mentioned in section 3, superalloys are among the hard-to-machine materials meaning that the required technology and the design of the whole machining process will cost relatively higher compared to the widely used engineering materials. Therefore, to reduce the amount of the tool wear and on some occasions to be able to machine the parts, the conventional approach is adopting cooling techniques with cutting fluids or cryogenic methods. However, cutting fluids add an extra cost in the process, and transferring the fresh cutting fluids and disposal of the fluid are raising environmental concerns. Although the cutting fluids reduce the cutting zone temperature and assist the lubrication of the contact area resulting in an improved tool life (approximately 30%), the fluid clean up procedure, maintenance, delivering the cutting fluid, method of application to the contact zone, and disposal adds extra costs to the production [109], [110]. Considering these issues, Kaynak [15] investigated the machining of Inconel 718 with MQL and cryogenic cooling methods. The MQL method reduced the cutting zone and tool wear amplitude slightly as compared to the dry machining. However, in this method, a minimum amount of cutting fluid is sprayed to the contact zone and adjustment of the nozzle angle and the air compressor pressure affect the results drastically. Moreover, there is a need for cutting fluid disposal in mass production applications. On the other hand, cryogenic cooling demonstrated promising results in reducing the machining outcomes (cutting forces, tool wear, and surface roughness). However, as mentioned earlier, same problems with the cleaning, disposal, and delivering of the fluids is valid in both approaches which adds to the machining costs. Additionally, the capital investment of the cooling setup should be added to the whole process costs. Keeping in mind the above-mentioned obstacles with the wet machining, an optimized dry machining method with the desired amount of tool wear can be beneficial from the economical perspective.

Generally, Conventional dry machining of superalloys is performed in low cutting speed and feed rate conditions. Therefore, the low material removal rate (MRR) consequent in economically inefficient machining operation. Keeping in mind these issues, the introduction of heat assistance in dry machining aggregate higher production rate in hard-to-machine materials and is demonstrated to be cost-efficient in mass production [111]. Preheating the workpiece reduces the shear strength of the material and has a better tool life influence compared to the cooling methods resulting in a reduction of machining costs [25]. Additionally, in heat-assisted superalloy machining, the amount of tool change is reduced which results in higher tool life and machining time. Anderson et al. [23] reported that LAM reduced the total machining time by approximately

30% at 2.2 m/s and 50% at 3 m/s cutting speed as compared to conventional machining. Figure 2.34 represents a cost evaluation of the LAM and conventional machining of Inconel 718.

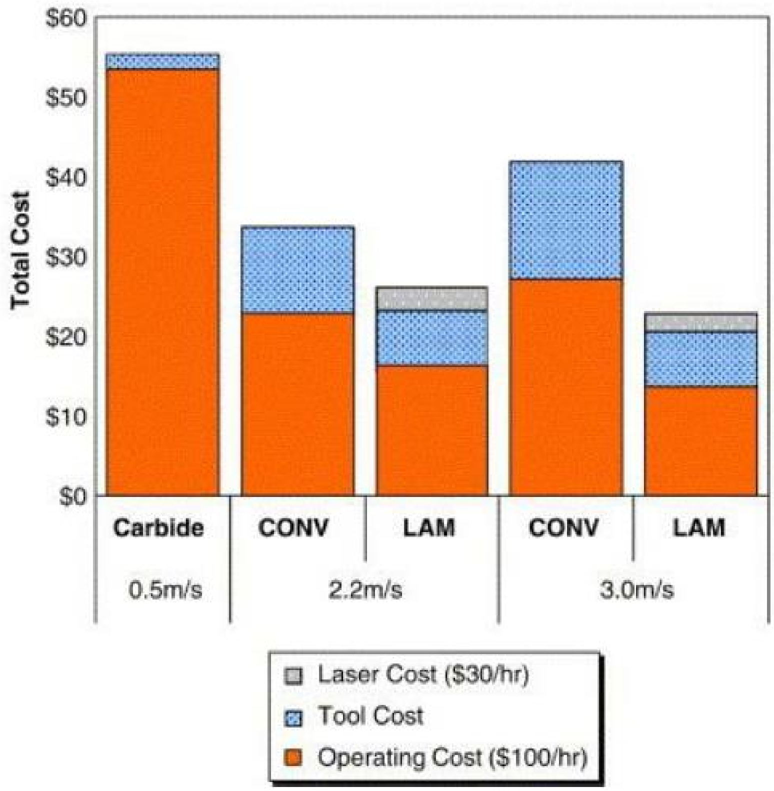

Figure 2.34: A cost comparison of conventional and LAM in 1m length of machining at various cutting velocities [23].

Similarly, Kong et al. [112] compared the total machining cost of the conventional and laser assistant machining at three different cutting speeds and showed that laser assistance results in a reduction of the total machining cost. Figure 2.35 represents the cost comparison between conventional and laser assistant machining in these conditions. As shown in the figure, at all these velocities, laser assistance results in lower machining costs (approximately 40%).

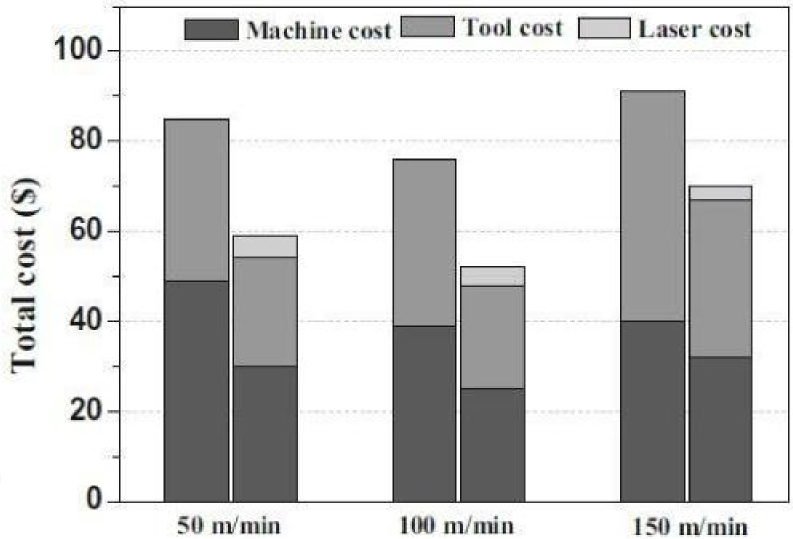

Figure 2.35: A cost comparison of conventional and LAM in 1m length of machining at various cutting speeds (0.5mm depth of cut, 0.1mm/rev feed rate) [112].

Although the laser assistance is showing promising results in better machining characteristics and cost efficiency, the assembly of the laser is not widely used in the industry due to the high laser setup cost. However, the usage of plasma and induction assistance can result in low investment costs [69]. , Moon et al. [40] reported that the plasma heat source is relatively cheaper than that of laser (approximately 10 times cheaper). Moreover, induction-assisted machining for the superalloys with high permeability to have the advantage of even lower machine investment cost and being eco-friendly [31].

3. COMPARISON OF CONVENTIONAL AND MODIFIED JHONSON-COOK MODEL FOR INCONEL 718

The assurance and achievement of finite element analysis are of significant importance for the constitutive model of the material. The material behavior can observe by the constitutive model, the effect of high strain, strain rate, and temperatures on the equivalent flow stresses can easily be evaluated. In this chapter, Inconel 718 was selected as the workpiece. A comparison has been done in detail on the conventional Johnson cook model and modified Johnson cook model. The JC material model extensively under consideration in the material constitutive law for simulation of machining [113]. There are mainly three independents in this empirical model. All of them are uncoupled from each other. Firstly, the isotropic hardening, where the yield surface endures the shape, but an expansion of shape happens with an increase in stresses. The main formula for isotropic hardening is in Eq. (3.1),

$$[\quad + \quad \varepsilon \quad] \qquad (3.1)$$

Where,

$= \qquad h$

$= \qquad h$

$\varepsilon =$

$= \qquad h$

Secondly, Strain rate hardening, the mechanical resistance, and hardness increase inside the metal because of this while the ductility of the metal decreases. The below relation in Eq. (3.2), expresses the strain rate hardening,

$$[1 + \quad (\frac{\varepsilon}{\varepsilon_0})] \qquad (3.2)$$

Where,

$=$

$=$

$_0 =$

Thirdly, and the most important parameter of the JC model is thermal softening, mostly authors neglect the thermal softening effect (= 0). On the other hand, authors also reported that the adiabatic shear bands produced because of the expansion of strain localization in finite element analysis of machining. Thermal softening is required for the beginning and amplification of strain localization [114]. Therefore, most of the authors considered the thermal softening in the JC model and modified it as required. Eq. (3.3) shows the thermal softening phenomena,

$$[1 - (\frac{-}{-})] \tag{3.3}$$

Where,

=

=

=

= h

by multiplying these three Eq.s, the equivalent flow stresses can be calculated and this is known as the conventional JC model as shown in Eq. (3.4),

$$= [\; + \; \mathcal{E} \;] \cdot [1 + \; (\frac{\mathcal{E}}{\mathcal{E}_0})] \cdot [1 - (\frac{-}{-}) \;] \tag{3.4}$$

The conventional JC model is limited to isotropic hardening, strain rate hardening, and thermal softening. In addition to the conventional JC Eq., Calamaz et al. [114] developed a TANH(tangent hyperbolic) model. The purpose of this modification is to consider strain softening at high temperature and strain rates. Eq. (4.5) and (4.6) expresses the Calmaz modified model,

$$= \; [\; + (1 - \;) \; h \, (\frac{1}{\mathcal{E} + \mathcal{E}})] \tag{3.5}$$

$$= 1 - (\frac{}{1 +}) \; h \, [(\frac{- \;\; _0}{- \;\; _0}) \;] \tag{3.6}$$

In this model, the author took benefits from the last conventional JC model by using the inputs (A, B, C, n, m). The flow behavior of metal can easily evaluate by these parameters. However, the other inputs (, , , ε ,) should be recognized so that softening of material take under consideration. Additionally, Sima et al. [115] made some changes in Calamaz et al. model, is taken as exponent in TANH function for the thermal softening. These amendments give improvement in control which is shown in Eq. (3.7).

$$= [+ (1 -) (h ((\varepsilon +)^{1}))] \tag{3.7}$$

Furthermore, Lurdos et al. [116] modified the conventional Voce model. The addition of supplementary strain hardening (ε) into the Voce model gives the steady state behavior. However, this behavior is not steady state if compared with divergent behavior of strain hardening in the JC model. The fluctuation in these inputs (, $_0$, , ,) directly related to the temperature sensitivity and strain rate. The Eq. (3.8) is given below,

$$= + (_0 - + \varepsilon) (-) \tag{3.8}$$

Where,

$_0 =$ h

$=$

Moreover, anis et al. reported that [117] the JC model does not consider the coupling phenomena between the temperature, strain, and strain rate. It is also reported that this constitutive model cannot be useful for the heavy machining processes at high temperature and strain rates. Due to an increase in strain, the flow stresses increase, this is known as strain-rate sensitivity which is directly proportional to the temperature in mostly metal cases [118]. Fang et al. [119] investigated the sensitivity flow stress analysis of Inconel 718 at different elevated temperatures to study the effect of strain rate hardening. The crucial point of temperature was noted which is 500°C, below this point sensitivity of Inconel 718 to the strain rate hardening is not showing. This is the reason that several authors explained the coupling in their models to study these effects of temperature and strain rate on the flow stress. In addition to that, Lin et al. [120]made amendments in the conventional JC model and investigated the coupled effects. The coupling between strain rate and temperature gives better results on the flow stress behavior on the material which was high strength steel. This improvement is limited to the low strain rate. This behavior has been noted in the case of aluminum alloys and high-strength steel. The six input parameters ($_1$, $_1$, $_2$, $_1$, $_1$, $_2$) of modified JC model are different for each material. It is necessary to calibrate them for each material separately. The model is shown in Eq. (3.9).

$$= (_1 - _1\mathcal{E} + _2\mathcal{E}^2)(1 + _1 \quad ^*) \quad [(_1 + _2 \quad ^*)(- \quad)] \tag{3.9}$$

Arrhenius model is known as the most accurate model which explained the flow stress briefly at elevated deformation temperature. The addition of the hyperbolic sine-typed Arrhenius model can give the advancement in conventional and modified JC, as shown in the below Eq. (3.10), is the Zenner-Hollomon parameter [121], [122]. Yong et al. [123] investigated the flow stresses in Inconel 718 in the metal forming process by using the Arrhenius model. The temperature range kept $(900 - 1060°C)$ while the Strain rates were kept low which is $(10^{-3} - 0.5 \quad ^{-1})$.

$$= \quad (\text{—}) \tag{3.10}$$

Wang et al. made advancements in the conventional JC model. In this modification as showing in Eq. (3.11) and (3.12), researchers studied the strain rate softening effect and consider it with the way of strain-rate sensitivity parameter. It is taken as the function of temperature. The range of temperature and high strain rate were kept $(500 - 800°C)$,$(5000 - 11000 \quad ^{-1})$ respectively [124].

$$= [\quad + \quad \mathcal{E} \quad] \cdot [1 + \quad (\;) \quad (\frac{\mathcal{E}^{\cdot}}{\mathcal{E}^{\cdot}_{0}})] \cdot [1 - (\frac{-}{-}) \quad] \tag{3.11}$$

$$(\;) = 0.0232 - (0.00372 + 0.0021 \quad (\frac{-500}{3000} \quad)) \quad (\frac{-500}{150} \quad) \tag{3.12}$$

The literature review of all the above constitutive modeling and development has great importance in finite element analysis of the machining process. The work material behavior is extensively studied under high strain, strain rate, and temperatures. Iturbe et al. [125]compared the conventional JC model with their own new coupled empirical modified JC model. The Inconel 718 is selected as a workpiece, experimental work has done in which softening phenomena playing a major role in material behavior. Moreover, coupling between the strain rate and temperature occurred experimentally. With the reference to these experimentally and simulated values, a comparison has been done for the Inconel 718 material behavior.

3.1 CONVENTIONAL JHONSON-COOK MODEL STRESS-STRAIN CURVE RESULT

The conventional JC modeling has been modeled in MATLAB. The picture showing the prediction result for the Inconel 718 with various strain rates and temperatures. It can be seen this conventional prediction is not valid in the case of Inconel 718. There is no yield point, ultimate tensile strength, and rupture point in this graph. The graph is showing that as strain increases, the stresses are increasing, and it diverges to infinity. This is because of the limitation of the conventional JC model. Thermal softening was not considered in this model. Thermal softening gives a remarkable improvement in results by taking this parameter under consideration in the empirical constitutive model.

Table 3.1: Reference parameters for Inconel 718 [115]

( )	( )	(−)	(−)	(−)	($^{-1}$)	Heat Treat.
1241	622	0.0134	0.6522	1.3	1.0	Aged

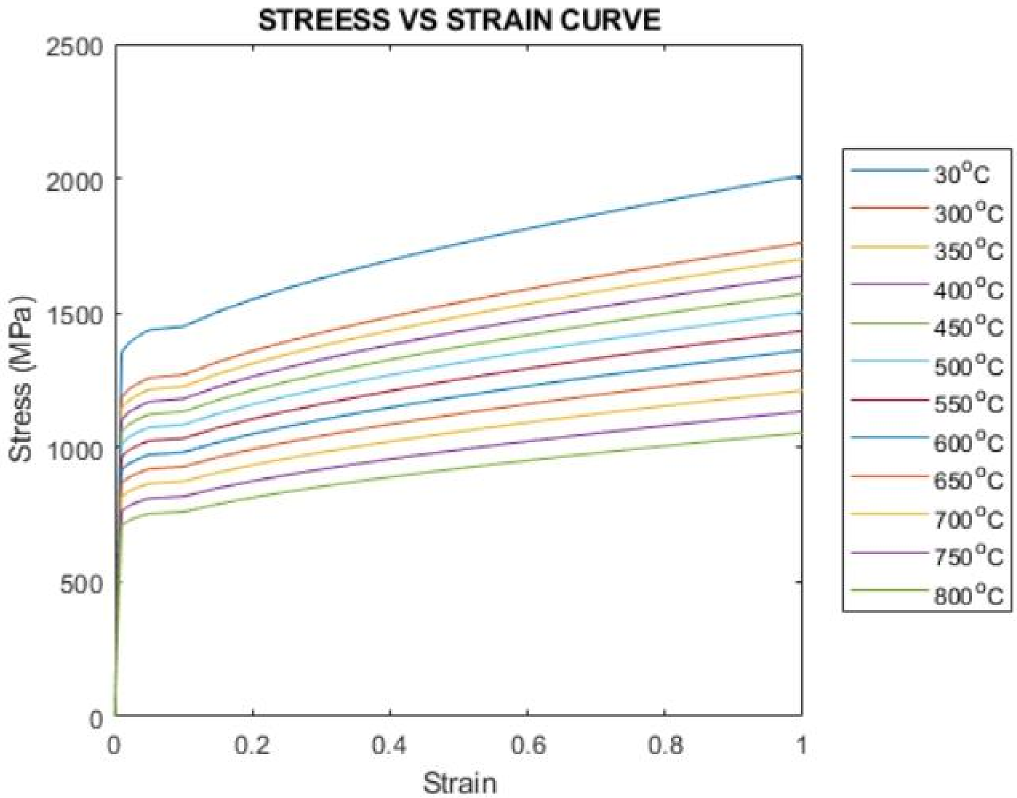

Figure 3.1: Stress-Strain curve result of conventional JC material model.

3.2 MODIFIED JHONSON-COOK MODEL STRESS-STRAIN CURVE RESULT

To get better results for the stresses in the conventional JC model, a new proposed model has been invented, which is given below, thermal softening parameter modified to do better optimization in finite element analysis simulation and on different elevated temperatures (30-1200°C). the exponential term has been introduced so that thermal softening can take nonlinear. the proposed model is coupled model, the coupling between the temperature and strain rate hardening affects the flow stress. For the proposed modified model, the values of the different parameters are mentioned in Tables 3.2,3.3 and 3.4.

The proposed model is given below in Eq. (3.13), where the Eqs. (3.14), (3.15), and (3.16) have been modeled for the strain hardening/softening, thermal softening, and strain rate hardening respectively.

$$= \quad (\ ) \cdot \quad (\ ) \cdot \quad (\ ,\ ) \tag{3.13}$$

$$(\ ) = \quad + (\ _0 - \quad + \quad) \exp(- \quad) \tag{3.14}$$

$$(\ ) = \frac{1}{1 + \ - \ (\ -\ )} \tag{3.15}$$

$$(\ ,\ ) = [1 + \quad (\ ) \ln (\ _0)] = [1 + (\quad + \quad -) \ln (\ \cdot_0)] \tag{3.16}$$

Table 3.2: Thermal softening values at different temperature for Inconel 718 [125].

		0	
Modified JC model TS term,	< 700℃	21℃	2
	> 700℃	700℃	0.0016 * T + 2.0031

Table 3.3: Thermal softening parameter values for the characterized Inconel 718 [125].

	0.00663	0832.27

Table 3.4: The reference value for the proposed model for Inconel 718 [125].

	0 ( )	( )			
Proposed Strain Hardening term, ( )	1388	1565	1600	0.06767	3

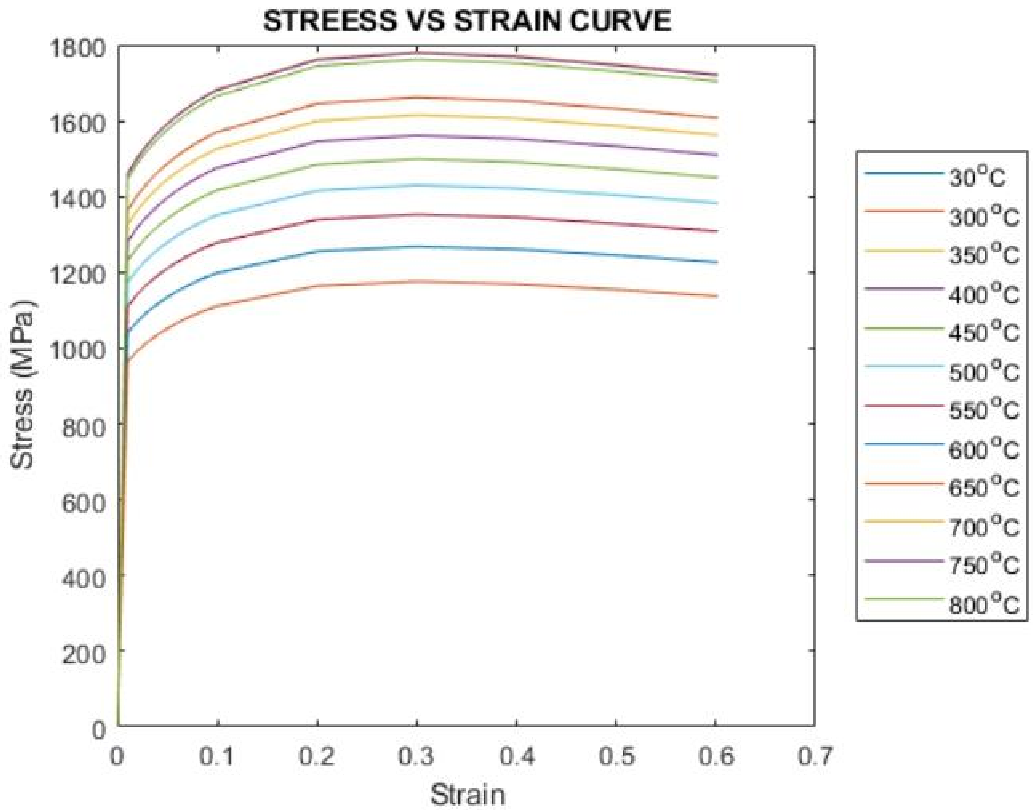

Figure 3.2: Stress-Strain curve results in modified conventional JC material model.

The graph gives the value of yield point, ultimate tensile strength, and most importantly it does not diverge to infinity while in the conventional JC model the divergence is a big failure. This is because of the consideration of the thermal softening parameter. This has significant importance especially in the intensification of strain localization.

4. ANALYTICAL SOLUTION OF INDUCTION HEATING POWER AND TEMPERATURE FOR THE INCONEL 718

An analytical approach is developed to obtain the thermal power of induction heating which is induced in the workpiece by electrical power through the electromagnetic field. As mentioned in the induction heating phenomena is detailed in section 2.1.2, this procedure is non-contact and gives a uniform heat distribution to the material as compared to the other heating methodology.

4.1 INDUCED INDUCTION POWER FOR THE SOLID BAR OF INCONEL 718

In this section, an Inconel 718 solid bar was selected as a workpiece. The dimension of the solid cylinder is taken as diameter $= 50$ and length $= 200$. The span factor is rely on the ratio of workpiece diameter to the coil diameter ( ). If the number of turns of the coil is 1 it gives the value in unity. The flux factor is important for calculating the coil's power factor. It has different values for the slab and rod. By Figure 5.1 we assumed the flux factor value ($= 1$), where the induced power can be calculated from Eq. (4.1). the skin effect during the induction heating calculated from Eq. (4.2).

$$= (\ *\ *\ )^2 * \frac{*\ *}{*} * \quad (\quad) \tag{4.1}$$

$$= \sqrt{2} \tag{4.2}$$

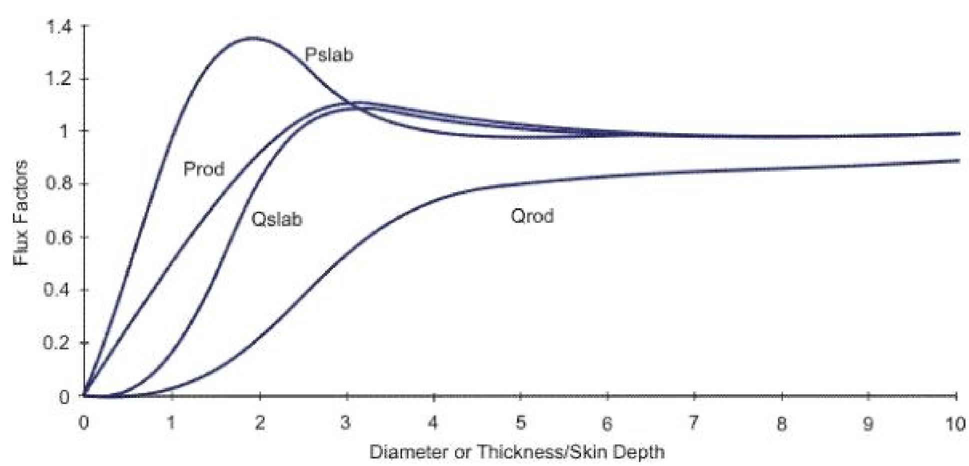

Figure 4.1: Flux factor value for the different diameters of a workpiece [126].

The most important parameter in induction heating is the skin effect, which is previously mentioned in section 2.4.2. Penetration depth (skin effect) is inverse relation to the square root of absolute magnetic permeability = $_0$. Where the value of magnetic permeability of free space is $_0 = 4\ 10^{-7}$ ( ) and the value of relative magnetic permeability for the Inconel 718 is =1.0011. the angular frequency is denoted by = 2 (—) and the value of frequency is considered = 2 . The electrical resistivity of Inconel 718 is taken as = 0.000125 (Ω − m)The number of turns is = 1. The modeling of these parameters has been evaluated on MATLAB. The results of the induced power in the Inconel 718 workpiece at various voltages are shown in Figure 4.2.

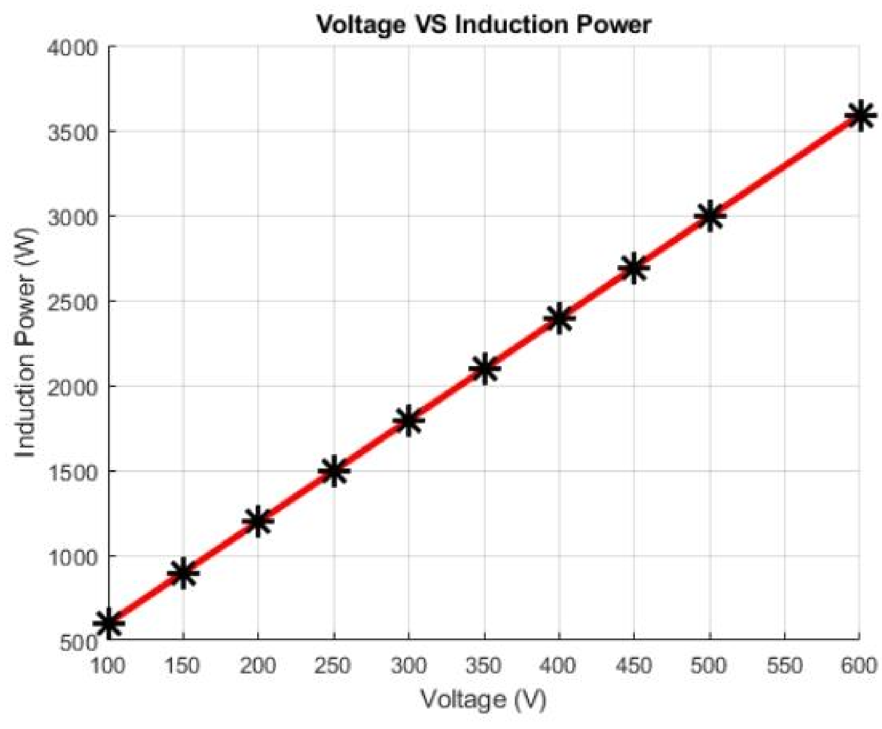

Figure 4.2: Induction Power at various Voltages.

4.2 TEMPERATURE REQUIRED TO HEATED-UP THE INCONEL 718 AT DIFFERENT TIME INTERVAL

The value of specific heat ( )describe the value of heat energy which is absorbed inside the metal by 1 gram of mass ( ) as a workpiece to attain a 1°Ctemperature increase. The specific heat = 435 ($\frac{}{*}$) is considered for the Inconel 718. The room temperature is taken = 30, and density of Inconel 718 is = 8230 ($\frac{}{3}$). By Eq. (4.3), we can get the value of rising in temperature at various induction power, where the mass of the workpiece is calculated by Eq. (5.4).

$$= \frac{-}{} \tag{4.3}$$

$$= \frac{4}{} 2 * \; * \tag{4.4}$$

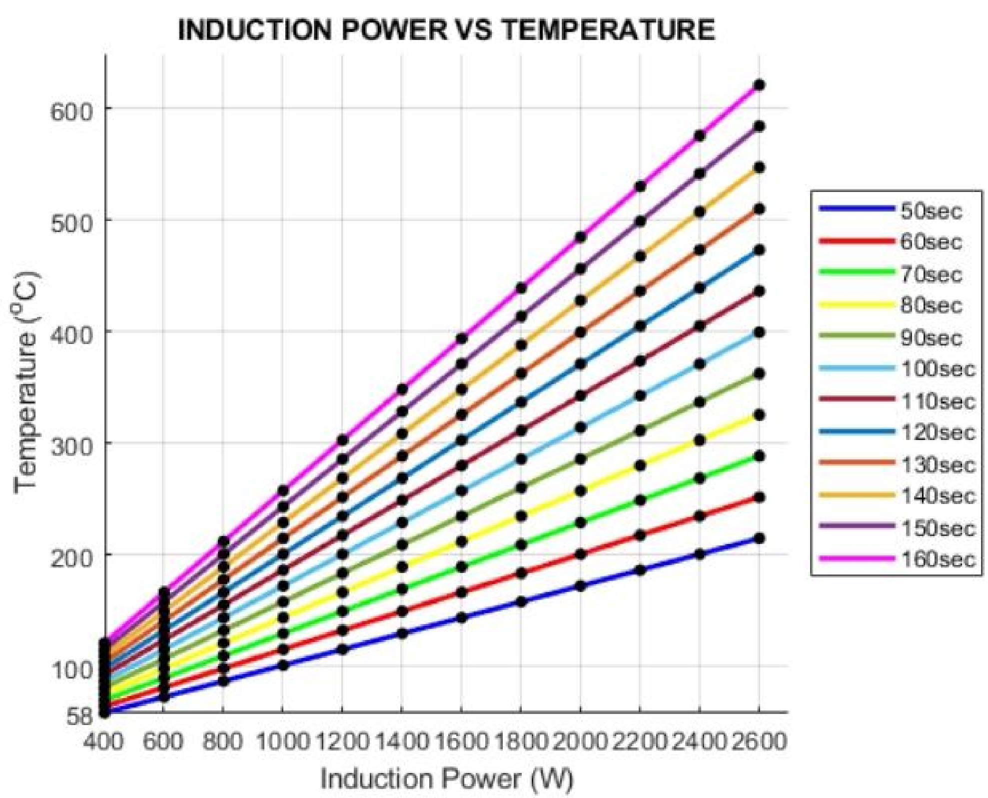

Figure 4.3: Induction power and temperature relation at different intervals.

5. MODELING OF INDUCTION HEATING FOR INCONEL 718 BAR IN COMSOL MULTIPHYSICS

In this chapter, the modeling of induction heating of metallic bar by using COMSOL multiphysics is studied in detail. The model includes Inconel 718 bar within a coil. A high-frequency excitation current is supplied to the coil which generates an alternating magnetic field. The alternating magnetic field interacts with the Inconel 718 bar and induced eddy current in it. The eddy current will heat up the bar due to joul effect. This modeling has done in 2D axisymmetry. In the Ac/Dc module, the induction heating inside the electromagnetic heating is selected as physics. This adds the heat transfer interface and the magnetic field interface and the electromagnetic heating is decoupled. The diameter and length of the bar are 6mm and 150mm respectively. The value of electrical conductivity [127], thermal conductivity, and specific heat [128] with various temperatures taken as showing in Figures 5.1,5.2, and 5.3 respectively. These properties are dependent on temperature.

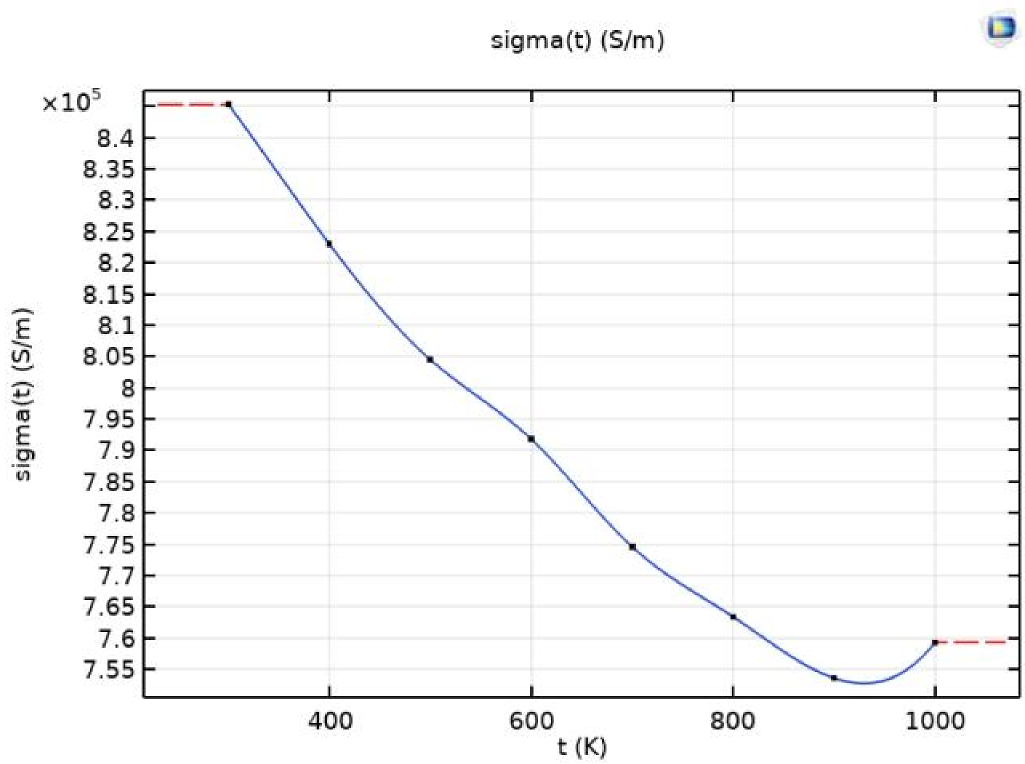

Figure 5.1: Electrical conductivity of Inconel 718 at various temperatures (K) [127].

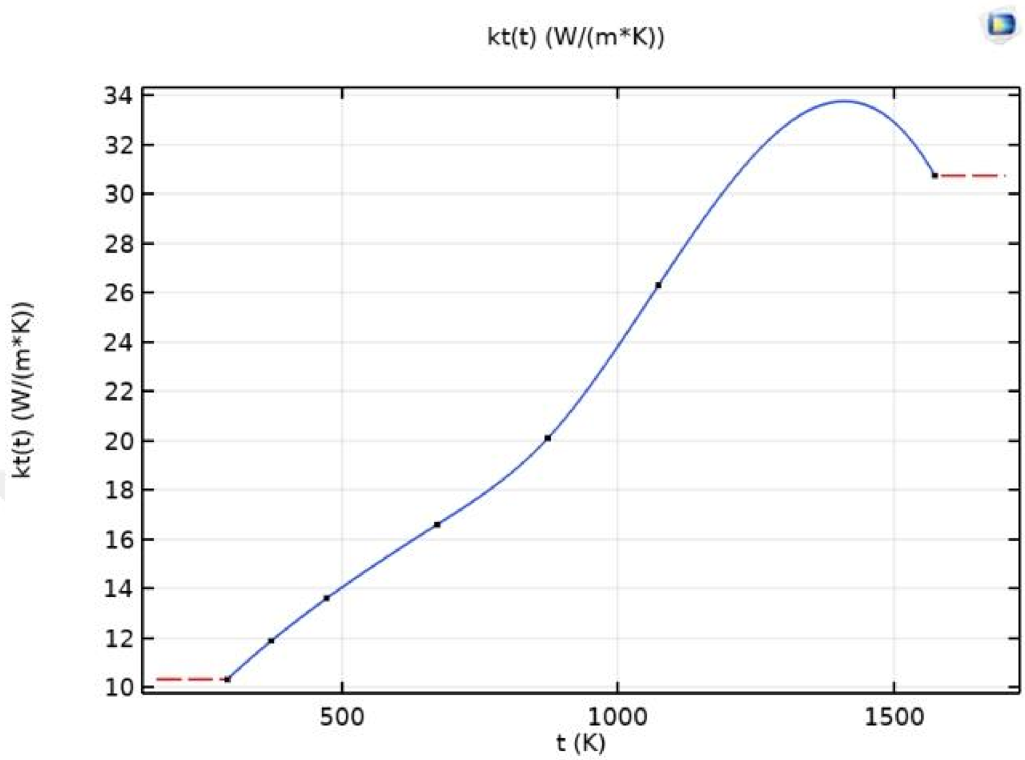

Figure 5.2: Thermal conductivity of Inconel 718 at various temperatures (K) [128].

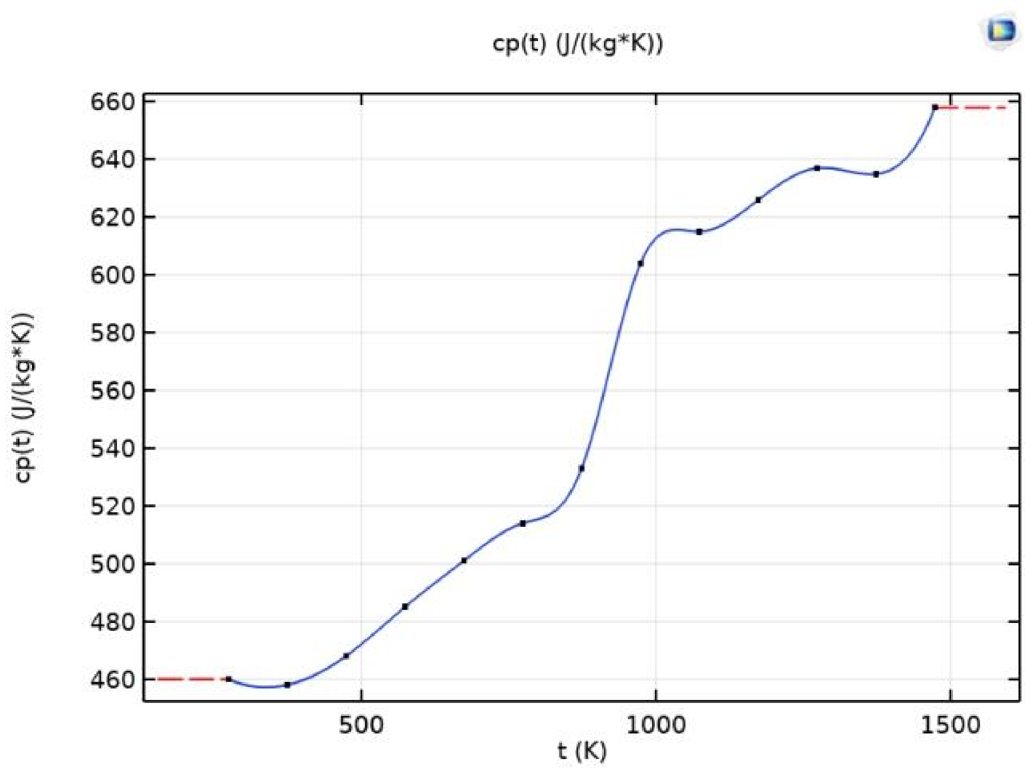

Figure 5.3: Specific Heat of Inconel 718 at various temperature (K) [128].

5.1 FREQUENCY-TRANSIENT STUDY RESULT

This heat transfer model has been studied in the time domain so the frequency-transient study selected. The input signal is sinusoidal so the excitation current is also sinusoidal. The magnetic field problems are modeled in the frequency domain and that information is transferred to the heat transfer physics which is solved by using a time-dependent solver.

These properties input manually in the material section to get the appropriate results. The sinusoidal currents with the various amplitudes and various values of frequency are taken under consideration. The term comes from joule heating that eddy currents generated in the interface of the magnetic fields will be transferring energy to heat up the cylinder in the heat transfer interface. The modeling of radiation and convection is considered to get better optimization in the model, the heat flux is inserted on the outer surface of the bar for the convection.

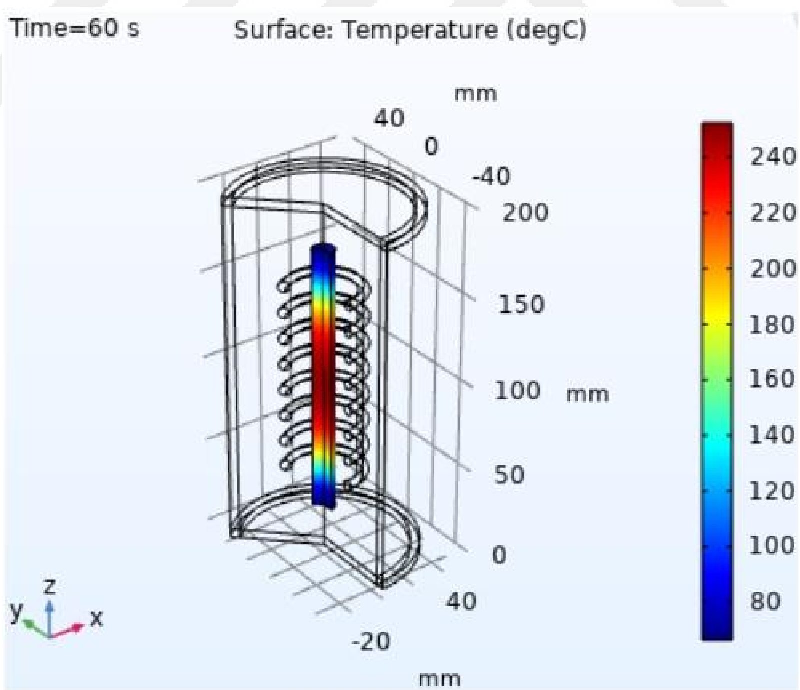

(a)

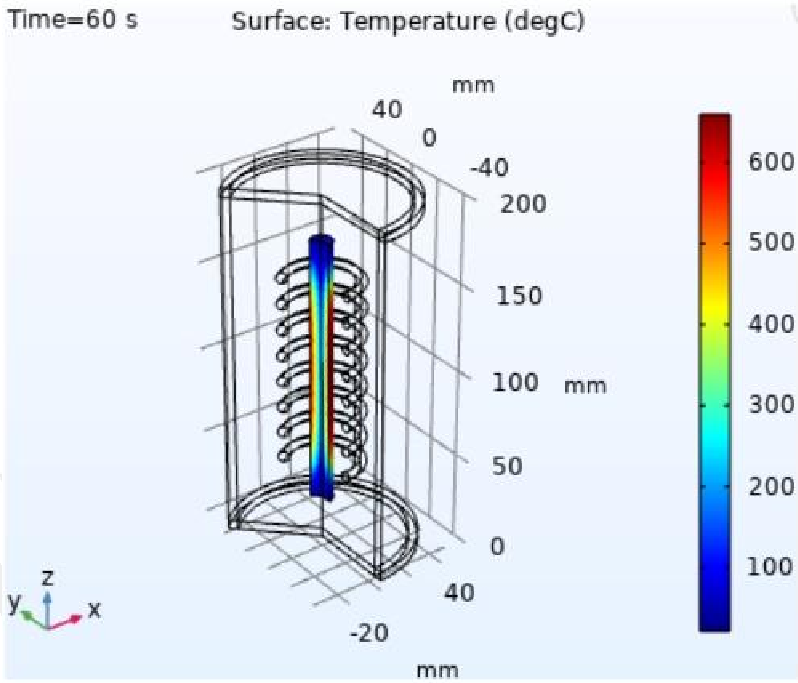

(b)

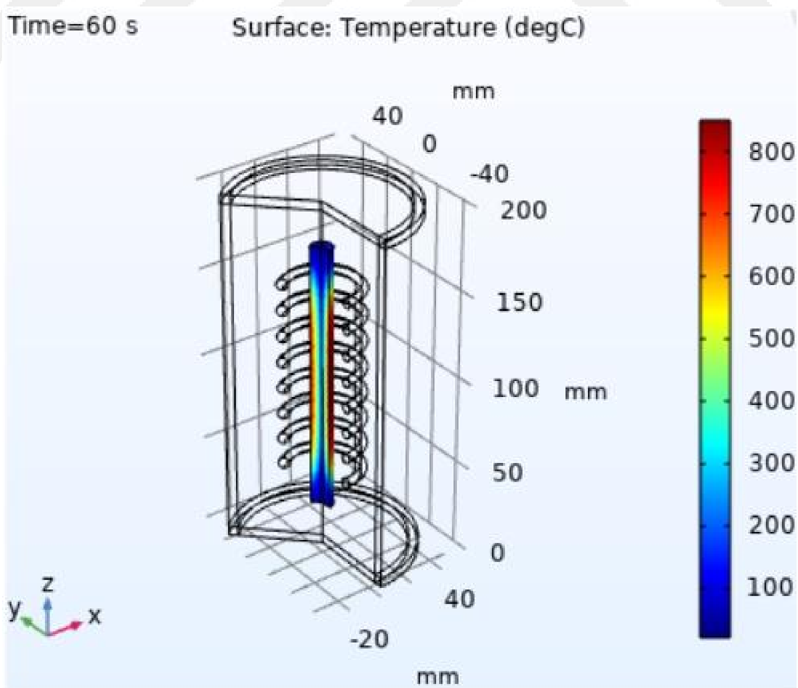

(c)

Figure 5.4: Temperature rise concerning time in the cylinder of Inconel 718 at = 2kHz (a) V = 150 (b) V = 200 (c) V = 250

At the constant frequency, the increase in voltages gives the temperature rise as shown in Figure 5.4. In Figure 5.5, the voltage value is kept constant and frequency value.

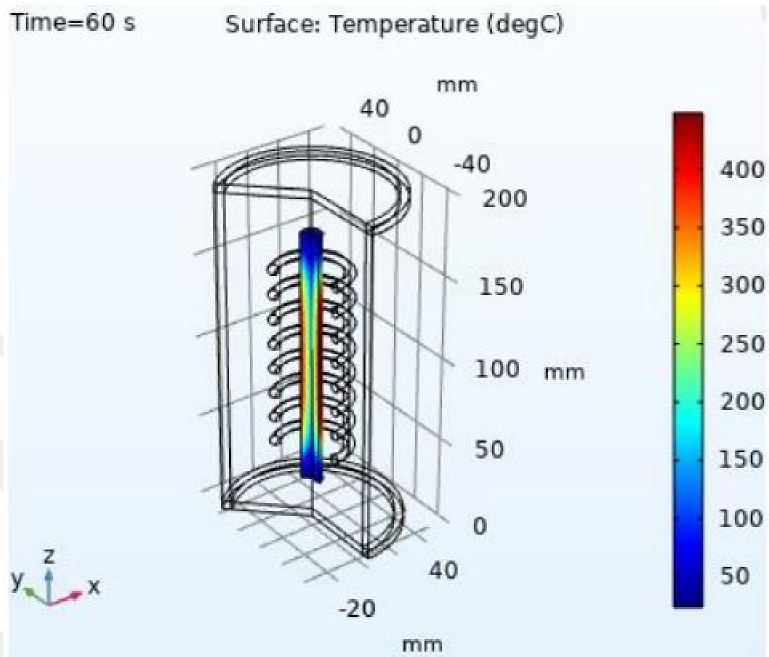

(a)

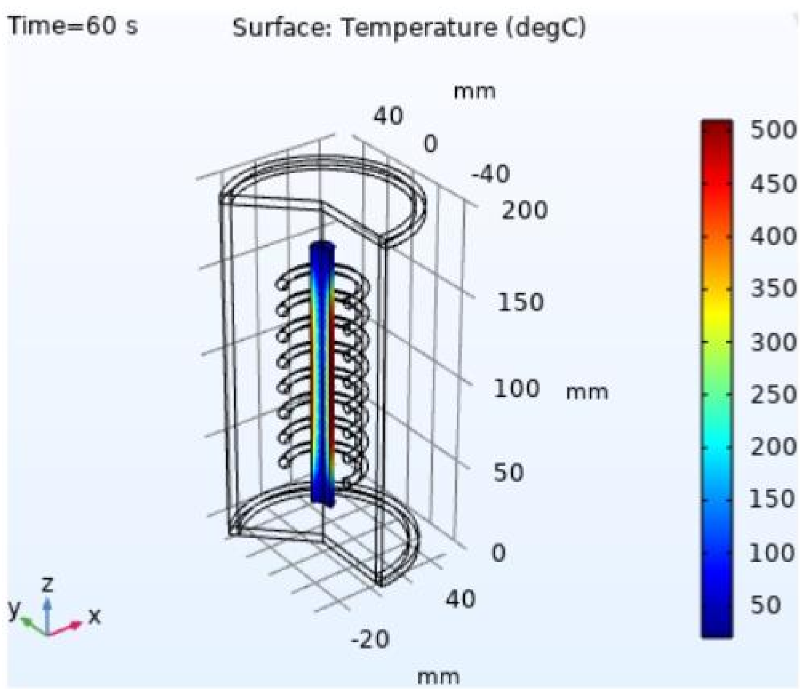

(b)

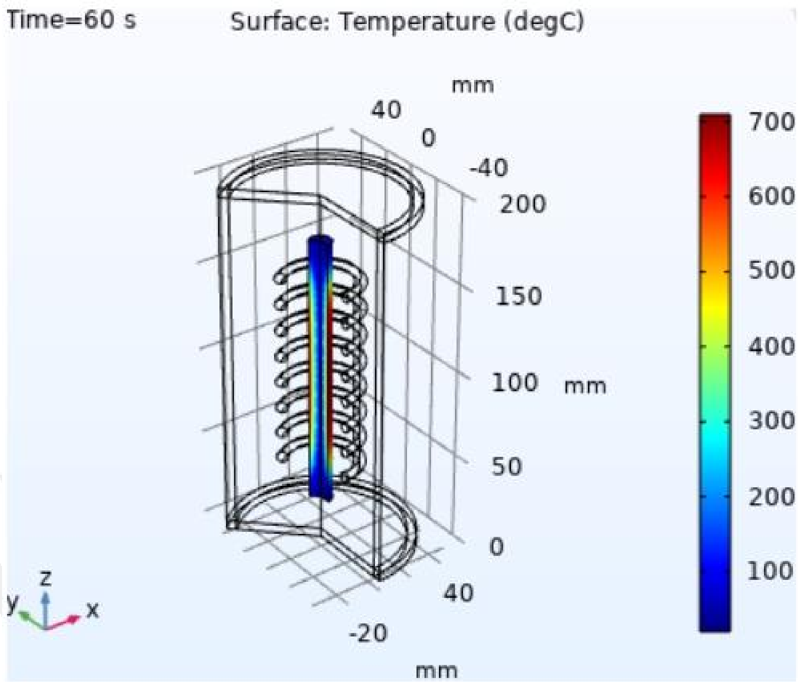

(c)

Figure 5.5: Temperature rise concerning time in the cylinder of Inconel 718 at V = 250 V, (a) = 1kHz (b) = 2kHz (c) = 3kHz.

5.2 SKIN EFFECT RESULTS

The high excitation frequency gives the high induced current in the cylinder and it is concentrated next to the surface so this is called the skin effect and the value of current moving away from the surface decay exponentially. This phenomenon happens in a very small depth so this factor is very important for the results. This value is calculated accordingly. The magnitude of J is called current density which value is showing zero except very near to surface, so this the skin effect. The current density is extremely high next to the surface and over a very small distance, it decays to almost zero. Figure 5.6 shows the results for the current density on the surface bar.

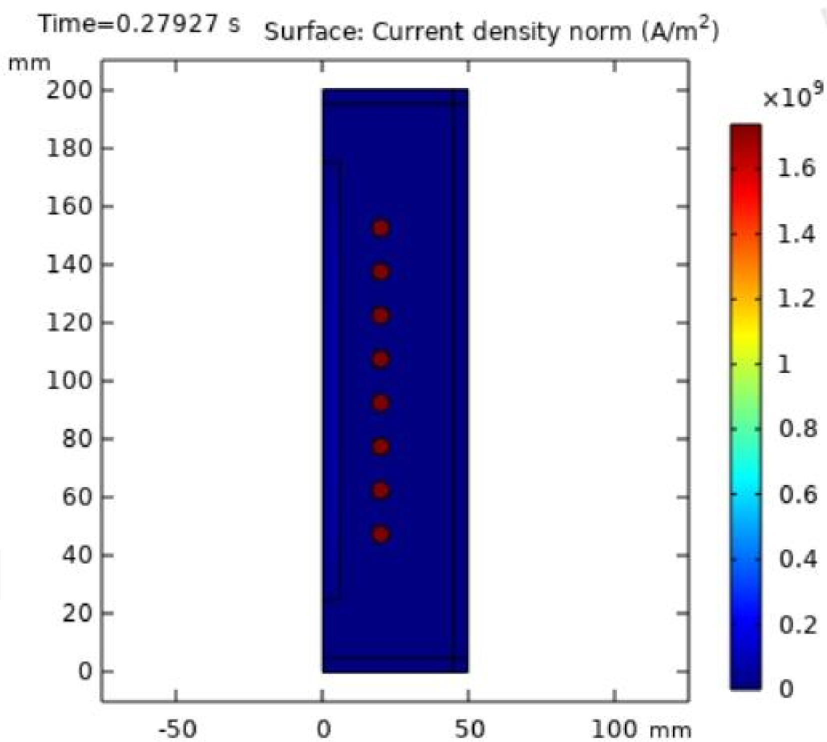

Figure 5.6: Skin effect at V = 250 V, = 2 .

6. FINITE ELEMENT ANALYSIS FOR THE ORTHOGONAL CUTTING OF INCONEL 718

The finite element analysis is carried out by using ANSYS 2021 R1. The orthogonal cutting operation analysis was investigated. The simulation is done on the rectangular bar. The dimension for the model is l=10 mm, width is 2 mm and thickness is 2 mm. A single-point cutting tool was used to perform the orthogonal cutting. The material for the workpiece selected Inconel 718, and the material for the tool is tungsten. The explicit dynamics analysis was investigated. The cutting velocity for the orthogonal operation kept 1000 mm/sec. the mesh to the model is showing in figure 6.1.

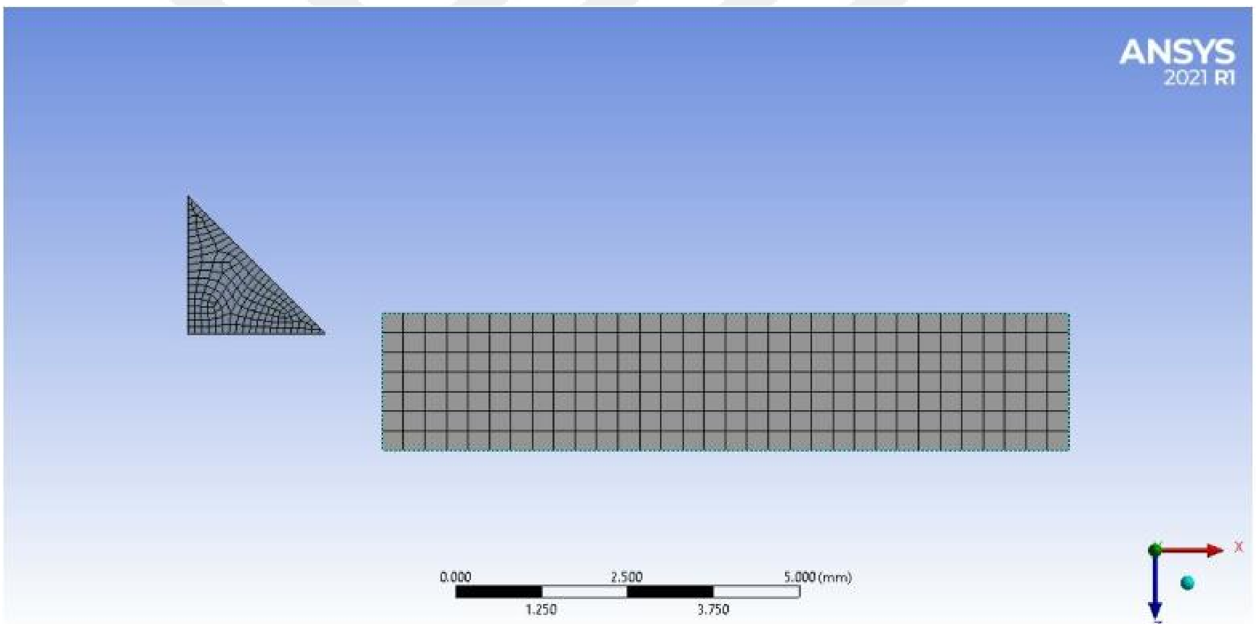

Figure 6.1: The meshing to the model.

The physics which is applied to the model are showing in the below figure. In displacement is given to bodies for the smooth simulation. Fixed support does not move the workpiece during orthogonal cutting so that required results can find easily.

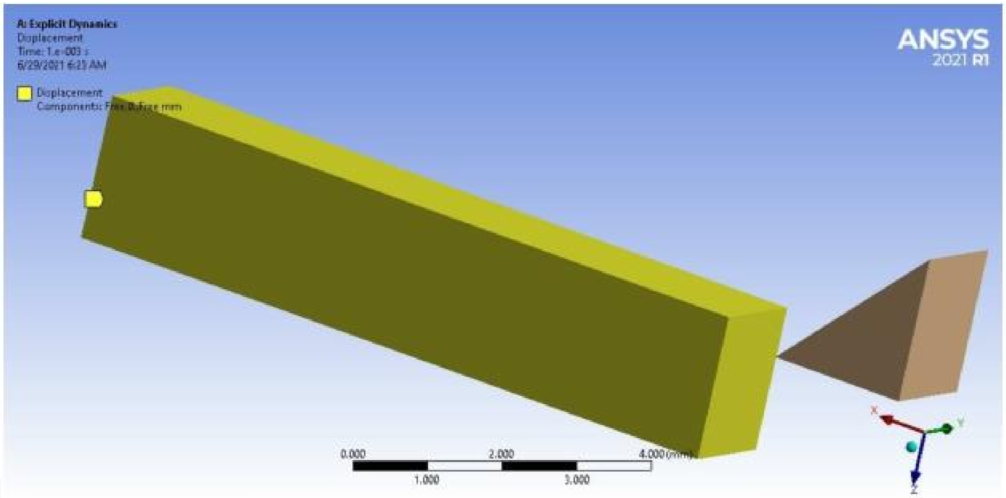
A: Explicit Dynamics
Displacement
Time: 1.e-003 s
6/29/2021 6:23 AM
Displacement
ANSYS
2021 R1
0.000
2.000
4.000 (mm)
1.000
3.000

(a)

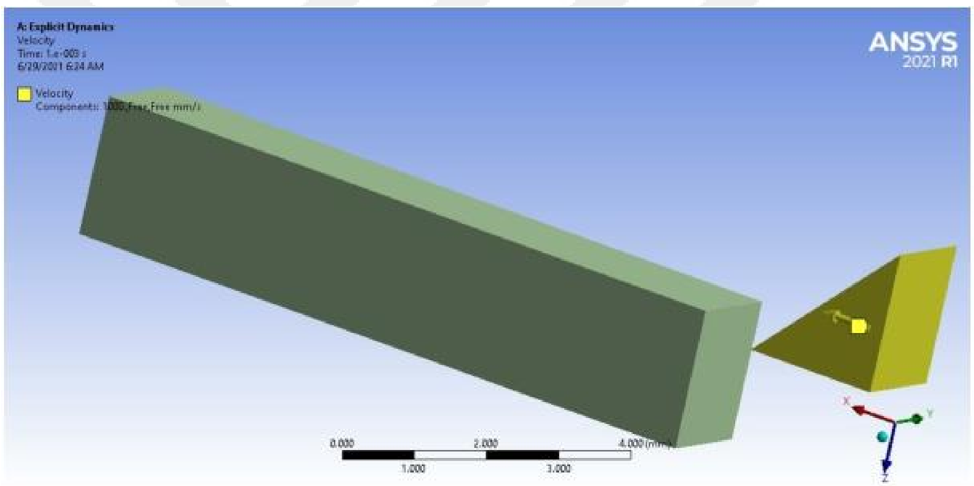
A: Explicit Dynamics
Velocity
Time: 1.e-003 s
6/29/2021 6:24 AM
Velocity
ANSYS
2021 R1
0.000
2.000
4.000 (mm)
1.000
3.000

(b)

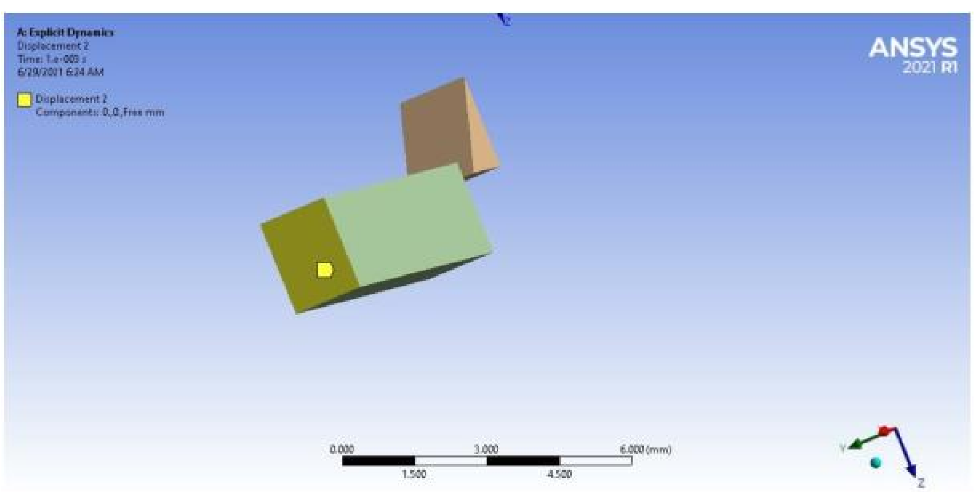
A: Explicit Dynamics
Displacement 2
Time: 1.e-003 s
6/29/2021 6:24 AM
Displacement 2
Components: 0,0,Free mm
ANSYS
2021 R1
0.000
3.000
6.000 (mm)
1.500
4.500

(c)

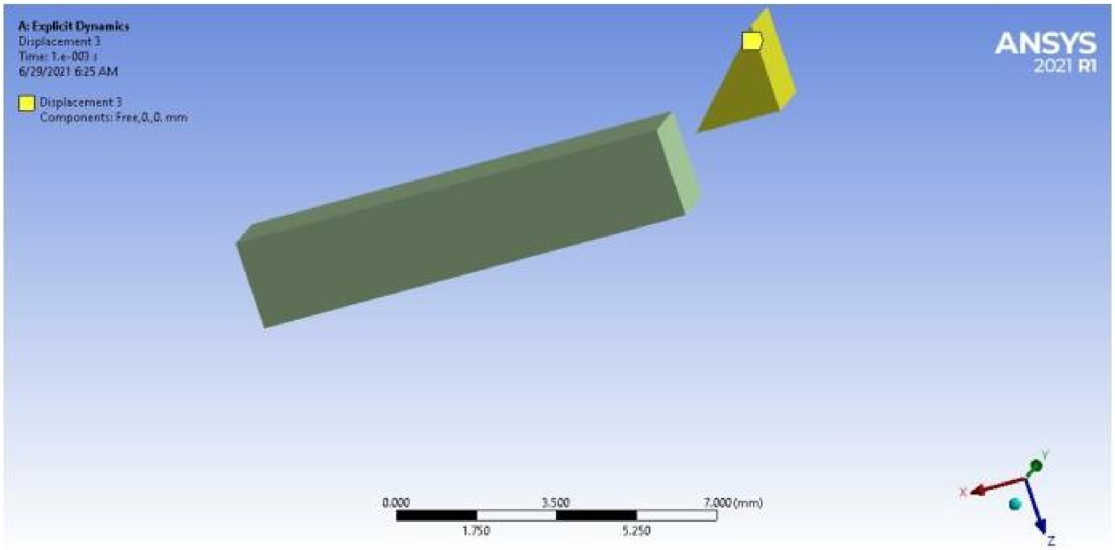

(d)

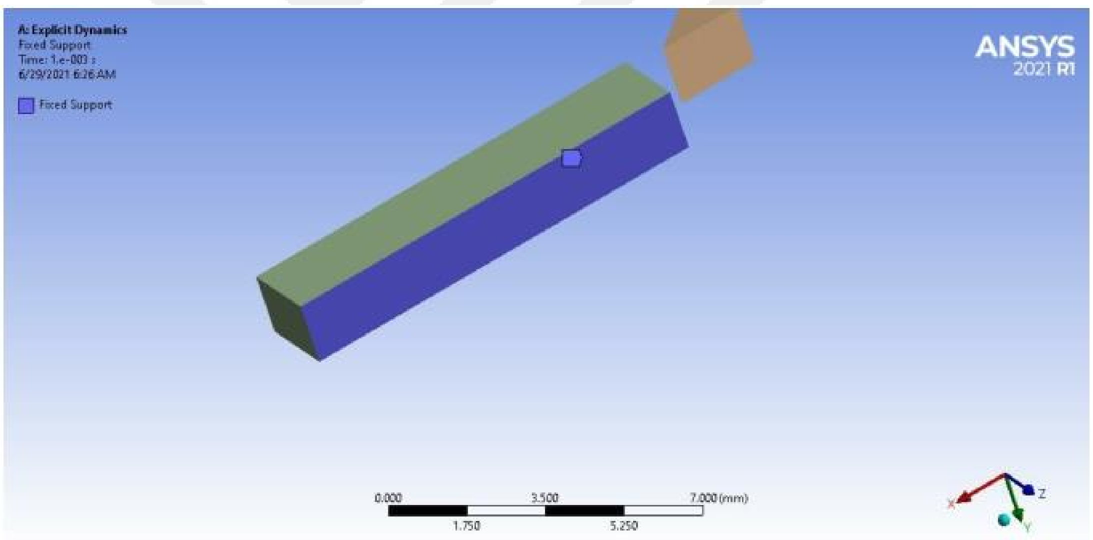

(e)

Figure 6.2: The physics for the simulation (a) Displacement to the workpiece (b) Velocity to the tool (c) Displacement to end face of workpiece (d) Displacement to the tool (e) Fixed support to the down face of the workpiece.

6.1 SIMULATION RESULTS

6.1.1 The Equivalent Stress And The Equivalent Strain

Figure 6.3 shows the equivalent stress results and figure 6.4 shows the results for equivalent elastic strain. Figure 6.5 shows the graphical representation between equivalent stresses and equivalent elastic strain.

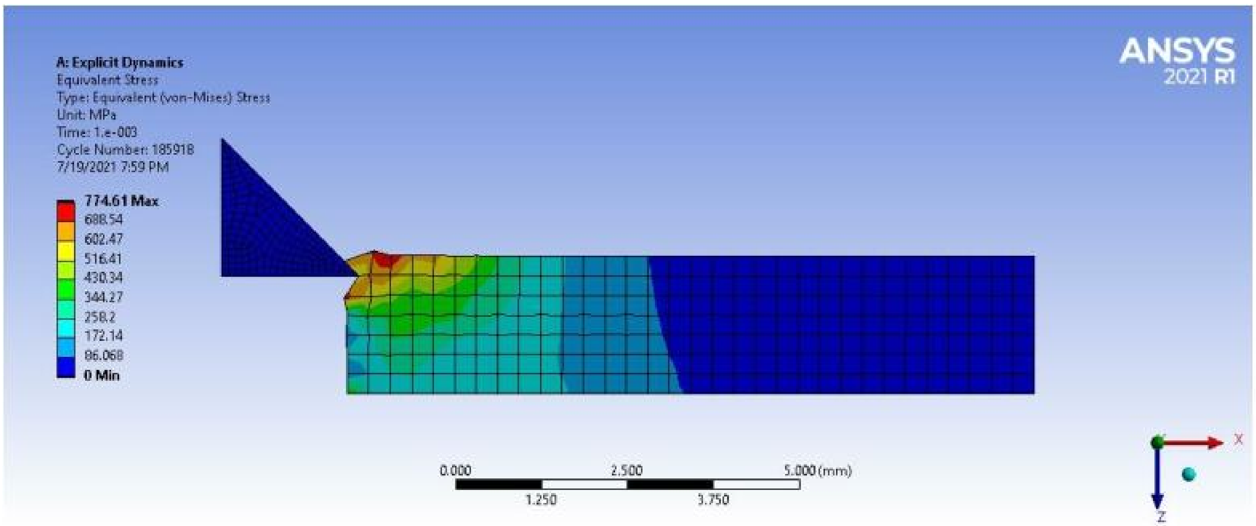

Figure 6.3: The equivalent stress results for the Inconel 718.

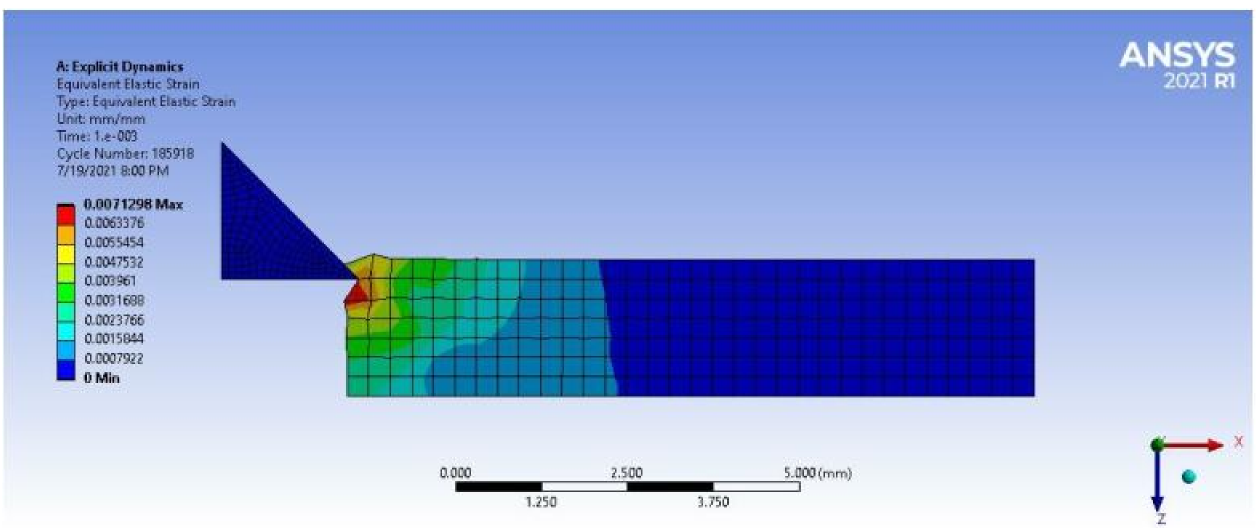

Figure 6.4: The equivalent elastic strain result for the Inconel 718.

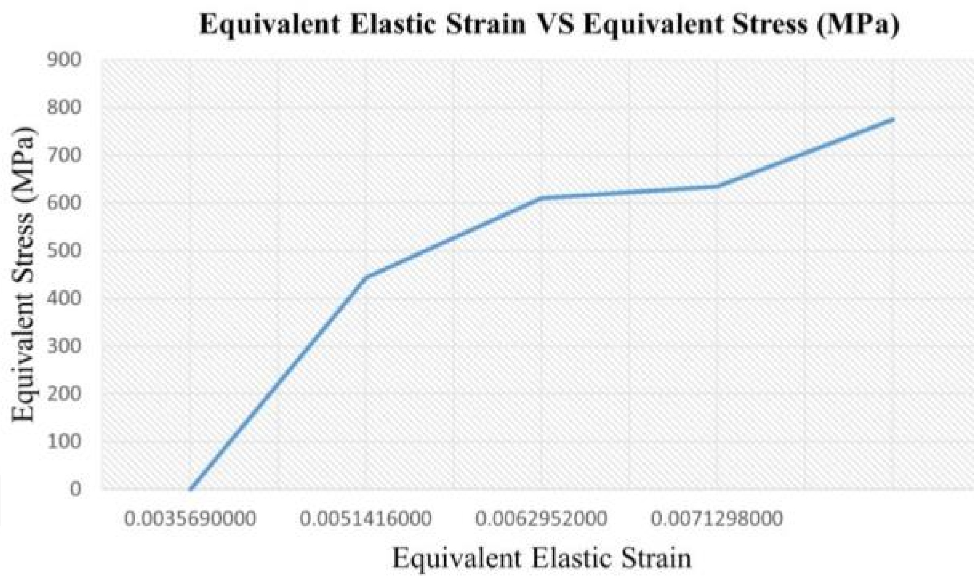

Figure 6.5: The equivalent stress and equivalent elastic strain curve for the Inconel 718.

6.1.2 The Maximum Principal Stresses And Maximum Elastic Strain

Figure 6.6 shows the maximum principal stress results and figure 6.7 shows the results for maximum principal elastic strain. Figure 6.8 shows the graphical representation between the maximum principal elastic strain and the maximum principal stress.

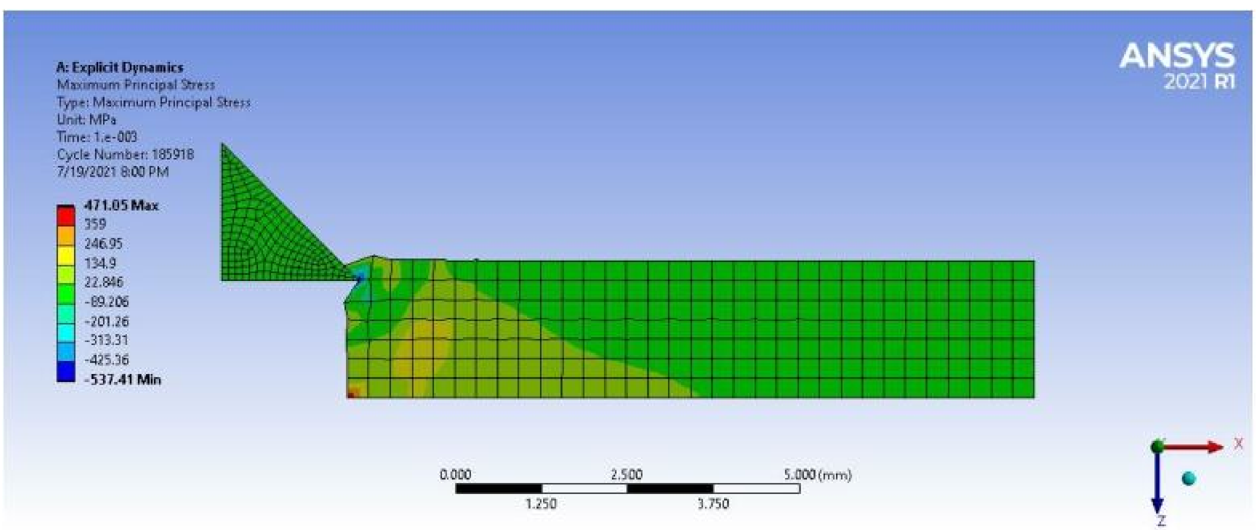

Figure 6.6: The maximum principal stress results for the Inconel 718.

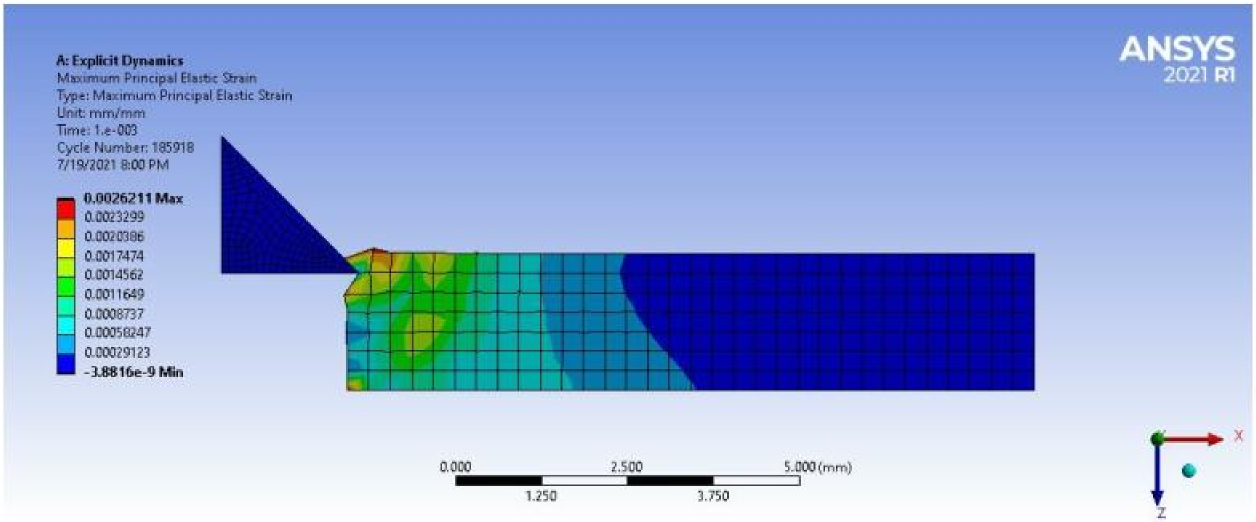

Figure 6.7: The maximum principal elastic strain results for the Inconel 718.

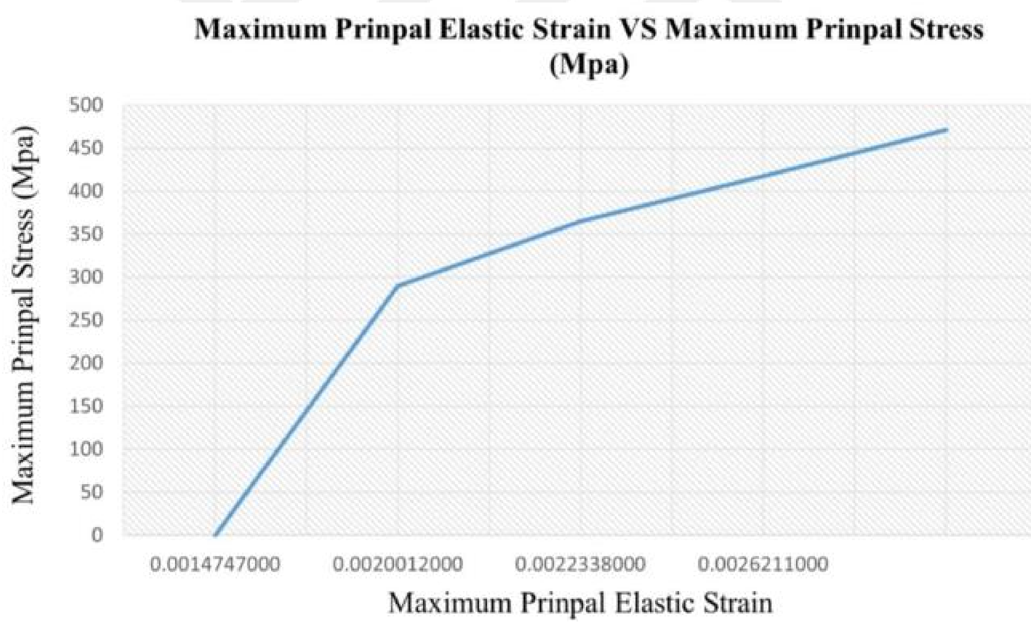

Figure 6.8: The maximum principal stress and maximum principal elastic strain curve for the Inconel 718.

6.1.3 Shear Stress And Shear Elastic Strain

Figure 6.9 shows shear stress results and figure 6.10 shows the results for shear elastic strain. Figure 6.11 shows the graphical representation between the shear elastic strain and the shear stress.

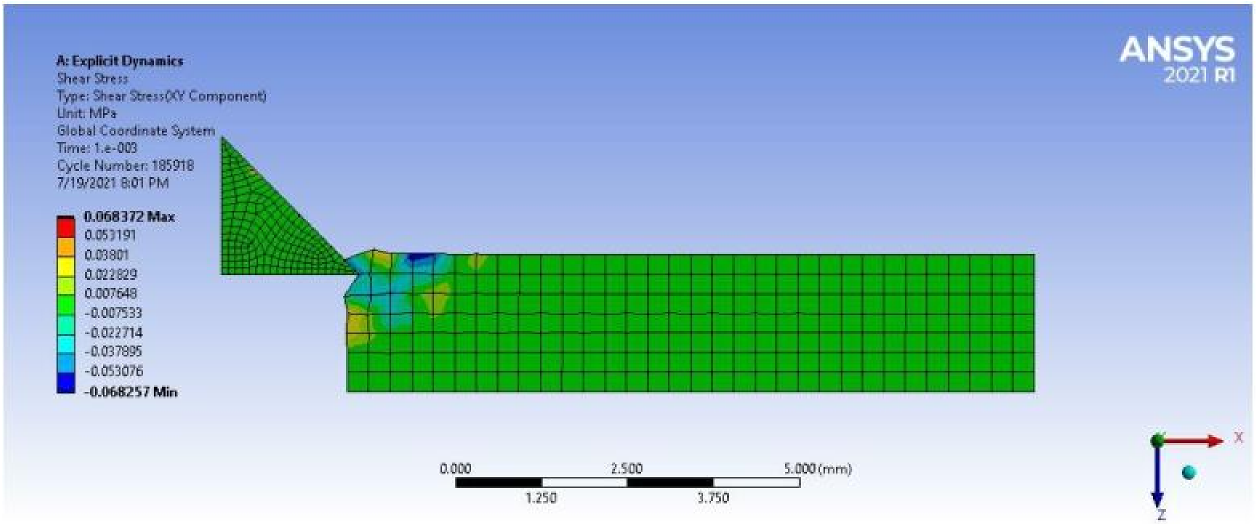

Figure 6.9: Shear stress results for the Inconel 718.

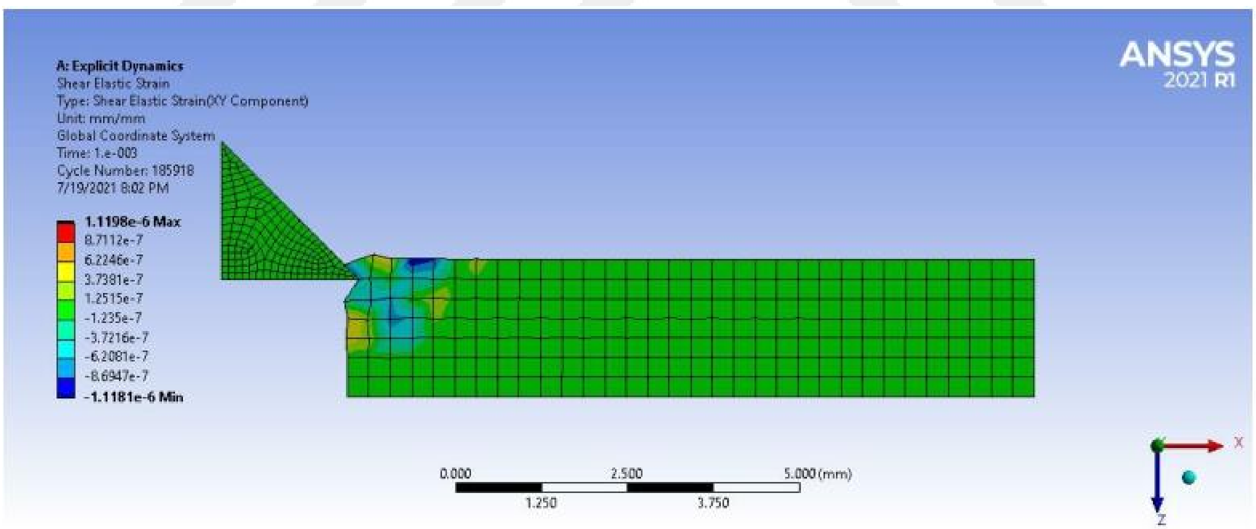

Figure 6.10: Shear elastic strain results for the Inconel 718.

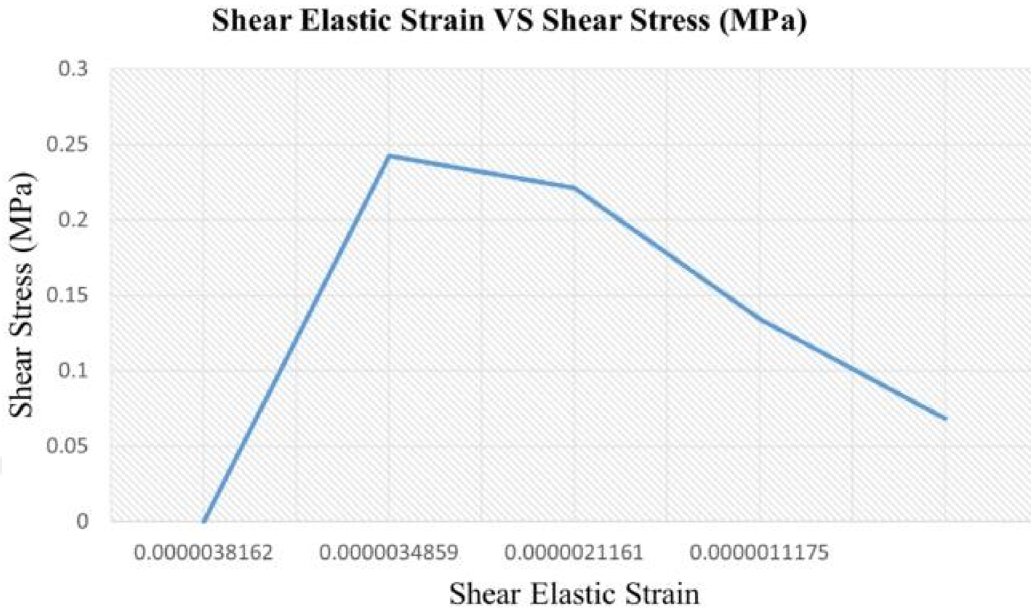

Figure 6.11: The shear stress and shear elastic strains curve for the Inconel 718.

7. CONCLUSION

Heat Assisted Machining (HAM) is a technique introduced to improve the machinability of superalloys. It employs various heat sources to preheat the workpiece and enhance its machinability. The applied heat causes a reduction in the yield, ultimate tensile, and shear strength of the superalloy workpiece leading to a tangible reduction in cutting forces. Additionally, by selecting the appropriate cutting tool (coated ceramic inserts), a raise in the tool life and Material Removal Rate (MRR) is visible experimentally. The main cause of the phenomenon is related to lower friction and lower shear stress in the cutting zone. Moreover, the preheated workpiece will demonstrate lower structural stiffness, and optimizing the appropriate cutting parameters (velocity, feed, and depth of cut) can reduce the workpiece vibration amplitudes which results in better surface quality.

In this study, four common heat sources as gas flame, induction, Laser, and plasma are investigated. The heating methodology and the application methods are discussed in detail and the heating efficiency of the techniques is compared. Furthermore, the effect of heating on the microstructure change of three main superalloy types is discussed and evaluated. Finally, the effect of the heating on the machining parameters (cutting forces, tool wear, surface roughness, and chip morphology) and the cost of the processes are explored.

The stresses inside the material have a direct relation to the temperature, in the modified JC model the stresses are reduced because of the consideration of thermal softening in the constitutive model. Moreover, finite element analysis shows that without heating the properties of Inconel are too hard for the tools. The induction power is a direct relationship with the voltage, number of turn N, and the current. Analytical study of estimation of induction heating power concerning temperature needs to be more focused. The electrical losses inside the coil and the workpiece should be more studied. The variation in frequency and current are directly proportional to the temperature.

Although HAM was introduced in the 1940s, the analytical and numerical analysis of the various techniques with optimized cutting parameters needs more investigation. Additionally, the kinetics of the process and the machinability estimation approaches need more research. The areas for future investigations can be entitled as:

a) Cutting tool life with HAM

The preheated workpiece adds external heat to the cutting zone. Therefore, depending on the cutting tool selection and the cooling technique, the effect can vary drastically resulting in impairment of the tool life. A deep investigation of the cutting tool microstructure, chemical stability, and wear mechanisms are necessary to evaluate the impact of the various external heat sources (interrupted, continuous, and local or a shallow area) on the tool wear. Additionally, most of the researchers explore the effect of heat enhancement on dry machining. However, the effect of various cooling and lubrication techniques on HAM needs a more focused study.

b) Real-time heat assistance module

Although several real-time heat applications are introduced by researchers, the heat source attachment in interrupted cutting operations (milling and drilling) is a challenging task. Additionally, in hybrid methods, the coalescing of the heat sources and their integration configurations for optimal machinability needs further investigation. The arrangement of the hybrid heat source has an essential impact on the heating efficiency and losses. Therefore, the effect of distance, angle and the order of the heat application needs to be explored in more detail. In addition to the heat source Integration problem in simple geometries (circular or rectangular shapes), suitable heat source selection and implementation remain a hurdle in the workpieces with free-from geometries (5-axis machining of impellers). Hence, there is a need for the development of flexible and reliable heat source integration methods for these applications. Moreover, when the diameter of the workpiece changes throughout the length, a constant heat source and workpiece distance need to be maintained to achieve a homogeneous heat distribution. This problem is more prominent in induction-assisted turning which needs the development of variable magnetic coil diameter design.

c) Optimization

The efficiency and the required period of heating play an important role in the productivity of the HAM processes. Additionally, the power losses are related to the nature of the heating method, thermal losses (convection, conduction, and radiation) during and after the heating processes. Therefore, a monitored controlled cycle with feedback is necessary to apply optimized power. Thermocouples, thermal cameras, and other related sensors can adjust the required timing for the heat application or elimination to achieve optimal efficiency. Additionally, a comprehensive study on the selection of desired power parameters (voltage, current, frequency, pulse type, gas pressure, nozzle diameter, and gas stream flow rate) concerning the superalloy workpiece, cutting tool material, cutting parameters (velocity, feed, and depth of cut), and environmental effects (temperature, humidity, chemical stability) is necessary.

d) Analytical evaluation

Most research in the HAM area and its effect on the machining parameters (force, tool life, surface roughness, and material removal rate) are performed experimentally and there is a lack of analytical evaluation of heat source impact on these parameters. Estimation of these effects ahead of experimenting has economic benefits which can result in better selection of the heat source, implementation technique, power consumption, and selection of the appropriate cutting tool material and geometrical parameters (rake angle, nose radius, and inclination angle). Therefore, an analytical and numerical simulation approach especially in cutting forces and tool life analysis leads to higher productivity.

e) Complex Geometry

Heat-assisted machining of complex freeform geometries such as turbine impellers remains a challenge for engineers. The development of more flexible heating systems/techniques can help overcome this problem in various aerospace industry applications.

8. REFERENCES

[1] D. Popli and M. Gupta, "Experimental study and optimization of cutting parameters in machining of super alloy with hybrid ultrasonic method," *Adv. Manuf.*, vol. 5, no. 3, pp. 199–216, 2017, doi: 10.1007/s40436-017-0185-6.

[2] Y. Shen *et al.*, "Surface integrity of Inconel 718 in high-speed electrical discharge machining milling using air dielectric," *Int. J. Adv. Manuf. Technol.*, vol. 90, no. 1–4, pp. 691–698, 2017, doi: 10.1007/s00170-016-9332-7.

[3] N. Fang, P. S. Pai, and N. Edwards, "A comparative study of high-speed machining of Ti-6Al-4V and Inconel 718 - Part I: Effect of dynamic tool edge wear on cutting forces," *Int. J. Adv. Manuf. Technol.*, vol. 68, no. 5–8, pp. 1839–1849, 2013, doi: 10.1007/s00170-013-4981-2.

[4] J. wei Ma, F. ji Wang, Z. yuan Jia, Q. Xu, and Y. yu Yang, "Study of machining parameter optimization in high speed milling of Inconel 718 curved surface based on cutting force," *Int. J. Adv. Manuf. Technol.*, vol. 75, no. 1–4, pp. 269–277, 2014, doi: 10.1007/s00170-014-6115-x.

[5] M. Z. A. Yazid, G. A. Ibrahim, A. Y. M. Said, C. H. CheHaron, and J. A. Ghani, "Surface integrity of Inconel 718 when finish turning with PVD coated carbide tool under MQL," *Procedia Eng.*, vol. 19, pp. 396–401, 2011, doi: 10.1016/j.proeng.2011.11.131.

[6] E. Akca and A. Gürsel, "A Review on Superalloys and IN718 Nickel-Based INCONEL Superalloy," *Period. Eng. Nat. Sci.*, vol. 3, no. 1, 2015, doi: 10.21533/pen.v3i1.43.

[7] A. Pramanik, "Problems and solutions in machining of titanium alloys," *Int. J. Adv. Manuf. Technol.*, vol. 70, no. 5–8, pp. 919–928, 2014, doi: 10.1007/s00170-013-5326-x.

[8] A. X. M, M. Manohar, P. M. Madhukar, and P. Jeyapandiarajan, "Experimental investigation of work hardening , residual stress and microstructure during machining Inconel 718 †," vol. 31, no. 10, pp. 4789–4794, 2017, doi: 10.1007/s12206-017-0926-2.

[9] Z. Qi, B. Li, and L. Xiong, "The formation mechanism and the influence factor of residual stress in machining," *Front. Mech. Eng.*, vol. 9, no. 3, pp. 265–269, 2014, doi: 10.1007/s11465-014-0311-0.

[10] X. Cai, S. Qin, J. Li, Q. An, and M. Chen, “Experimental investigation on surface integrity of end milling nickel-based alloy-inconel 718,” *Mach. Sci. Technol.*, vol. 18, no. 1, pp. 31–46, 2014, doi: 10.1080/10910344.2014.863627.

[11] D. Jin and Z. Liu, “Effect of cutting speed on surface integrity and chip morphology in high-speed machining of PM nickel-based superalloy FGH95,” *Int. J. Adv. Manuf. Technol.*, vol. 60, no. 9–12, pp. 893–899, 2012, doi: 10.1007/s00170-011-3679-6.

[12] E. O. Ezugwu, “High Speed Machining of Aero-Engine Alloys,” *J. Brazilian Soc. Mech. Sci. Eng.*, vol. 26, no. 1, pp. 1–11, 2004, doi: 10.1590/S1678-58782004000100001.

[13] A. T. Kuzu, A. Bijanzad, and M. Bakkal, “Experimental Investigations of Machinability in the Turning of Compacted Graphite Iron using Minimum Quantity Lubrication,” *Mach. Sci. Technol.*, vol. 19, no. 4, pp. 559–576, 2015, doi: 10.1080/10910344.2015.1085313.

[14] G. R. Singh, M. K. Gupta, M. Mia, and V. S. Sharma, “Modeling and optimization of tool wear in MQL-assisted milling of Inconel 718 superalloy using evolutionary techniques,” *Int. J. Adv. Manuf. Technol.*, vol. 97, no. 1–4, pp. 481–494, 2018, doi: 10.1007/s00170-018-1911-3.

[15] Y. Kaynak, “Evaluation of machining performance in cryogenic machining of Inconel 718 and comparison with dry and MQL machining,” *Int. J. Adv. Manuf. Technol.*, vol. 72, no. 5–8, pp. 919–933, 2014, doi: 10.1007/s00170-014-5683-0.

[16] A. K. Nandy, M. C. Gowrishankar, and S. Paul, “Some studies on high-pressure cooling in turning of Ti-6Al-4V,” *Int. J. Mach. Tools Manuf.*, vol. 49, no. 2, pp. 182–198, 2009, doi: 10.1016/j.ijmachtools.2008.08.008.

[17] D. Dudzinski, A. Devillez, A. Moufki, D. Larrouquère, V. Zerrouki, and J. Vigneau, “A review of developments towards dry and high speed machining of Inconel 718 alloy,” *Int. J. Mach. Tools Manuf.*, vol. 44, no. 4, pp. 439–456, 2004, doi: 10.1016/S0890-6955(03)00159-7.

[18] D. Umbrello, “Investigation of surface integrity in dry machining of Inconel 718,” *Int. J. Adv. Manuf. Technol.*, vol. 69, no. 9–12, pp. 2183–2190, 2013, doi: 10.1007/s00170-013-5198-0.

[19] J. Zhou, V. Bushlya, P. Avdovic, and J. E. Ståhl, "Study of surface quality in high speed turning of Inconel 718 with uncoated and coated CBN tools," *Int. J. Adv. Manuf. Technol.*, vol. 58, no. 1–4, pp. 141–151, 2012, doi: 10.1007/s00170-011-3374-7.

[20] Z. P. Hao, Y. H. Fan, J. Q. Lin, and Z. X. Yu, "Wear characteristics and wear control method of PVD-coated carbide tool in turning Inconel 718," *Int. J. Adv. Manuf. Technol.*, vol. 78, no. 5–8, pp. 1329–1336, 2015, doi: 10.1007/s00170-014-6752-0.

[21] S. Sun, M. Brandt, and M. S. Dargusch, "International Journal of Machine Tools & Manufacture Thermally enhanced machining of hard-to-machine materials — A review," *Int. J. Mach. Tools Manuf.*, vol. 50, no. 8, pp. 663–680, 2010, doi: 10.1016/j.ijmachtools.2010.04.008.

[22] A. M. Ravi, S. M. Murigendrappa, and P. G. Mukunda, "Experimental investigation on thermally enhanced machining of high-chrome white cast iron and to study its machinability characteristics using Taguchi method and artificial neural network," *Int. J. Adv. Manuf. Technol.*, vol. 72, no. 9–12, pp. 1439–1454, 2014, doi: 10.1007/s00170-014-5752-4.

[23] M. Anderson, R. Patwa, and Y. C. Shin, "Laser-assisted machining of Inconel 718 with an economic analysis," *Int. J. Mach. Tools Manuf.*, vol. 46, no. 14, pp. 1879–1891, 2006, doi: 10.1016/j.ijmachtools.2005.11.005.

[24] M. J. Bermingham, P. Schaffarzyk, S. Palanisamy, and M. S. Dargusch, "Laser-assisted milling strategies with different cutting tool paths," *Int. J. Adv. Manuf. Technol.*, vol. 74, no. 9–12, pp. 1487–1494, 2014, doi: 10.1007/s00170-014-6093-z.

[25] A. Kumar and K. Maity, "Engineering Science and Technology , an International Journal Experimental investigation on tool life and chip morphology in hot machining of Monel-400," *Eng. Sci. Technol. an Int. J.*, vol. 21, no. 3, pp. 371–379, 2018, doi: 10.1016/j.jestch.2018.04.003.

[26] A. Kumar and K. Maity, "Numerical and experimental analysis of specific cutting energy in hot turning of Inconel 718," *Measurement*, vol. 133, pp. 361–369, 2019, doi: 10.1016/j.measurement.2018.10.033.

[27] S. Lei and F. Pfefferkorn, "A review of thermally assisted machining," *Proc. ASME Int. Manuf. Sci. Eng. Conf. 2007, MSEC2007*, pp. 325–336, 2007, doi: 10.1115/MSEC2007-31096.

[28] S. Lupi, M. Forzan, and A. Aliferov, *Induction and Direct Resistance Heating*. 2015.

[29] J. H. Ha and C. M. Lee, "A study on the thermal effect by multi heat sources and machining characteristics of laser and induction assisted milling," *Materials (Basel).*, vol. 12, no. 7, 2019, doi: 10.3390/ma12071032.

[30] T. Machinability, M. Baili, V. Wagner, and G. Dessein, "An Experimental Investigation of Hot Machining with Induction to Improve An experimental investigation of hot machining with induction to improve Ti-5553 machinability," no. February 2015, pp. 2018–2022, 2011, doi: 10.4028/www.scientific.net/AMM.62.67.

[31] E. J. Kim and C. M. Lee, "A study on the optimal machining parameters of the induction assisted milling with Inconel 718," *Materials (Basel).*, vol. 12, no. 2, 2019, doi: 10.3390/ma12020233.

[32] G. Kibria, B. Doloi, and B. Bhattacharyya, "Investigation and analysis on pulsed Nd:YAG laser micro-turning process of aluminium oxide (Al2O3) ceramic at various laser defocusing conditions," *Int. J. Adv. Manuf. Technol.*, vol. 76, no. 1–4, pp. 17–27, 2013, doi: 10.1007/s00170-013-5254-9.

[33] Y. Feng *et al.*, "Analytical prediction of temperature in laser-assisted milling with laser preheating and machining effects," pp. 3185–3195, 2019.

[34] J. Meijer, "Laser beam machining (LBM), state of the art and new opportunities," *J. Mater. Process. Technol.*, vol. 149, no. 1–3, pp. 2–17, 2004, doi: 10.1016/j.jmatprotec.2004.02.003.

[35] A. K. Dubey and V. Yadava, "Laser beam machining-A review," *Int. J. Mach. Tools Manuf.*, vol. 48, no. 6, pp. 609–628, 2008, doi: 10.1016/j.ijmachtools.2007.10.017.

[36] S. Azhdari Tadavani, R. Shoja Razavi, and R. Vafaei, "Pulsed laser-assisted machining of Inconel 718 superalloy," *Opt. Laser Technol.*, vol. 87, pp. 72–78, 2017, doi: 10.1016/j.optlastec.2016.07.020.

[37] N. Ahmed, S. Darwish, A. M. Alahmari, and M. A. Shar, "Micro-channels by Nd:YAG laser beam machining: fabrication, microstructures, and micro-hardness profiles," *Int. J. Adv. Manuf. Technol.*, vol. 85, no. 9–12, pp. 1955–1968, 2016, doi: 10.1007/s00170-015-7257-1.

[38] D. H. Kim and C. M. Lee, "A study of cutting force and preheating-temperature prediction for laser-assisted milling of Inconel 718 and AISI 1045 steel," *Int. J. Heat Mass Transf.*, vol. 71, pp. 264–274, 2014, doi: 10.1016/j.ijheatmasstransfer.2013.12.021.

[39] Y. Lee and C. Lee, "A Study on Optimal Machining Conditions and Energy E ffi ciency in Plasma Assisted Machining of Ti-6Al-4V," 2019.

[40] S. H. Moon and C. M. Lee, "A study on the machining characteristics using plasma assisted machining of AISI 1045 steel and Inconel 718," *Int. J. Mech. Sci.*, vol. 142–143, no. January, pp. 595–602, 2018, doi: 10.1016/j.ijmecsci.2018.05.020.

[41] S. H. Chen and K. T. Tsai, "The study of plasma-assisted machining to Inconel-718," *Adv. Mech. Eng.*, vol. 9, no. 12, pp. 1–7, 2017, doi: 10.1177/1687814017735789.

[42] A. B. M. Hadzley, S. M. Hafiz, W. Azahar, R. Izamshah, K. M. Shahir, and A. Abu, "Heat-assisted machining for material removal improvement," *IOP Conf. Ser. Mater. Sci. Eng.*, vol. 88, no. 1, 2015, doi: 10.1088/1757-899X/88/1/012052.

[43] O. A. Shams, A. Pramanik, and T. T. Chandratilleke, "Thermal-Assisted Machining of Titanium Alloys," 2017, doi: 10.1007/978-3-319-56099-1.

[44] L. N. López De Lacalle, J. A. Sánchez, A. Lamikiz, and A. Celaya, "Plasma assisted milling of heat-resistant superalloys," *J. Manuf. Sci. Eng. Trans. ASME*, vol. 126, no. 2, pp. 274–285, 2004, doi: 10.1115/1.1644548.

[45] V. V. K. Prasad Rambabu, N. Eswara Prasad and R. J. H. Wanhill, "Aerospace Materials and Material Technologies, Volume 1: Aerospace Material Technologies," *Aerosp. Mater. Mater. Technol. Vol. 1 Aerosp. Mater.*, vol. 1, p. 586, 2017, doi: 10.1007/978-981-10-2134-3.

[46] A. S. M. International and A. Rights, *ASM specialty handbook: nickel, cobalt, and their alloys*, vol.

38, no. 11. 2001.

[47] M. Zielińska, M. Yavorska, M. Poreba, and J. Sieniawski, “Thermal properties of cast nickel based superalloys,” *Arch. Mater. Sci. Eng.*, vol. 44, no. 1, pp. 35–38, 2010.

[48] H. A. Youssef, *Machining of Stainless Steels and Super Alloys*. 2015.

[49] J. A. Lee, “Hydrogen embrittlement of nickel, cobalt and iron-based superalloys,” *Gaseous Hydrog. Embrittlement Mater. Energy Technol. Probl. its Characterisation Eff. Part. Alloy Classes*, pp. 624–667, 2012, doi: 10.1533/9780857093899.3.624.

[50] K. J. Ducki, “Analysis of the Precipitation and Growth Processes of the Intermetallic Phases in an Fe-Ni Superalloy,” *Superalloys*, 2015, doi: 10.5772/61159.

[51] H. Kitaguchi, “Microstructure-Property Relationship in Advanced Ni-Based Superalloys,” *Metall. - Adv. Mater. Process.*, 2012, doi: 10.5772/52011.

[52] B. Graybill, M. Li, D. Malawey, C. Ma, J. M. Alvarado-Orozco, and E. Martinez-Franco, “Additive manufacturing of nickel-based superalloys,” *ASME 2018 13th Int. Manuf. Sci. Eng. Conf. MSEC 2018*, vol. 1, no. June, 2018, doi: 10.1115/MSEC2018-6666.

[53] M. Heilmaier and B. Reppich, “Creep lifetime prediction of oxide-dispersion-strengthened nickel-base superalloys: A micromechanically based approach,” *Metall. Mater. Trans. A Phys. Metall. Mater. Sci.*, vol. 27, no. 12, pp. 3861–3870, 1996, doi: 10.1007/bf02595635.

[54] Z. Zhang, D. Liu, Y. Yang, J. Wang, Y. Zheng, and F. Zhang, “Microstructure evolution of nickel-based superalloy with periodic thermal parameters during rotary tube piercing process,” *Int. J. Adv. Manuf. Technol.*, vol. 104, no. 9–12, pp. 3991–4006, 2019, doi: 10.1007/s00170-019-04126-x.

[55] V. I. Razumovskiy *et al.*, “New Cr-Ni-base alloy for high-temperature applications designed on the basis of first principles calculations,” *Adv. Condens. Matter Phys.*, vol. 2018, 2018, doi: 10.1155/2018/9383981.

[56] Y. C. Tsai and J. M. Hsieh, “An analysis of cutting-edge curves and machining performance in the

Inconel 718 machining process," *Int. J. Adv. Manuf. Technol.*, vol. 25, no. 3–4, pp. 248–261, 2005, doi: 10.1007/s00170-003-1869-6.

[57] Nickel Development Institute, "Machining Nickel Alloys," *A Nickel Dev. Inst. Ref. B.*, pp. 2–6, 1995.

[58] B. Geddes Hugo Leon Xiao Huang, *Senior Content Developer; Ann Britton, Editorial Assistant; Bonnie Sanders, Manager of Production; Madrid Tramble, Senior Production Coordinator; Diane Whitelaw, Production Coordinator; and Patricia Conti*. 2009.

[59] C. H. Superalloy, "Examining of Tool Wear in Cryogenic Machining of," vol. 9, no. 8, pp. 751–755, 2015.

[60] X. Tian, J. Zhao, J. Zhao, Z. Gong, and Y. Dong, "Effect of cutting speed on cutting forces and wear mechanisms in high-speed face milling of Inconel 718 with Sialon ceramic tools," *Int. J. Adv. Manuf. Technol.*, vol. 69, no. 9–12, pp. 2669–2678, 2013, doi: 10.1007/s00170-013-5206-4.

[61] S. Montazeri, M. Aramesh, and S. C. Veldhuis, "An investigation of the effect of a new tool treatment technique on the machinability of Inconel 718 during the turning process," *Int. J. Adv. Manuf. Technol.*, vol. 100, no. 1–4, pp. 37–54, 2019, doi: 10.1007/s00170-018-2669-3.

[62] D. Stephenson and J. Agapiou, *Metal Cutting Theory and Practise*, Third Edit. CRC Press, 2016.

[63] Y. ALTINTAS, *MANUFACTURING AUTOMATION*, Second. Cambridge University Press, 2012.

[64] J. M. C. Filho, "Prediction of cutting forces in mill turning through process simulation using a five-axis machining center," *Int. J. Adv. Manuf. Technol.*, vol. 58, no. 1–4, pp. 71–80, 2012, doi: 10.1007/s00170-011-3391-6.

[65] J. Krystof, "Berichte uber Betriebswissenschaftliche Arbeiten, VDI Verlag," vol. Bd., 12 , 1939.

[66] B. W. Shaffer and E. H. Lee, "Theory of plasticity applied to the problem of machining," *J. Appl. Mech.*, vol. 18, pp. 405–413, 1951.

[67] M. E. Merchant., “Mechanics of the metal cutting process,” *J. Appl. Phys.*, vol. 16, pp. 267–279, 1945.

[68] A. Kumar and K. Maity, “Engineering Science and Technology , an International Journal Comparison the machinability of Inconel 718 , Inconel 625 and Monel 400 in hot turning operation,” *Eng. Sci. Technol. an Int. J.*, vol. 21, no. 3, pp. 364–370, 2018, doi: 10.1016/j.jestch.2018.03.018.

[69] Y. H. Choi and C. M. Lee, “A study on the machining characteristics of AISI 1045 steel and inconel 718 with circular cone shape in induction assisted machining,” *J. Manuf. Process.*, vol. 34, no. February, pp. 463–476, 2018, doi: 10.1016/j.jmapro.2018.06.023.

[70] J. T. Baek, W. S. Woo, and C. M. Lee, “A study on the machining characteristics of induction and laser-induction assisted machining of AISI 1045 steel and Inconel 718,” *J. Manuf. Process.*, vol. 34, no. July, pp. 513–522, 2018, doi: 10.1016/j.jmapro.2018.06.030.

[71] T. W. Kim and C. M. Lee, “A study on the development of milling process for silicon nitride using ball end-mill tools by laser-assisted machining,” *Int. J. Adv. Manuf. Technol.*, vol. 77, no. 5–8, pp. 1205–1211, 2015, doi: 10.1007/s00170-014-6525-9.

[72] S. J. Hwang, W. J. Oh, and C. M. Lee, “A study of preheating characteristics according to various preheating methods for laser-assisted machining,” *Int. J. Adv. Manuf. Technol.*, vol. 86, no. 9–12, pp. 3015–3024, 2016, doi: 10.1007/s00170-016-8387-9.

[73] X. Kong, L. Yang, H. Zhang, K. Zhou, and Y. Wang, “Cutting performance and coated tool wear mechanisms in laser-assisted milling K24 nickel-based superalloy,” *Int. J. Adv. Manuf. Technol.*, vol. 77, no. 9–12, pp. 2151–2163, 2015, doi: 10.1007/s00170-014-6606-9.

[74] H. Ding and Y. C. Shin, “Improvement of machinability of Waspaloy via laser-assisted machining,” *Int. J. Adv. Manuf. Technol.*, vol. 64, no. 1–4, pp. 475–486, 2013, doi: 10.1007/s00170-012-4012-8.

[75] K. Venkatesan, R. Ramanujam, and P. Kuppan, “Investigation of machinability characteristics and chip morphology study in laser-assisted machining of Inconel 718,” *Int. J. Adv. Manuf. Technol.*, vol. 91, no. 9–12, pp. 3807–3821, 2017, doi: 10.1007/s00170-017-9987-8.

[76] X. Wu and J. Chen, "The temperature process analysis and control on laser-assisted milling of nickel-based superalloy," *Int. J. Adv. Manuf. Technol.*, vol. 98, no. 1–4, pp. 223–235, 2018, doi: 10.1007/s00170-018-1809-0.

[77] A. K. M. N. Amin, M. I. Hossain, and A. U. Patwari, "Enhancement of machinability of Inconel 718 in end milling through online induction heating of workpiece," *Adv. Mater. Res.*, vol. 415–417, pp. 420–423, 2012, doi: 10.4028/www.scientific.net/AMR.415-417.420.

[78] J. Baek, W. Woo, and C. Lee, "A study on the machining characteristics of induction and laser-induction assisted machining of AISI 1045 steel and Inconel 718 A study on the machining characteristics of induction and laser-induction assisted machining of AISI 1045 steel and Inconel 718," in *Journal of Manufacturing Processes*, vol. 34, no. August, Elsevier, 2018, pp. 513–522.

[79] C. Brecher, M. Emonts, C. Rosen, and J. Hermani, "Laser-assisted Milling of Advanced Materials," vol. 12, pp. 599–606, 2011, doi: 10.1016/j.phpro.2011.03.076.

[80] C. E. Leshock, J. N. Kim, and Y. C. Shin, "Plasma enhanced machining of Inconel 718: Modeling of workpiece temperature with plasma heating and experimental results," *Int. J. Mach. Tools Manuf.*, vol. 41, no. 6, pp. 877–897, 2001, doi: 10.1016/S0890-6955(00)00106-1.

[81] J. W. Novak, Y. C. Shin, and F. P. Incropera, "Assessment of plasma enhanced machining for improved machinability of Inconel 718," *Am. Soc. Mech. Eng. Prod. Eng. Div. PED*, vol. 68–1, no. February 1997, pp. 443–451, 1994.

[82] C. Ezilarasan, V. S. Senthil Kumar, and A. Velayudham, "Effect of machining parameters on surface integrity in machining nimonic C-263 super alloy using whisker-reinforced ceramic insert," *J. Mater. Eng. Perform.*, vol. 22, no. 6, pp. 1619–1628, 2013, doi: 10.1007/s11665-012-0439-1.

[83] X. Li, Y. Wang, R. Xu, S. Yang, C. Guan, and Y. Zhou, "Influence of surface integrity on fatigue behavior of Inconel 718 and Ti6Al4V workpieces with CBN electroplated wheel," *Int. J. Adv. Manuf. Technol.*, vol. 102, no. 5–8, pp. 2345–2356, 2019, doi: 10.1007/s00170-019-03345-6.

[84] F. Jafarian, H. Amirabadi, and M. Fattahi, "Improving surface integrity in finish machining of Inconel 718 alloy using intelligent systems," *Int. J. Adv. Manuf. Technol.*, vol. 71, no. 5–8, pp. 817–

827, 2014, doi: 10.1007/s00170-013-5528-2.

[85] L. Qiang, G. Ya-dong, C. Ming, and L. Ming-jun, "Research on surface integrity in milling Inconel718 superalloy," *Int. J. Adv. Manuf. Technol.*, vol. 92, no. 1–4, pp. 1449–1463, 2017, doi: 10.1007/s00170-017-0080-0.

[86] G. de Paula Oliveira, M. Cindra Fonseca, and A. C. Araujo, "Analysis of residual stress and cutting force in end milling of Inconel 718 using conventional flood cooling and minimum quantity lubrication," *Int. J. Adv. Manuf. Technol.*, vol. 92, no. 9–12, pp. 3265–3272, 2017, doi: 10.1007/s00170-017-0381-3.

[87] Y. Hua and Z. Liu, "Effects of cutting parameters and tool nose radius on surface roughness and work hardening during dry turning Inconel 718," *Int. J. Adv. Manuf. Technol.*, vol. 96, no. 5–8, pp. 2421–2430, 2018, doi: 10.1007/s00170-018-1721-7.

[88] X. Ren and Z. Liu, "A simulation model for predicting surface integrity coupled thermal–mechanical effect in turning of Inconel 718 super alloy," *Int. J. Adv. Manuf. Technol.*, vol. 100, no. 5–8, pp. 1825–1837, 2019, doi: 10.1007/s00170-018-2704-4.

[89] M. S. Kasim *et al.*, "Chip morphology in ball nose end milling process of nickel-based alloy material under MQL condition," *Int. J. Adv. Manuf. Technol.*, pp. 4621–4625, 2019, doi: 10.1007/s00170-019-03948-z.

[90] M. Pacella, "A new low-feed chip breaking tool and its effect on chip morphology," *Int. J. Adv. Manuf. Technol.*, vol. 104, no. 1–4, pp. 1145–1157, 2019, doi: 10.1007/s00170-019-03961-2.

[91] G. C. Behera, J. Thrinadh, and S. Datta, "Influence of cutting insert (uncoated and coated carbide) on cutting force, tool-tip temperature, and chip morphology during dry machining of Inconel 825," *Mater. Today Proc.*, no. xxxx, pp. 0–6, 2020, doi: 10.1016/j.matpr.2020.08.332.

[92] K. Venkatesan *et al.*, "Study of forces, surface finish and chip morphology on machining of Inconel 825," *Procedia Manuf.*, vol. 30, pp. 611–618, 2019, doi: 10.1016/j.promfg.2019.02.086.

[93] G. Germain, J. L. Lebrun, T. Braham-Bouchnak, D. Bellett, and S. Auger, "Laser-assisted

machining of Inconel 718 with carbide and ceramic inserts," *Int. J. Mater. Form.*, vol. 1, no. SUPPL. 1, pp. 523–526, 2008, doi: 10.1007/s12289-008-0213-y.

[94] C. E. Leshock, J. Kim, and Y. C. Shin, "Plasma enhanced machining of Inconel 718: modeling of workpiece temperature with plasma heating and experimental results," vol. 41, pp. 877–897, 2001.

[95] K. Zhuang, X. Zhang, D. Zhu, and H. Ding, "Employing preheating- and cooling-assisted technologies in machining of Inconel 718 with ceramic cutting tools: towards reducing tool wear and improving surface integrity," *Int. J. Adv. Manuf. Technol.*, vol. 80, no. 9–12, pp. 1815–1822, 2015, doi: 10.1007/s00170-015-7153-8.

[96] U.S. Department of Energy., "Technical Support Documents for Residential cooking Products, Vol. 2: Potential Impact of Alternative Efficiency Levels for Residential Cooking."

[97] M. B. Valery Rudnev, Don Loveless, Raymond Cook, "Handbook of Induction Heating," 2003.

[98] D. Istardi and A. Triwinarko, "Induction Heating Process Design Using COMSOL ® Multiphysics Software Induction Heating Process Design Using COMSOL ® Multiphysics Software," no. August, 2011, doi: 10.12928/telkomnika.v9i2.704.

[99] G. Pastras, A. Fysikopoulos, P. Stavropoulos, and G. Chryssolouris, "An approach to modelling evaporation pulsed laser drilling and its energy efficiency," pp. 1227–1241, 2014, doi: 10.1007/s00170-014-5668-z.

[100] D. Bergström, "The Absorption of Laser Light by Rough Metal Surfaces," 2008.

[101] H. Kügler, "Effects of Short-Term Laser Beam Heating on the Absorptivity of Steel Sheets," 2019, doi: 10.3390/jmmp3020041.

[102] R. Daub, R. Wiedenmann, A. Mahrle, J. Duong, and M. F. Zaeh, "Influence on the efficiency of the heat conduction mode laser beam welding process regarding different laser spot geometries INFLUENCE ON THE EFFICIENCY OF THE HEAT CONDUCTION MODE LASER BEAM," vol. 200, no. 2010, 2018, doi: 10.2351/1.5062026.

[103] W. Woo and C. Lee, “Innovative use of multi-heat sources for improvement of tool life in thermally assisted machining of high-strength material,” *J. Manuf. Process.*, vol. 38, no. June 2018, pp. 30–37, 2019, doi: 10.1016/j.jmapro.2018.12.031.

[104] A. K. M. N. Amin and T. L. Ginta, *Heat-Assisted Machining*, vol. 11. Elsevier, 2014.

[105] A. Bogaerts and E. C. Neyts, “Plasma Technology: An Emerging Technology for Energy Storage,” 2018, doi: 10.1021/acsenergylett.8b00184.

[106] B. K. Hinds and S. M. De Almeida, “Plasma arc heating for hot machining,” *Int. J. Mach. Tool Des. Res.*, vol. 21, no. 2, pp. 143–152, 1981, doi: 10.1016/0020-7357(81)90005-6.

[107] N. V. Pashatskii and A. V. Prokhorov, “Analytical model of heating a component by plasma- assisted machining,” *Weld. Int.*, vol. 16, no. 5, pp. 405–407, 2002, doi: 10.1080/09507110209549550.

[108] H. R. Siebner *et al.*, *Introduction to Mechanical Engineering*, vol. 22, no. 7. Springer International Publishing, 2018.

[109] R. S. Revuru, N. R. Posinasetti, V. R. Vsn, and M. Amrita, “Application of cutting fluids in machining of titanium alloys—a review,” *Int. J. Adv. Manuf. Technol.*, vol. 91, no. 5–8, pp. 2477–2498, 2017, doi: 10.1007/s00170-016-9883-7.

[110] K. M. Hubbard, R. N. Callahan, and S. D. Strong, “A standardized model for the evaluation of machining coolant/lubricant costs,” *Int. J. Adv. Manuf. Technol.*, vol. 36, no. 1–2, pp. 1–10, 2008, doi: 10.1007/s00170-006-0806-x.

[111] V. Ganta and D. Chakradhar, “An Experimental Investigation of Hot Machining Performance Parameters using Oxy-Acetylene gas setup,” no. Aimtdr, pp. 1–6, 2014.

[112] X. Kong, L. Yang, H. Zhang, G. Chi, and Y. Wang, “Optimization of surface roughness in laser-assisted machining of metal matrix composites using Taguchi method,” *Int. J. Adv. Manuf. Technol.*, vol. 89, no. 1–4, pp. 529–542, 2017, doi: 10.1007/s00170-016-9115-1.

[113] G. R. Johnson and W. H. Cook, “A CONSTITUTIVE MODEL AND DATA FOR METALS

SUBJECTED TO LARGE.”

[114] M. Calamaz, “NUMERICAL SIMULATION OF TITANIUM ALLOY DRY MACHINING WITH A STRAIN SOFTENING CONSTITUTIVE LAW,” no. October 2013, pp. 37–41, doi: 10.1080/10910344.2010.500957.

[115] P. Taylor, “Machining Science and Technology: An 3D FINITE ELEMENT MODELLING OF CHIP FORMATION PROCESS FOR MACHINING INCONEL 718 : COMPARISON OF FE SOFTWARE PREDICTIONS,” no. May 2013, pp. 37–41, doi: 10.1080/10910344.2011.557950.

[116] O. Lurdos, F. Montheillet, G. Damamme, and C. Fauriel, “Empirical and physically based flow rules relevant to high speed processing of 304L steel,” pp. 1431–1434, 2008, doi: 10.1007/s12289-008-0105-1.

[117] A. Hor, F. Morel, and J. Lebrun, “International Journal of Mechanical Sciences An experimental investigation of the behaviour of steels over large temperature and strain rate ranges,” vol. 67, pp. 108–122, 2013, doi: 10.1016/j.ijmecsci.2013.01.003.

[118] Marc Andr´e MeyersKrishan Kumar Chawla, *Mechanical behavior of material*, Second. Cambridge University Press.

[119] S. Analysis, O. F. The, M. Flow, and S. In, “IMECE2003-4 1655,” pp. 1–10, 2016.

[120] Y. C. Lin, K. Li, H. Li, J. Chen, X. Chen, and D. Wen, “New constitutive model for high-temperature deformation behavior of inconel 718 superalloy,” *J. Mater.*, vol. 74, pp. 108–118, 2015, doi: 10.1016/j.matdes.2015.03.001.

[121] A. He, G. Xie, H. Zhang, and X. Wang, “A comparative study on Johnson – Cook , modified Johnson – Cook and Arrhenius-type constitutive models to predict the high temperature flow stress in 20CrMo alloy steel,” vol. 52, pp. 677–685, 2013, doi: 10.1016/j.matdes.2013.06.010.

[122] L. Chen, G. Zhao, and J. Yu, “Hot deformation behavior and constitutive modeling of homogenized 6026 aluminum alloy,” *J. Mater.*, 2015, doi: 10.1016/j.matdes.2015.02.024.

[123] J. Yong, "Flow Behavior and Constitutive Modeling of Delta-processed Inconel 7 1 8 alloy," 2012, doi: 10.1016/S1006-706X(15)30078-9.

[124] X. Wang, C. Huang, B. Zou, H. Liu, and H. Zhu, "Materials Science & Engineering A Dynamic behavior and a modi fi ed Johnson – Cook constitutive model of Inconel 718 at high strain rate and elevated temperature," *Mater. Sci. Eng. A*, vol. 580, pp. 385–390, 2013, doi: 10.1016/j.msea.2013.05.062.

[125] A. Iturbe *et al.*, "Mechanical characterization and modelling of Inconel 718 material behavior for machining process assessment To cite this version: HAL Id : hal-02283291," 2019.

[126] J. Davies, *Conduction and Induction Heating*. P. Peregrinus Ltd. London, U.K., 1990.

[127] VDM-Metals, "VDM Alloy 718 Nicrofer 5219 Nb," no. 4127, 2016.

[128] J. Díaz-Álvarez, A. Tapetado, C. Vázquez, and H. Miguélez, "Temperature measurement and numerical prediction in machining inconel 718," *Sensors (Switzerland)*, vol. 17, no. 7, 2017, doi: 10.3390/s17071531.